Daniel Cantero
Anders Rønnquist

NTNU
Norwegian University of Science and Technology

Parametric excitation of mooring systems

Trondheim – May 2018

Report

NTNU
Norwegian University of Science and Technology
Faculty of Engineering
Department of Structural Engineering

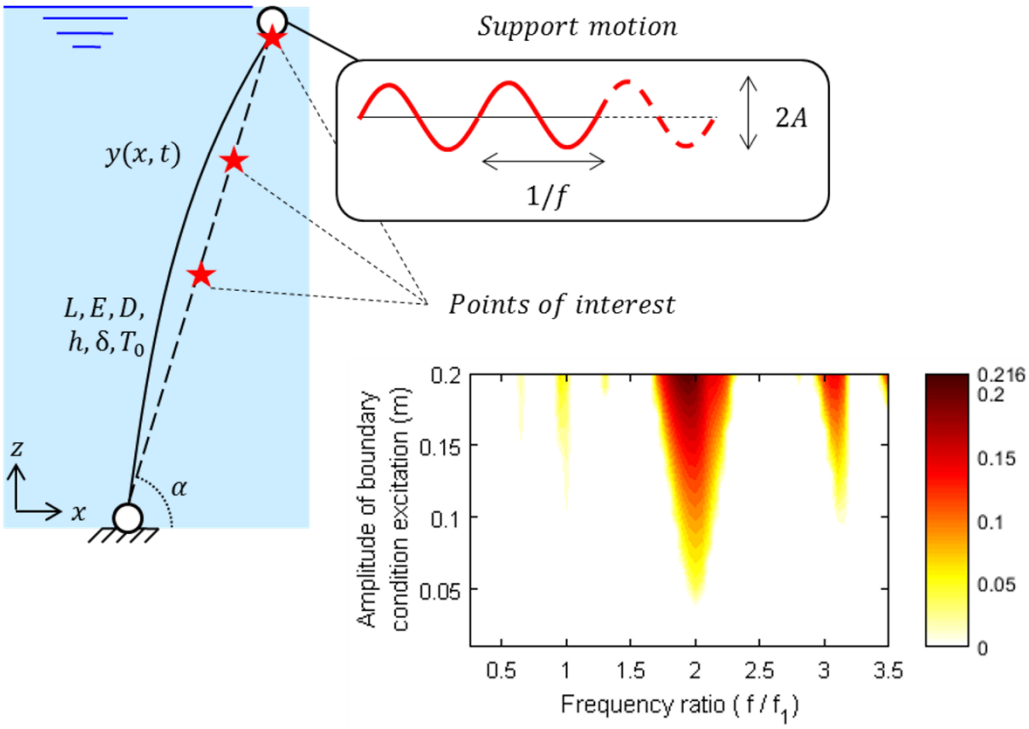

NTNU
Norwegian University of Science and Technology

Executive summary

This document gathers all the results obtained by the post-doc Daniel Cantero in the course of the investigations related to the parametric excitation of mooring systems. This project is part of the research program within the E39 Ferry-free project.

This document consist of two distinct parts:

First, the main body of the document consists of a brief summary of the project and the results obtained. This first part gives an introduction to the problem of parametric resonance in mooring systems, highlights relevant results and finishes providing conclusions.

The second part of the document consists of a list of Appendices. In here, the reader can find copies of the scientific work produced during this project (conference proceedings and journal publication), an additional small report related to the E39 project, as well as complementary theoretical derivations.

Table of contents

1. Introduction
2. What is parametric excitation?
    2.1 Simple example of 1-DOF system
    2.2 Parametric excitation in a mooring system
3. Analytical investigations
    3.1 Equations of motion
    3.2 Analytical solution of transition curves
4. Numerical modelling
5. Results
    5.1 System frequency vs. Excitation frequency
        5.1.1 Study of pretension
        5.1.2 Marine Growth
    5.2 Influence of hydrodynamic effects
        5.2.1 Dry tether
        5.2.2 Submerged tether
    5.3 Numerical validation of analytical expressions
    5.4 Extreme tension values
    5.5 Fatigue calculations
    5.6 Influence of pretension
    5.7 Influence of tether length
    5.8 Influence of inclination angle
    5.9 Extreme bending moment values
    5.10 Influence of boundary conditions
6. Conclusions

References

Appendices
    Appendix A: Conference paper – IABSE 2016, Guangzhou
    Appendix B: Conference paper – IABSE 2016, Stockholm
    Appendix C: Conference paper – SUFTUS 2016, Chongqing
    Appendix D: Journal article – Applied Ocean Research, 2017
    Appendix E: Conference paper – IABMAS 2018, Melbourne
    Appendix F: Static deformation of cable.
    Appendix G: Parametric excitation of Arch bridge
    Appendix H: Equations of motion of inclined cable

1. Introduction

The National Roads Authority (NRA) in Norway is planning to cross several fjords along the west coast of the country as part of the “Ferry-free E39” project [1]. These crossings are characterized by large widths (up to 5 km) and depths (up to 1 km) that require unconventional engineering solutions. The preliminary designs suggest the construction of floating suspension bridges and submerged floating tunnels, as illustrated in Figure 1. A floating bridge is not a new idea and several examples can be found worldwide [2]. However, no precedent exists of a suspension bridge with multiple floating towers. A submerged floating tunnel is a structural concept that has been considered several times during the last century [3]; this tunnel essentially consists of a watertight buoyant tube at a certain depth underwater. To date, no such structure has ever been built. Both a long floating bridge and a submerged floating tunnel require a mooring system (Figure 1) to position these floating structures and to resist any imposed motion due to environmental loading. Since these structures would be located near the end of the fjord next to the sea, they would be exposed to sea states with wind waves and swell. In particular, swells have a long period and can last for several hours with effects that decrease linearly with water depth. There are concerns that these environmental loads can parametrically excite the tethers of the mooring system, leading to parametric resonance or Mathieu instability.

a) b)

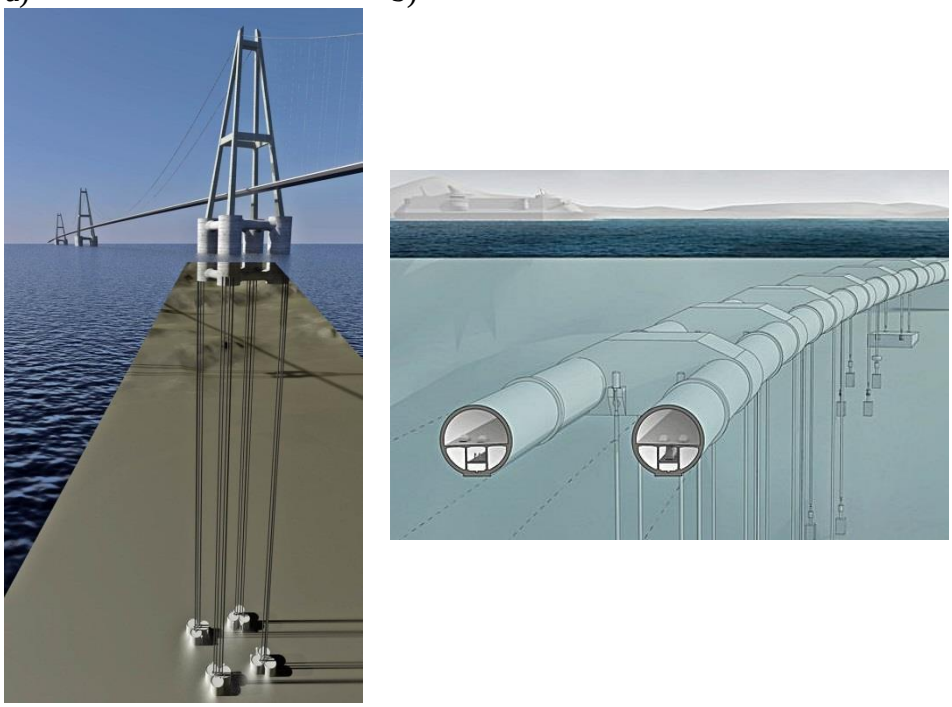

Figure 1: a) Floating cable-stayed bridge (Source: The Norwegian Public Roads Administration; https://flic.kr/p/pcgEt3); b) Submerged floating tunnel (Source: Snøhetta; https://flic.kr/p/yGeftB)

The taut mooring systems proposed in Figure 1 are similar to those used in Tension-Leg Platforms (TLP), which are usually made of steel tubes [4]. These tension pipes or tethers are designed to avoid slack cable configurations while also considering the peak and fatigue loading conditions [5]. As a result, these tethers have high pretension levels, zero net buoyancy and such massive dimensions that they cannot be considered to be compliant in the axial direction [4]. The environmental loads on the bridge towers or the submerged tunnel lead to

varying tension levels and imposed motions on the tether that define a parametrically excited system.

A tether excited by harmonically varying imposed displacements of one of its ends is a parametrically excited system. Under certain conditions, parametric excitation leads to parametric resonance, which is an unstable situation that produces excessive lateral motion. The principal parametric resonance occurs when the frequency of the upper support motion is twice the fundamental frequency of the tether, i.e., a 2:1 frequency ratio. However, there are many more frequencies that induce instability in the system. Reasonably small amplitudes of anchorage oscillations may lead to important steady-state tether responses [6, 7]. Furthermore, the greater the amplitude of the support motion is, the more frequencies there are that lead to unstable motion. Parametric excitation has been extensively studied in the field of differential equations and dynamic systems [8] and is generally described by the nonlinear Mathieu equation, where the excitation appears as time-varying coefficients. In bridge engineering, this phenomenon has been theoretically studied [6], investigated in laboratory experiments [7] and examined in cable-stayed bridges [9] where girder or mast oscillations have parametrically excited the stay cables.

Therefore, the goal of this study is to provide a clear description of parametric excitation on taut mooring lines with an emphasis on tension values; additionally, special attention is given to extreme tether tension values. Very high cable tension could produce tether breakage, while very small or no tether tension could result in a momentarily slack member, which might induce large impulse forces on the moored structure when the cable becomes a taut line again. Moreover, a better understanding of the difference between the maximum and the minimum tension will allow us to suggest appropriate design procedures with respect to the tether's fatigue life. This document also aims to clarify the relation between lateral displacement and tether tension in the event of parametric resonance.

This document starts with a clear explanation of what parametric excitation is, first illustrated for a simple 1-DOF configuration followed by a description of the phenomenon in taut mooring systems. Next, Section 3 derives the equations of motion of a cable under parametric excitation due to imposed motions at the boundary conditions and determines the analytical expression of the instability regions. The description of the numerical model used in this study in given Section 4 that consists on a full numerical model of the tether, which includes geometric and hydrodynamic nonlinear effects. Section 5 presents the results from a variety of numerical investigations that explore different aspects of the problem. Finally, the conclusions are summarized in Section 6.

2. What is parametric excitation?

2.1 Simple example of 1-DOF system

In order to understand what parametric excitation is, it is convenient to start with the simplest configuration. Assume that we have a single degree of freedom system, like the one shown in Figure 2. This system is not subjected to any external load ($F = 0$). However, the system features a time-varying parameter, in this case the spring stiffness ($k(t)$). The system's response depends on the values of that parameter, thus called parametric excitation.

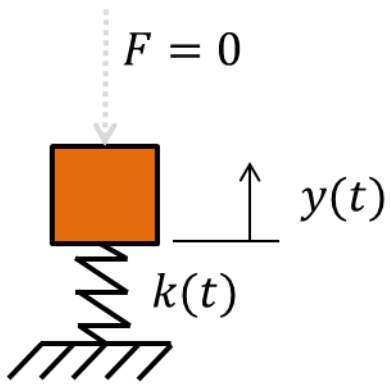

Figure 2: Model of single DOF system

The equation of motion of the system in Figure 2 is:

$$m\,\ddot{y}(t) + k(t)y(t) = 0 \qquad \text{Eq. (1)}$$

If we say that the variation of the spring stiffness is harmonic, it can be described by:

$$k(t) = k_0 + \ A\cos\,(\Omega t) \qquad \text{Eq. (2)}$$

where k_0 is the initial stiffness, A the amplitude of variation and Ω the frequency of variation. Performing the change of variable:

$$\tau = \Omega\, t \qquad \text{Eq. (3)}$$

renders the equation:

$$m\Omega^2\ddot{y}(\tau) + (k_0 + A\cos(\tau))y(\tau) = 0 \qquad \text{Eq. (4)}$$

which can be rearranged by dividing over $m\,\Omega^2$ to:

$$\ddot{y}(\tau) + \left(\frac{k_0}{m\Omega^2} + \frac{A}{m\Omega^2}\cos(\tau)\right)y(\tau) = 0 \qquad \text{Eq. (5)}$$

We know that the system frequency is:

$$\omega = \sqrt{\frac{k_0}{\mathrm{m}}} \qquad \text{Eq. (6)}$$

thus Eq. (5) can be written as:

$$\ddot{y}(\tau) + \left(\frac{\omega^2}{\Omega^2} + \frac{A}{m\Omega^2}\cos(\tau)\right)y(\tau) = 0 \qquad \text{Eq. (7)}$$

that can be expressed in the classic Mathieu equation format as:

$$\ddot{y}(\tau) + (\alpha + \beta\cos(\tau))y(\tau) = 0 \qquad \text{Eq. (8)}$$

where

$$\alpha = \frac{\omega^2}{\Omega^2} \qquad \text{Eq. (9)}$$

$$\beta = \frac{A}{m\Omega^2} \qquad \text{Eq. (10)}$$

It can be shown that for certain combinations of (α, β) pairs, the solution of the equation leads to ever-larger results. Then, it is said that the solution is unstable. This instability is called parametric resonance (PR). It is worth noting that parametric excitation (PE) is the general description of the way the system is excited, whereas parametric resonance (PR) corresponds to those situations where the system is unstable.

Therefore, when the solutions of the equation are studied for any combination of (α, β) values, some combinations render unstable results. All possible (α, β) pairs that lead to parametric resonance are grouped together in the so-called instability tongues. The separations between stable and unstable solutions in the (α, β) plane are defined by the transition curves. The following figure (Figure 3a) shows the transition curves for the classic Mathieu equation. Figure 3b shows the influence of damping on the shape of the instability tongues.

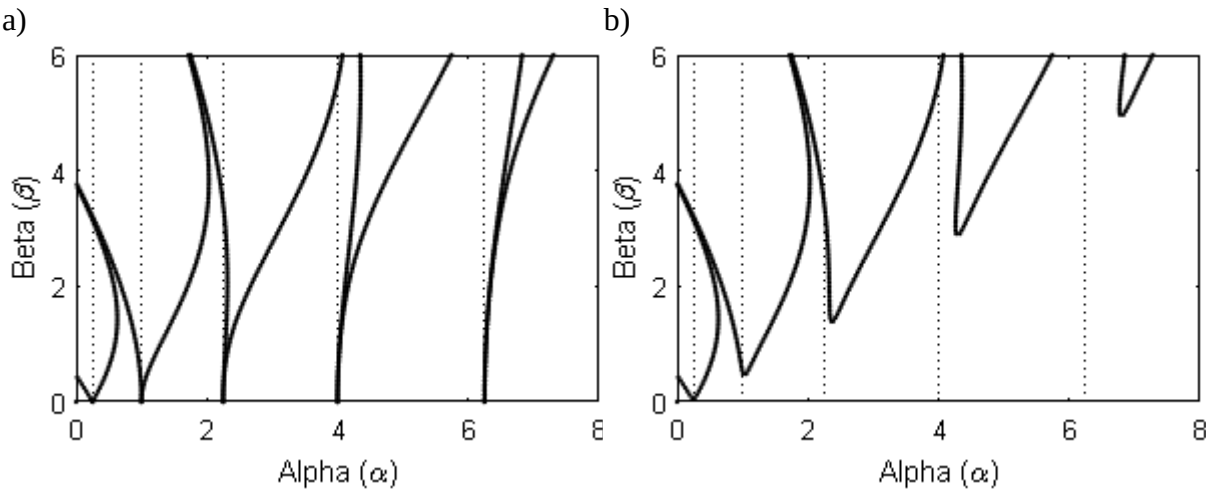

Figure 3: Transition curves; a) No damping; b) With damping

Note that Eq. (9) is a ratio that relates the fundamental frequency of the structure to the excitation frequency. This ratio α is commonly used in studies in the field of parametric excitation. Alternatively, it is possible to define the ratio between frequencies, as the relation between the excitation frequency and the fundamental frequency of the structure (Eq. (11)). The frequency ratio (FR) is thus the ratio of the excitation frequency (f) to the fundamental frequency (f_1). The principal parametric resonance tongue emanates from $FR = 2$, that corresponds to $\alpha = 0.25$ in Figure 3. The authors believe that this definition leads to a more intuitive interpretation of the results. Furthermore, this definition confines all the critical frequencies in a range from 0 to 2.

$$FR = \frac{\omega}{\Omega} = \frac{f}{f_1} \qquad \text{Eq. (11)}$$

2.2 Parametric excitation in a mooring system

The tether is a mooring system cannot be represented as a single DOF configuration. This is now a continuous structure that features (at least theoretically) an infinite number of modes of vibration. The response of such a system is therefore more complex due to the multiple modes to consider and the possible coupling between them. Furthermore, it is necessary to include the internal dissipative effects as well as the hydrodynamic contributions of the surrounding water. However, the main ideas discussed for the 1-DOF system in previous subsection, can be applied to more complex systems such as a tether, to explain parametric excitation.

A mooring system will have imposed motions on one of its ends. This will lead to variations in the axial forces inside the tether that result in a cyclic variation of the system properties. Depending on the frequency and amplitude of the imposed motion, the mooring system can reach parametric resonance and result in large lateral motions.

To better understand parametric excitation in a mooring system, the response of the tether can be illustrated using a 3D graphical representation. The time-histories of the horizontal displacement at mid-span (u_x^{mid}) and the vertical motion at the upper support (u_y^{upper}) are plotted together in Figure 4 for the 2:1 frequency ratio example. Both displacements are presented at the same scale to clearly visualize the large magnification observed during parametric resonance. Here, the colour code is proportional to the system's energy content, where blue values indicate low energy levels and red values indicate high energy levels. Figure 4 shows only the part of the response that has a rapid growth due to parametric instability. First, due to the boundary condition motion, only vertical displacements with small energy values are observed. However, as soon as the parametric resonance is triggered, the horizontal displacements quickly increase to several times greater than the imposed vertical motion. While the vertical motion ranges between ±0.1 m, the lateral displacement ranges between ±0.5 m.

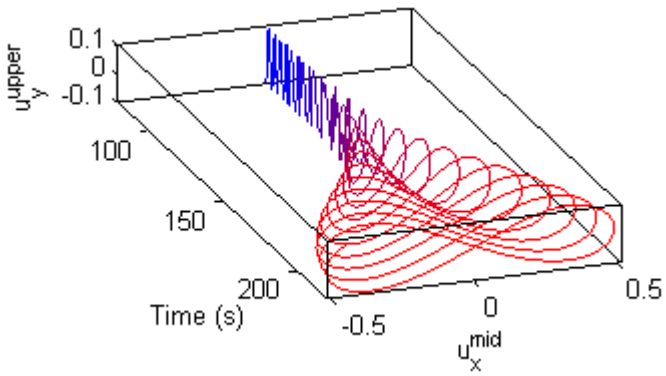

Figure 4: 3D plot of the tether response at the mid-span

The physical explanation of why the lateral displacements of the tether increase so much is illustrated in Figure 5. The figure shows several instances (A-E) of one full cycle of the tether's lateral motion. Because of the 2:1 frequency ratio, during a single cycle, the upper support moves vertically two full cycles. Every time that the tether is fully bent and is returning to its static equilibrium position (instances A, C and, E in Figure 5), the upper support is moving upwards. This positive vertical movement makes the tether move faster. For every repetition of this cycle, the imposed motion adds more energy to the system until it eventually becomes unstable. Section 2.1 shows that other frequency ratios can also lead to unstable responses, and that the instability mechanism for those cases is similar to the one presented in Figure 5.

However, the 2:1 frequency ratio provides the most intuitive example and reaches instability more quickly (requires fewer cycles); therefore, this example is generally called principal parametric resonance.

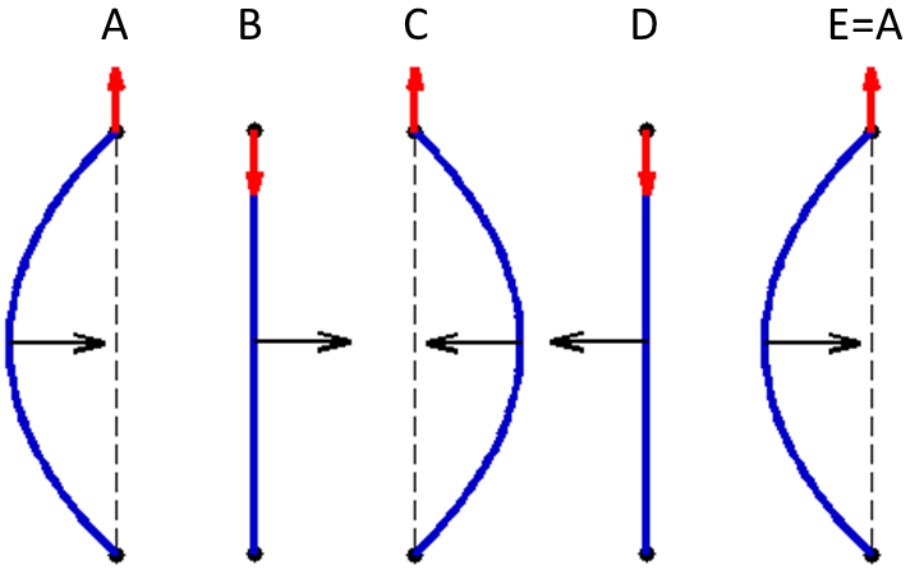

Figure 5: Multiple instances of one full cycle of tether lateral displacement for the 2:1 frequency ratio (blue lines = tether lateral deformation; black dashed lines = static equilibrium position; black horizontal arrow = direction of movement; and red vertical arrow = imposed vertical motion)

3. Analytical investigations

This section obtains the equations of motion of suspended cable under imposed motions of one of its supports. Then it derives the analytical expression of the Transition Curves (TC), which define the boundaries between stable and unstable solutions of a cable under parametric excitation. Then the expression is compared to the results obtained from a numerical model.

3.1 Equations of motion

A mooring line of an SFT can be modelled as a cable suspended between two points. The wave loading excites the submerged structure inducing oscillations on one of the cable ends. This is represented as a cyclic imposed displacement of the upper boundary condition (Figure 6a). The equation of motion can be derived considering a differential element of the cable, establishing the dynamic equilibrium and using D'Alembert's principle:

$$m\frac{\partial^2 y}{\partial t^2} + c\frac{\partial y}{\partial t} - \left(N + \Delta N(t)\right)\frac{\partial^2 y}{\partial x^2} - \Delta N(t)\frac{\partial^2 y_0}{\partial x^2} = 0 \qquad \text{Eq. (12)}$$

The equation can be solved by separation of variables, in which it is assumed that the solution is in the form of Eq. (13), where $Y_j(t)$ are the generalized coordinates and the $\Phi_j(x)$ the modes of vibration.

$$y(x,t) = \sum_{j=1}^{n} Y_j(t)\phi_j(x); \qquad \phi_j(x) = sin\left(\frac{j\pi x}{L}\right) \qquad \text{Eq. (13)}$$

The variation of the tension in the cable is proportional to the cable length increment, which is equal to the combined contribution of three terms, as seen in Eq. (14). First, the cable length increment is equal to the displacement of the boundary condition along the cable chord. For displacements perpendicular to cable chord it can be approximated using a Taylor expansion and including the terms up to second degree. Similarly, the increment in length due to the cable dynamic deformation is approximated upon Taylor expansion and discarding higher order terms.

$$\Delta N(t) = \frac{EA}{L}\left(\Delta x(t) + \frac{\Delta y(t)^2}{2L} + \sum_{j=1}^{n} \frac{j^2\pi^2 Y_j(t)^2}{4L^2}\right) \qquad \text{Eq. (14)}$$

Applying Galerkin's method [6], the partial differential equation (Eq. (12)) is transformed into a system of second order differential equations. The general case is a set of coupled Mathieu equations. However, the coupling terms are small when the relation between sag and span is small [6]. This condition can be expressed in terms of Irvine's parameter λ^2 [10] that quantifies the relative importance of elastic and geometric effects. When $\lambda^2 < 0.1$, the system of equations can be uncoupled, obtaining a second order differential equation for each mode-*j*:

$$mL^2\ddot{Y}_j + cL^2\dot{Y}_j + \frac{j^4\pi^4 EA}{4L^2} Y_j^3 + j^2\pi^2\left(N + \frac{EA\,\Delta x}{L} + \frac{EA\,\Delta y^2}{2L^2}\right) Y_j = 0 \qquad \text{Eq. (15)}$$

The support's displacement in time is assumed to be harmonic with frequency Ω and amplitude A, which can be written in terms of the cable's inclination angle α as follows:

$$\Delta x(t) = A\,sin(\alpha)\,cos(\Omega t); \qquad \Delta y(t) = A\,cos(\alpha)\,cos(\Omega t) \qquad \text{Eq. (16)}$$

3.2 Analytical solution of transition curves

Eq. (15) is the non-linear Mathieu equation where the excitation appears as time-varying coefficients [8] or parameters, thus called parametric excitation. A small parametric excitation can generate an unbounded solution (unstable solution). It is of great importance to identify when instability might occur. The boundaries that separate the stable from unstable solutions are termed Transition Curves (TC). One possibility to calculate the TC is through the Harmonic Balance Method (HBM) that essentially approximates the solution to Eq. (15) as a Fourier series (Eq. (17)). Because the phase shift is unknown, both *sin* and *cos* must be included [6].

$$Y_j(t) = \sum_{n=0}^{M} \Upsilon_{(2n-1)}\,sin(n\Omega t) + \Upsilon_{2n}\,cos(n\Omega t) \qquad \text{Eq. (17)}$$

Substituting Eq. (17) into Eq. (15), multiplying the result by the basis $\{\sin(\Omega t), \cos(\Omega t), \ldots, \sin(n\Omega t), \cos(n\Omega t)\}$, integrating over one full cycle and balancing harmonic terms gives a system of equations with the Fourier coefficients Υ_i as the unknowns. Solutions of the system provide the Fourier coefficients that define periodic solutions for Eq. (15). The transition curves are thus defined when the determinant of the coefficient matrix of the system is zero. The number of harmonic terms considered M defines the accuracy of the solution. In the literature only one term is generally considered. However, here two terms are considered ($N = 2$) because there is a significant increase in accuracy. Analytical expressions for the TC are obtained with the aid of symbolic calculation software [11]. Two separate expressions are defined in Eq. (18) and Eq. (19), corresponding to periods 2π and 4π, which correspond

respectively to the sum of all even and odd n values in Eq. (15) respectively. See the Appendix C for complete definition of the auxiliary expressions B_i and C_i.

$$A = \pm B_1 \left(2L\sqrt{B_2(B_3 \pm \sqrt{B_4})} \right) \quad for\ T = 2\pi \qquad \text{Eq. (18)}$$

$$A = \pm C_1 \left(L\sqrt{2}\sqrt{C_2 \pm \sqrt{C_3}} \right) \quad for\ T = 4\pi \qquad \text{Eq. (19)}$$

The expressions of the TC can be used to calculate the stability regions associated to any mode of vibration j. Figure 6b shows the stability chart derived from the analytical expressions for mode-j without damping.

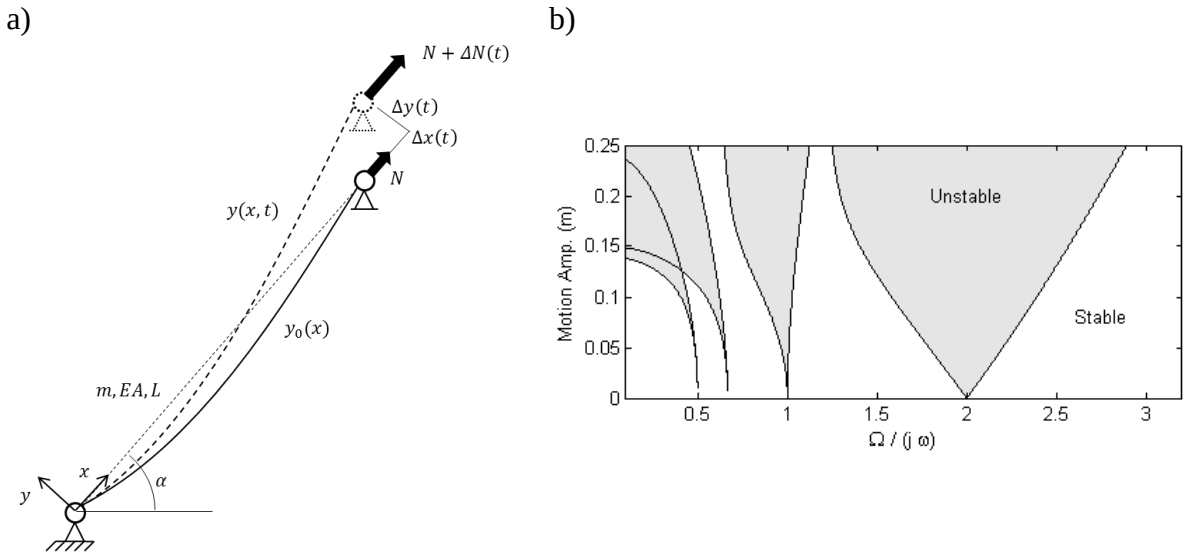

Figure 6: (a) Sketch of mooring line model; (b) Analytical stability tongues for mode-j.

4. Numerical model

Each tether of a mooring system can be modelled as a submerged beam. In addition, the wave loading on the bridge towers or the tube of the tunnel depends on the random sea state. However, due to the transfer function from wave action to structural movements, this random process leads to a narrow banded excitation of the mooring line [12, 13]. Thus, the wave-induced motion is represented as a sinusoidal imposed vertical displacement of the upper beam support. Figure 7 shows a schematic representation of the tether and its support motion. Specifically, the numerical model is developed in ABAQUS [14] using 40 beam elements (B21) including nonlinear geometric effects. Each element consists of in-plane slender beam elements with two nodes and linear interpolation that translates to two degrees of freedom per node The type and number of elements was decided based on a convergence study (not reported here) that ensured accuracy and stability of the numerical results. Since large deformations are expected in the model, equilibrium is formulated in the deformed state, i.e. considering nonlinear geometric effects. The same configuration is used throughout this study. The contribution of the hydrodynamic effects (drag and added mass) is represented by the Morison equation using the Aqua toolbox in ABAQUS. Two important parameters are necessary, namely the added mass coefficient C_A and the drag coefficient C_D. A beam of total length L is assumed to have an initial pretension T_0 and supports that are free to rotate (pin), while the upper support also follows a prescribed motion. Additionally, it is possible to model the beam

rotational stiffness (k_r) at the ends. The fundamental frequency f_1 is calculated considering the beam's self-weight and the added mass contribution of the surrounding water. The imposed cyclic motion of the upper support is defined by its amplitude A and frequency f. This numerical model is used to calculate the displacement, tension and bending moments at several points of interest along the tether's length. This analysis in ABAQUS was done with a direct numerical integration of the equations of motions, in order to correctly account for the nonlinear effects. The numerical time integration of the solution is done using a sufficiently small time step that gives a minimum sampling rate of 100Hz. For each simulated case, over 100 cycles of the support motion are considered, which is more than sufficient time to develop parametric resonance or to reach a steady state situation.

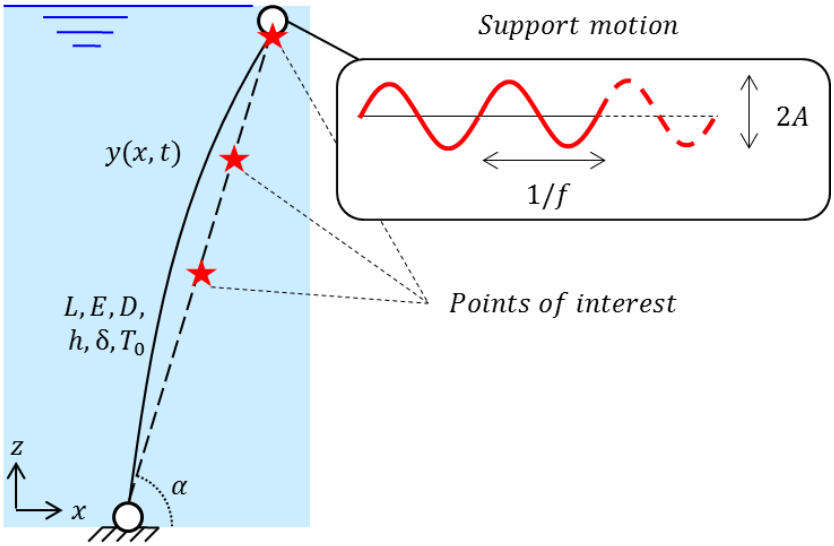

Figure 7: Sketch of tether and support motion

5. Results

This section provides an overview of some of the results obtained during the course of this project. The result represent a combination of analytical solutions and numerical results.

The particular tether properties used in this study are listed in Table 1 and are used throughout the document unless otherwise specified in the text. The values in Table 1 correspond to those suggested in the preliminary design of the mooring system for the floating bridge and submerged tunnel of the Bjørnafjord crossing, which is part of the "Ferry-free E39" project [1]. Moreover, similar tether dimensions and pretensions can be found in [15, 16, 17]. To correctly account for the hydrodynamic effects, two important parameters are needed, namely, the added mass coefficient C_A and the drag coefficient C_D. The numerical values of these coefficients are listed in Table 1 and they are taken from the recommendations in [18]. Furthermore, a small internal damping of only 0.1% is assumed to avoid any spurious numerical effects. Mooring system damping is difficult to assess precisely [19], but a higher internal damping can be expected. Therefore, the results presented here can be considered conservative. In the numerical simulation, 120 loading cycles of the upper support motion are computed for every simulated case presented here; this is more than sufficient for developing parametric resonance and/or reaching a steady-state situation. The numerical time integration of the solution is performed using a sufficiently small time step that gives a minimum sampling rate of 100 Hz. The numerical stability and accuracy of the solution was assessed in a preliminary convergence study that is not shown here.

Table 1: Tether properties

Description	Symbol	Value	Unit
Length	L	400	m
Young's modulus	E	$2.1 \cdot 10^{11}$	N/m^2
Diameter	D	1.119	m
Thickness	h	38	mm
Density	δ	7800	kg/m^3
Initial pretension	T_0	$18.5 \cdot 10^6$	N
Inclination angle	α	90	degrees
Fundamental frequency	f_1	0.1299	Hz
2nd frequency	f_2	0.2648	Hz
3rd frequency	f_3	0.4096	Hz
Added mass coefficient	C_A	1	-
Drag coefficient	C_D	1.5	-

5.1 System frequency vs. Excitation frequency

This section performs a preliminary evaluation of the possibilities of Parametric Resonance (PR) actually occurring in a tether with the dimensions given in Table 1. This can easily be done by comparing the fundamental frequency of the mooring system to the possible excitation frequency due to swell. According to [20] the wind waves and swell have periods as listed in Table 2.

Table 2: Range of loading periods *T* according to [20].

wind sea	4-7s
primary swell	12-20s
secondary swell	6-10s

Parametric resonance can occur in a wide range of frequencies. However, for simplicity only two situations will be considered below, namely for Frequency Ratios (FR) 1 and 2. Frequency Ratio is defined as the ratio of the excitation frequency (f_e) to the fundamental frequency of the tether (f_1) as seen in Eq. (20).

$$FR = \frac{loading\ frequency}{fundamental\ frequency} = \frac{f_e}{f_1} \qquad \text{Eq. (20)}$$

Once parametric resonance has been reached the levels of lateral tether motions are similar in magnitude regardless the FR. However, to reach parametric resonance the minimum amplitude of the excitation and/or the minimum excitation time needed changes drastically with FR. The case of $FR = 2$ is called the principal parametric resonance, which is the most likely resonance since the minimum amplitude and duration of excitation required is the smallest. The next likely occurrence might be for $FR = 1$, however the possibility of this occurring are greatly reduced. Other parametric resonant situations are possible but very unlikely and therefore not considered here.

The results show the fundamental frequency of tethers with different lengths (from 40 m to 480 m) in Figure 8. Superimposed are the possible parametric resonance frequency ranges for

FR = 1 or 2. The two different figures correspond to primary swell (Figure 8a) and secondary swell (Figure 8b).

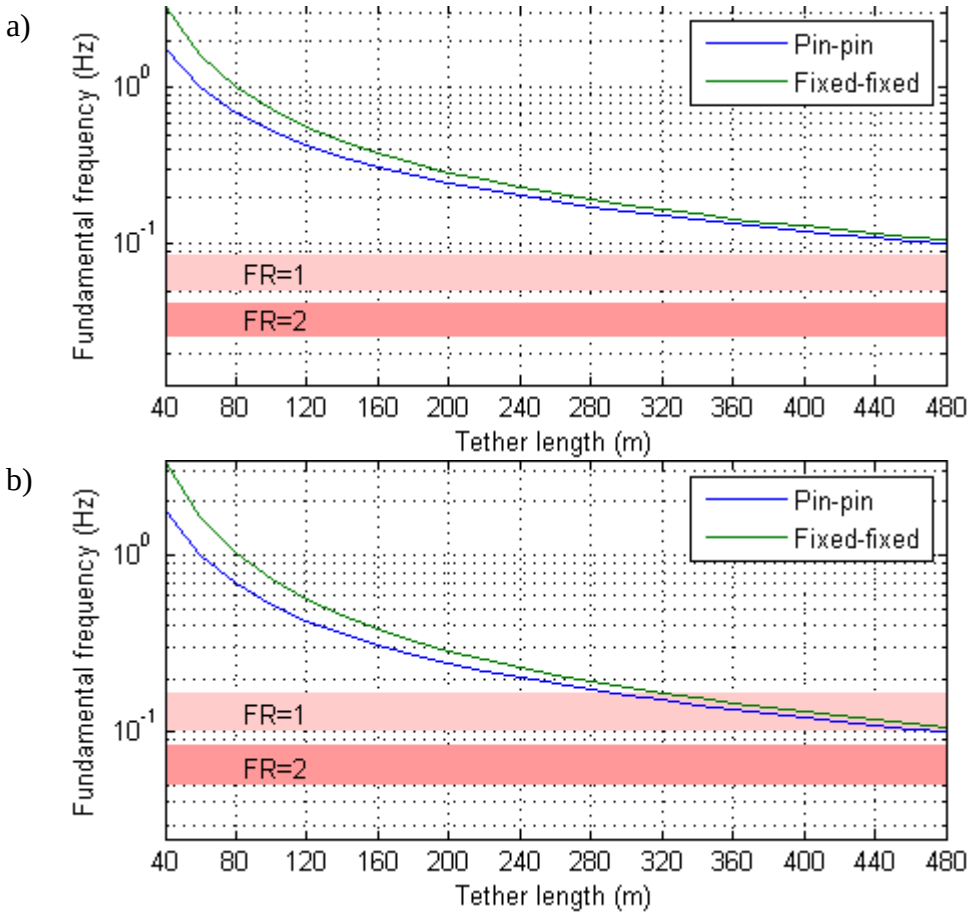

Figure 8: Tether fundamental frequencies and parametric resonance areas for a) Primary swell; b) secondary swell

The results show that there is a possibility of PR only for the longest cables (>300 m) with a FR=1 resonance due to secondary swell waves. In order to have tethers that might be closer to parametric resonance ranges one of the following must happen:

- Lower pretension values
- Longer tethers
- Thicker pipes (more massive elements)
- Effect of marine growth. This effect not only adds mass to the tether reducing its fundamental frequency, but also increases the cross-section increasing and displacing more water, thus increasing the added mass.

5.1.1 Study of pretension

Now we consider the particular case of a 400 m long tether, which is roughly the most common tether length for the Bjørnafjorden project. Decreasing its pretension will decrease the fundamental frequency and thus getting closer to unstable situations.

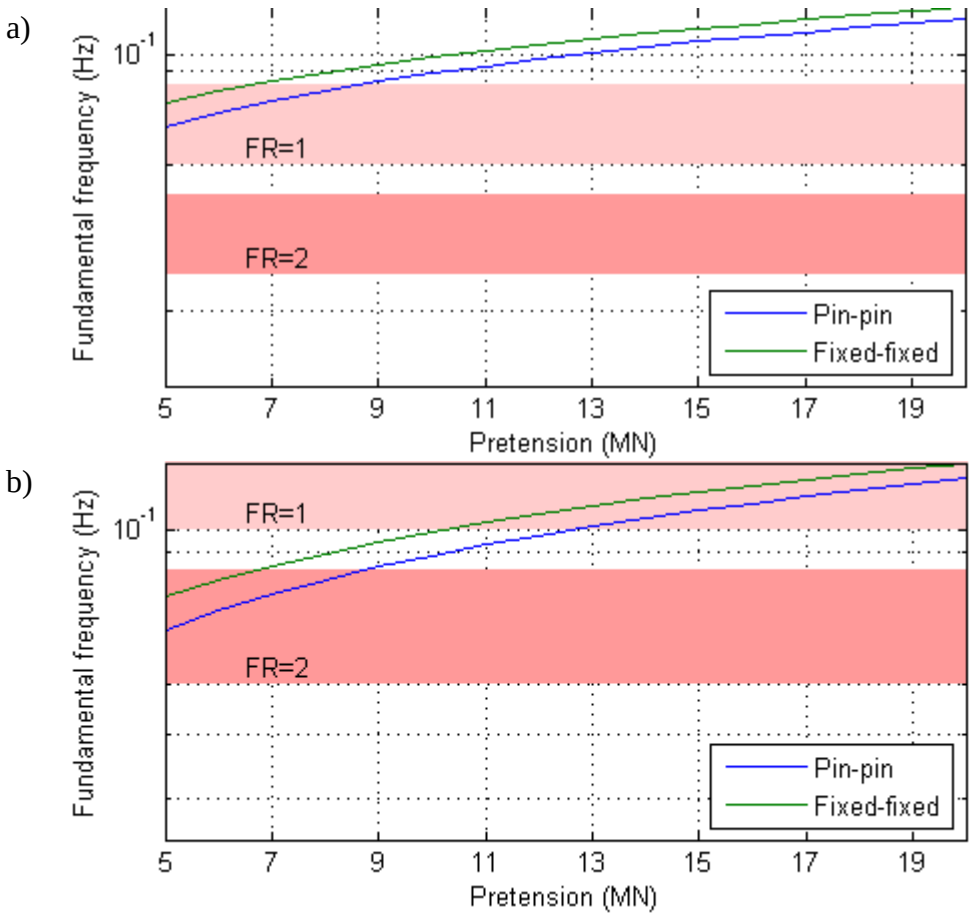

Figure 9: Tether (400 m) fundamental frequencies and parametric resonance areas for a) Primary swell; b) secondary swell

It is also well-known fact that decreasing tension increases the instability areas. This means that a wider range of excitation frequencies can induce parametric resonance.

Additionally, the smaller the pretension the smaller is the allowed vertical displacement. The, main design criteria for the tethers is to avoid any slack situation during its lifetime. The floating structure will have vertical motions that will be imposed as vertical support motions on the tethers. If the tethers have only small pretension, all the tension might disappear having a slack cable even for a small vertical displacement. Figure 10 shows the maximum vertical displacement that would be allowed for each of the range of pretension values studied for the 400 m long tether.

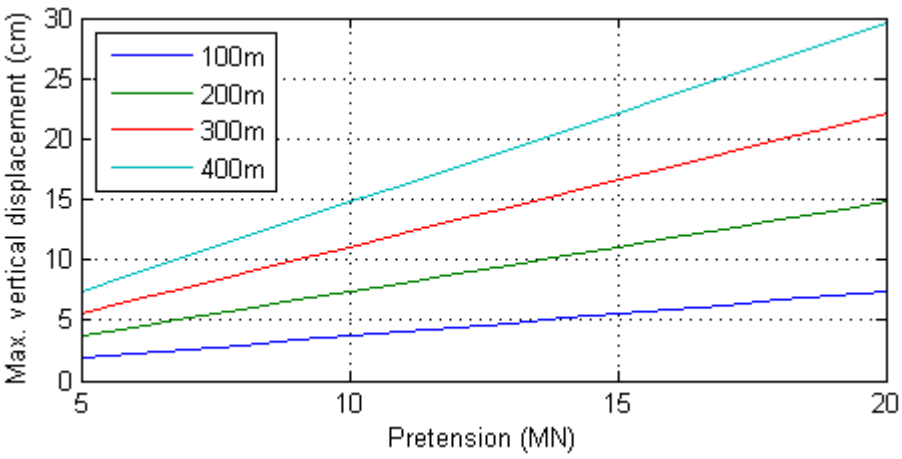

Figure 10: Maximum vertical displacement allowed to avoid a slack tether

5.1.2 Marine Growth

Over time, the tether will have marine growth attached to its surface. The amount of marine growth depends on its depth, but mainly concentrating near the sea surface and seabed. The influence of marine growth is predicted to be minor in [21]. However, the influence of marine growth on the fundamental frequency of the tethers is assessed below.

Following assumptions considered:

- The density of marine growth is 1300 kg/m^3
- The thickness of marine growth is 5 cm. Note that this is a significant overestimation of the marine growth expected along the tether (See [21])

The marine growth has been considered in the calculations as:

- Added non-structural mass along the beam element
- Increased buoyancy load
- Increased effective beam radius for the added mass calculation in the eigenvalue analysis

The new results are given in Figure 11. Compared to Figure 8 there are almost no differences. This confirms that the marine growth can be neglected in the calculations of the dynamic response of the tethers.

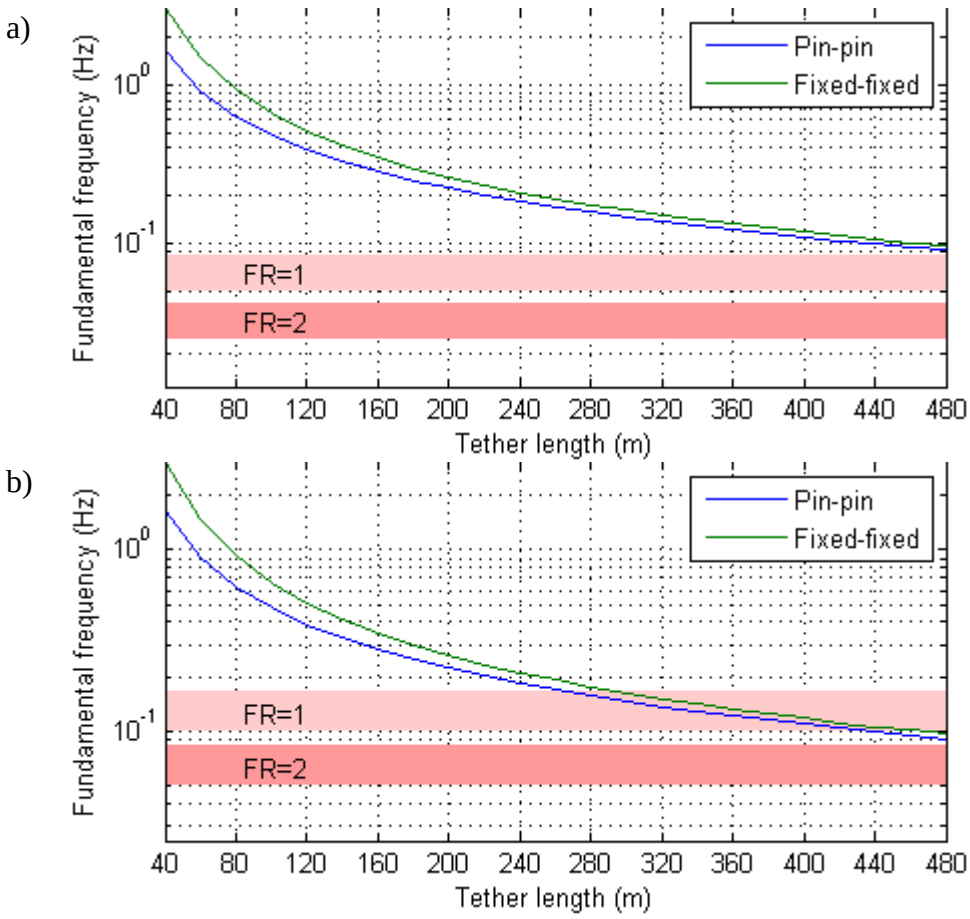

Figure 11: Tether fundamental frequencies and parametric resonance areas for a) Primary swell; b) secondary swell

Already the results presented in this Section 5.1 indicate that the possibilities of achieving parametric resonance are low. This is particularly true due to the particular tether lengths and the levels of prestressing to be used at the Bjørnafjorden crossing. However, it is still a possibility. Therefore, it is important to investigate further the possible parametric resonance scenario and its structural effect on a mooring system .

5.2 Influence of hydrodynamic effects

The response of a submerged tether differs significantly to that of a dry tether because of the influence of hydrodynamic drag, which is the most important nonlinear contribution [22] and acts as an additional damping component. Moreover, it has been shown [23, 24] that the out-of-plane motion can be neglected when calculating the response of submerged slender structures. For a tether in an unstable condition, the quadratic fluid damping force limits the amplitude of the lateral motion [25]. An example of instability analysis for TLP tethers is given in [26]. Reference [27] derives an approximate analytical expression of tether displacements including hydrodynamic effects for principal parametric resonance. Additional literature reviews of the instabilities of risers and immersed slender structures can be found in [28, 29].

5.2.1 Dry tether

A tether modelled as a linear system and parametrically excited at a critical frequency has an unbounded solution. The result is the classic parametric resonance of the linear Mathieu

equation featuring exponential growth. In a truly linear system, the amplitude increases until the system is destroyed [8]. However, real physical systems do not exhibit unbounded responses. By including the nonlinear effects, a more realistic model is obtained. During parametric resonance, the nonlinearities limit the oscillation amplitudes. Therefore, the tether is modelled to include nonlinear geometric effects. Figure 12a shows the time-history of the mid-span lateral displacements, which exhibit exponential growth over time until a certain maximum (or minimum) value is reached. Then, the displacements decay and repeat the exponential growth again. For this particular example, the maximum displacement is 4.47 m, while the amplitude of the upper support motion is only 0.10 m. This beating-like behaviour during parametric resonance is also reported in [6, 27, 30].

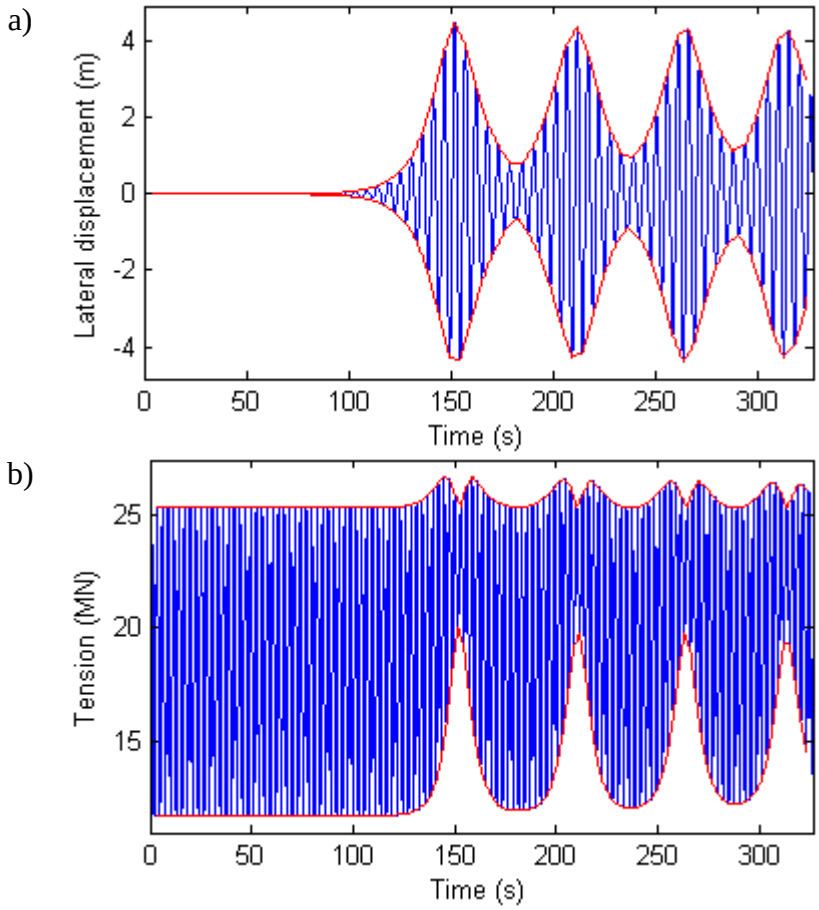

Figure 12: Dry tether response at the mid-span for a 2:1 frequency ratio: a) Horizontal displacement; b) Total tension (red lines = outer envelopes to response)

Intuition suggests that the internal tether tension should have a similar evolution over time or should at least feature some extreme values at the same times as those reported for the displacements in Figure 12a; however, this is not the case. Figure 12b shows the time-history of the total tension at the upper support. Before instability is triggered, the tension values oscillate according to the imposed motion of the support. After parametric resonance has started, both the maximum tension values and the minimum tension values increase. Moreover, the difference between the tension extremes is lowest exactly when the maximum displacements occur. This counterintuitive behaviour of the tension was also reported in [6] and explained as the synchronous compensation of the tension oscillations by the support motions.

5.2.2 Submerged tether

However, the hydrodynamic effects are the greatest contributors to the damping of the system. Parametric resonance of the submerged tether can still occur, but the displacement and tension responses differ significantly. The time-history response of the lateral displacement is given in Figure 13a, which also includes the hydrodynamic effects. The figure shows that the lateral displacement of the tether starts to increase rapidly after 100 s of excitation and reaches steady-state conditions after 220 s. This increase is mainly limited by the dissipative effects of the hydrodynamic contributions. The extreme lateral displacement values at mid-span are indicated by the labels $u_{x,max}^{mid}$ and $u_{x,min}^{mid}$. For reference, the figure shows the amplitude of the vertical motion (±0.1 m) of the upper support in dashed black lines; in addition, the envelopes of the time series are indicated with a solid red line. Parametric resonance plays an important role in the rapid growth. However, compared to the dry tether example (Section 5.2.1), the extreme displacements only reach 0.55 m, and more interestingly, no beating phenomenon is observed. These differences between dry tether (Figure 12a) and submerged tether (Figure 13a) can only be attributed to the additional damping of the hydrodynamic effects.

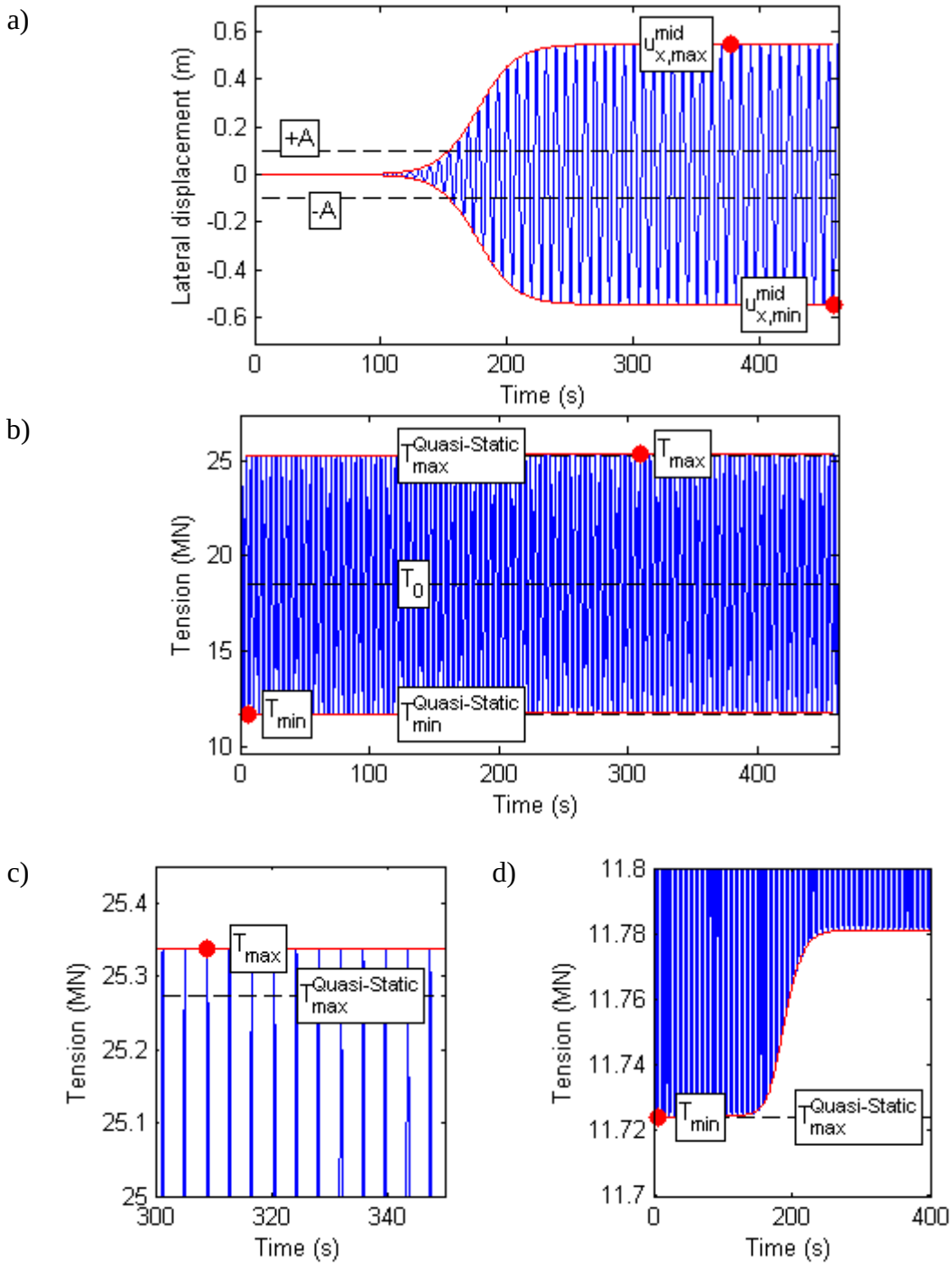

Figure 13: Submerged tether response at the mid-span for a 2:1 frequency ratio: a) Horizontal displacement; b) Total tension; c) Zoomed view near T_{max}; d) Zoomed view near T_{min} (red lines = outer envelopes to response)

Figure 13b presents the total tension of the submerged tether at the mid-span; this figure shows that the tension values are barely affected by the parametric resonance. For reference, the initial tether tension T_0 is indicated in the figure. The horizontal dashed black lines labelled $T_{max}^{Quasi-Static}$ and $T_{min}^{Quasi-Static}$ reveal the extreme quasi-static tension values expected due to the imposed cyclic motion ($A = 0.1\ m$). While the system response is stable ($t < 100\ s$), the tension values oscillate following the expected quasi-static response due to the imposed motion. However, when parametric resonance starts, only a small change can be observed. Then, the maximum tension values slowly increase to T_{max}, which is only slightly greater

than $T_{max}^{Quasi-Static}$ (Figure 13c). On the other hand, the minimum tension value T_{min} occurs at the beginning of the time series because the minimum tension values actually increase over time, even if only marginally (Figure 13d). Therefore, the effect of parametric excitation on the dynamic tension is very small. This result is somewhat counterintuitive: a situation that has large lateral motion (Figure 13a) features only very small dynamic tension effects (Figure 13b). This can be explained analysing the lateral displacement response. Even though the parametric resonance has been triggered, the steady-state response features constant amplitude due to the energy dissipation effects of the hydrodynamic contribution. In addition, this amplitude is an order of magnitude smaller for the submerged tether (Figure 13a), compared to the dry example in Figure 12a. These smaller and stationary lateral motions are not big enough to induce significant changes in the tension variation compared to the quasi-static response (Figure 13b).

5.3 Numerical validation of analytical expressions

The expressions derived in Section 3 allow us to identify situations that would produce large displacements in the mooring line due to harmonic movements of one of the boundary conditions. However, the analytical expression is only an approximation that needs to be compared against a numerical solution of the problem at hand. Therefore, a mooring line was modelled with ABAQUS [14] considering geometric nonlinearities. The cable is submerged in water and is thus influenced by drag forces and additional mass effects. These effects have been included by means of the Morison Equation using the toolbox AQUA provided by the software. Two important parameters are necessary, namely the added mass coefficient C_A and the drag coefficient C_D whose numerical values are 1 and 1.5 respectively as recommended in [18]. The particular cable properties used in this study are provided in Table 1.

The analytical expression derived in Section 3.2 is compared against the numerical solution in Figure 14. In order to find the analytical stability map for our model it is necessary to consider the contribution of several modes. This can be achieved by superimposing as many modes as deemed necessary. Figure 14 shows the stability chart for the particular cable defined in Table 1 considering 3 modes and 5% damping. The formulation allows us to easily include the contribution of higher modes of vibration. In particular it is important to include the first and second instability regions of each mode. The numerical stability map is obtained analyzing the results from 1320 separate simulations for a range of excitation frequencies and amplitudes. In particular, the ratio f/f_1 is varied in a discrete space with values from 0.25 to 3.5 in increments of 0.05, whereas the considered amplitudes are from 0.005m to 0.2m in 0.005m increments.

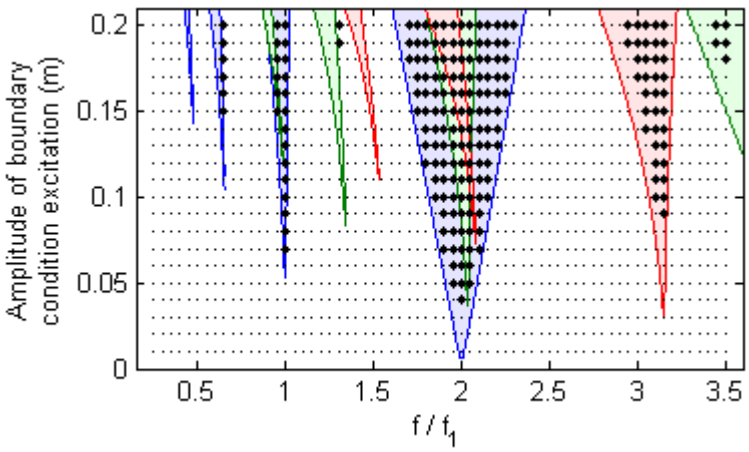

Figure 14: Instability map for numerical results (stable = small dot, unstable = large dot) and theoretical instability tongues (see Appendix C) associated to tether's 1st mode (Blue), 2nd mode (Green) and 3rd (Red) mode;

Figure 14 shows the instability diagram based on the lateral displacement of the tether at the mid-span. Each of the studied f/f_1 and A combinations is represented as a dot. If the particular case renders a stable solution, it is depicted as a small black dot; when the combination leads to an unstable result, it is represented by a larger dot. As expected, the results clearly feature distinct areas with parametric resonance, which are usually called instability tongues. The biggest tongue emanates from the 2:1 frequency ratio and corresponds to the principal parametric resonance. In addition, several other tongues correspond to other frequency ratios, higher vibration modes and/or a combination of harmonics. Figure 14 also shows the theoretical tongues associated to the Mathieu equation. These theoretical instability regions are drawn based on the analytical expressions reported in Section 3. These analytical expressions derive from the theoretical analysis of a taut simply supported cable using the harmonic balance method considering two harmonic terms. The direct comparison of the numerical and theoretical instability regions shows a good agreement.

5.4 Extreme tension values

The majority of the publications that have studied the parametric excitation of cables (either dry or submerged) mainly focus on lateral motion. As indicated in [31], tension has been overlooked in many studies. However, displacement is not the most important load effect. In fact, tension and stress values are of greater relevance when designing a taut mooring line. Some publications have specifically investigated tension to some extent. For example, reference [6] numerically shows how tension values develop on a dry cable during parametric excitation. In addition, [32] studies numerically tension using an experimentally validated model, while [31] shows that to achieve correct tension values, the model must account for spatiotemporal variations of tension along the cable. Moreover, [30] shows that the difference in magnitude (in spatial distribution) between the maximum and minimum tensions increases for a cable with significant sag. Furthermore, [33] concludes that the increase in pretension is ultimately equivalent to the increase in damping. In addition, [34] includes tension in the numerical analysis and states the need for understanding the impacts of parametric excitation. In [24], the dynamic tension values are measured for a submerged cable with sag in a scaled laboratory experiment, and recommendations are provided for the scaling and the support's boundary conditions. Other examples in the literature study the cable tension, but they do not consider the particular case of parametric excitation. For instance, [35] derives an approximate analytical expression of dynamic cable tension, and [13] obtains an analytical approximation

of the probability distribution of the dynamic tension envelope for a random sea state. Therefore, even though some investigations have considered tether tension, additional studies are needed to characterize parametrically excited taut mooring systems.

Figure 14 is the standard stability map, which is also called a Strut diagram. This map allows us to clearly identify the instability regions of the problem. However, it is difficult to assess the relative importance of each of the tongues. In theory, for infinitely long excitations, all unstable cases will reach steady-state and similar extreme displacement values. However, in practice, it is interesting to examine the maximum displacements achieved during parametric resonance for a finite duration of excitation. Figure 15 shows the maximum lateral displacements normalized by the amplitude of the support motion. In all the simulated cases, the excitation lasted for 120 cycles. The results clearly show that the 2:1 frequency ratio tongue has the highest values, indicating a quicker instability and confirming its importance compared to the other tongues.

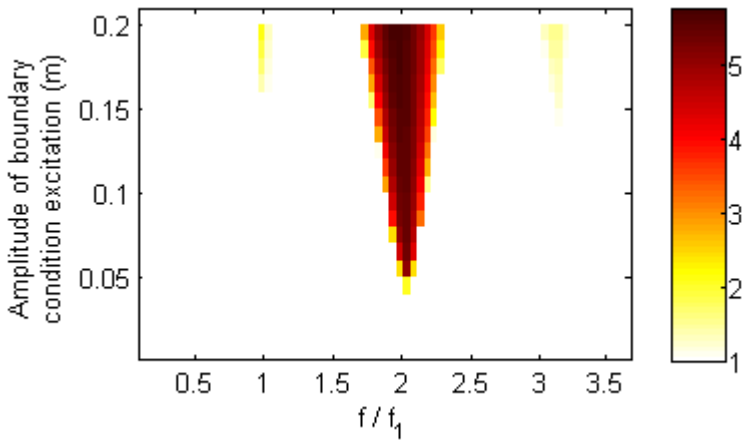

Figure 15: Normalized lateral displacement values

To characterize the effects of parametric resonance on the total tension values of the tether, it is necessary to quantify both extremes, i.e., maximum and minimum tension values, which are convenient to analyse in terms of dynamic factors. Here, we introduce the Dynamic Amplification Factor (*DAF*) and the Dynamic Reduction Factor (*DRF*), which are defined in Eq. (21) and Eq. (22) respectively using the notation presented in Figure 15. In essence, these factors are the normalizations of the dynamic tension increments with respect to the quasi-static tension increments due to the imposed upper support motions. For the particular case shown in Figure 15, *DAF* is 1.0094, which means that the quasi-static increment $\Delta T_{max}^{Quasi-Static}$ has to be increased by only 0.94% to account for the dynamic effects. On the other hand, *DRF* is 0.9923, which is equivalent to decreasing $\Delta T_{min}^{Quasi-Static}$ by 0.77%. Values of *DRF* that are less than one indicate that the total minimum tension is larger than the quasi-static minimum, as shown in Figure 15.

$$DAF = \frac{\Delta T_{max}}{\Delta T_{max}^{Quasi-Static}} = \frac{T_{max} - T_0}{T_{max}^{Quasi-Static} - T_0} \qquad \text{Eq. (21)}$$

$$DRF = \frac{\Delta T_{min}}{\Delta T_{min}^{Quasi-Static}} = \frac{T_{min} - T_0}{T_{min}^{Quasi-Static} - T_0} \qquad \text{Eq. (22)}$$

The effect of tether instability is evaluated in Figure 16 for the extreme tension values in terms of the dynamic factors *DAF* and *DRF*. There is a clear correlation between the instability tongues shown in Figure 14 and the results in Figure 16. However, the actual numerical values of the factors are remarkably small. In the case of *DAF* in Figure 16a, the overall maximum value is 1.019, meaning that the maximum total tension (static + dynamic) is only 1.9% greater than that in the static case. The results in Figure 16b show that the minimum tension in the tether is either equal to or slightly less than the minimum static tension. In particular, the absolute minimum *DRF* value is 0.977, which corresponds to a 2.3% decrease in the static tension.

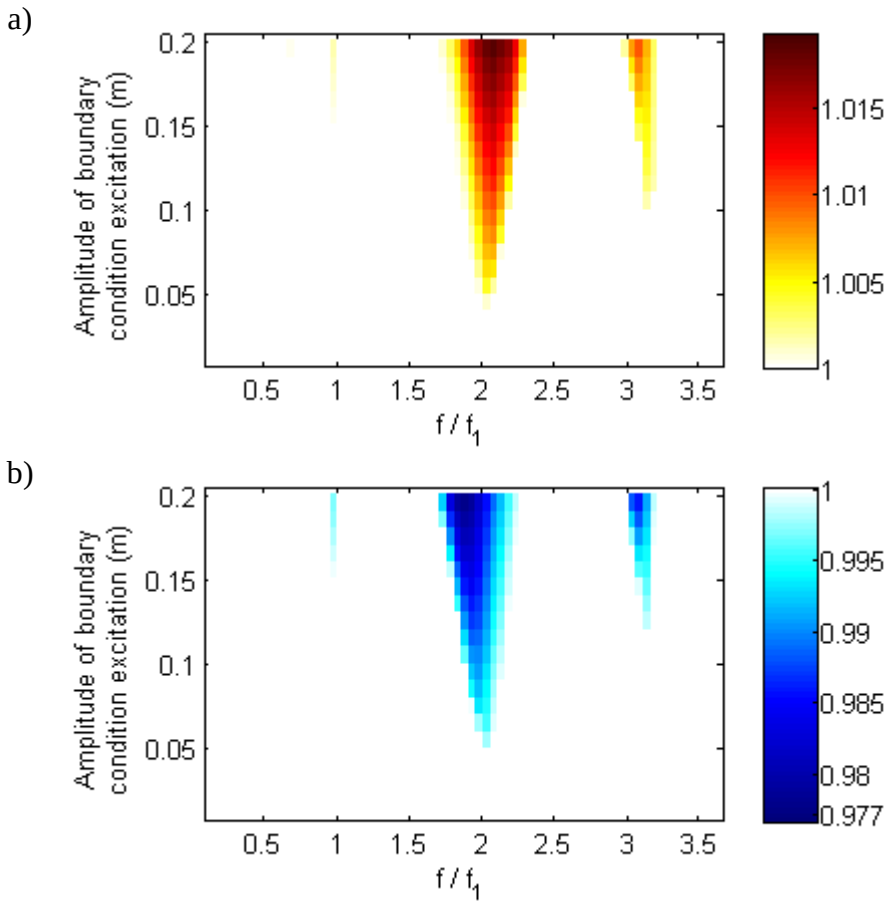

Figure 16: Tension dynamic factors: a) *DAF*; b) *DRF*

The main conclusion drawn from the results in Figure 16 is that the dynamic tension contribution during parametric resonance is very small. It is also interesting to note that outside of the instability tongues, the dynamic factors are virtually equal to one. In other words, the total tension during stable conditions is the same as the total tension due to quasi-static loading. Therefore, if the design of a tether is based on a maximum displacement criterion, the results in Figure 15 suggest that any possibility of parametric resonance should be avoided. However, in reality, a tether is designed with respect to the maximum stress levels. According to the results in Figure 16, the extreme tension levels are either close to or identical to the tension based on a quasi-static response, indicating that the dynamic effects of parametric resonance are very small. Furthermore, this conclusion can be refined when directly exploring the consequences on fatigue calculations.

5.5 Fatigue calculations

Correct tether design should include the fatigue limit state [16] to avoid failure due to crack growth initiated from a welded joint in the tether. Detailed fatigue design recommendations can be found in [36]. The magnitude of the stress cycle and the number of load cycles are the key parameters that determine the accumulated fatigue damage of the studied member. However, based on the studies published to date, it is not possible to assess correctly the stress values of a taut mooring line with parametric resonance or its effects on the tether's fatigue life. The total stress in a tether is the combined result of several load effects, namely the axial load, bending moments and hydrostatic pressures. In most parts of the tether's length, the main contributor to the stress is the total (static + dynamic) tension, whereas bending moment has only a marginal effect [16]. On the other hand, bending moments can be very important near the tether ends and is further investigated in Section 5.9.

This section evaluates the effect of parametric excitation on the fatigue life calculations of tethers by introducing a new factor that facilities this analysis. The main parameter in any fatigue calculation is the stress range *S*; this range is directly proportional to the tension increment ΔT, which can be written as:

$$\Delta T = T_{max} - T_{min} \qquad \text{Eq. (23)}$$

Using the definitions of *DAF* and *DRF* given in Eq. (21) and Eq. (22):

$$\Delta T = DAF \cdot \Delta T_{max}^{Quasi-Static} - DRF \cdot \Delta T_{min}^{Quasi-Static} \qquad \text{Eq. (24)}$$

In the case of taut tethers, it can generally be assumed that the static tension increment (ΔT_{max}^{Static}) due to positive vertical displacement of the support is of the same magnitude but opposite sign as the static tension increment (ΔT_{min}^{Static}) due to lowering the support motion. Thus, representing both tension increments as $\frac{1}{2}\Delta T^{Static}$, we can rewrite expression Eq. (24) as:

$$\Delta T = \frac{(DAF + DRF)}{2} \cdot \Delta T^{Quasi-Static} = DF \cdot \Delta T^{Quasi-Static} \qquad \text{Eq. (25)}$$

Eq. (25) introduces the Dynamic Factor (*DF*) and can be used to easily determine the total tension increment (including static and dynamic effects) by simply factoring the tension increment obtained from quasi-static analysis. Moreover, *DF* is the average of the *DAF* and *DRF* values. Figure 17 gives the numerical values of this new factor for the same frequency ratios and amplitudes studied in the previous subsections. Similarly, the results show the presence of multiple instability tongues, and the tongue emerging near the 2:1 frequency ratio shows the highest values. In particular, the maximum value in Figure 17 is 1.006, and the minimum value is 0.987, which are equivalent to 0.6% and -1.3% changes in the tension increment, respectively. The *DF* values for a given critical frequency ratio (say 2:1) may be either negative or positive depending on its excitation frequency with respect to the centre of the corresponding instability tongue. Therefore, the stress range *S* obtained from a quasi-static analysis should be decreased or increased, effectively increasing or decreasing the calculated fatigue life of the member, respectively. However, the *DF* values are very small regardless of their sign, which supports the assertion that it is safe to perform only quasi-static simulations

for the fatigue calculations of a tether. Even if parametric resonance occurs, the dynamic effects on tension are sufficiently small to be covered by the general safety factors of the design process.

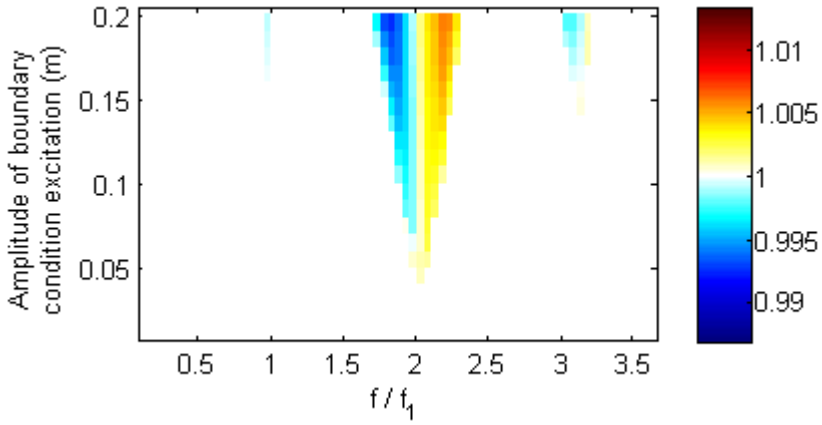

Figure 17: Tension Dynamic Factor (*DF*)

5.6 Influence of pretension

The influence of pretension is first evaluated in terms of the normalized mid-span tether displacement in Figure 18a, which clearly shows a decrease with increasing pretension. That is, the system's stability increases with increasing pretension. This fact is also shown as an increase in the number of cycles needed to trigger parametric resonance, as plotted in Figure 18b. Similarly, the dynamic factors that quantify extreme tension increments (*DAF* for maximum and *DRF* for minimum) also decrease with increasing pretension. Nevertheless, the numerical values of these factors are still quite small. Even for the lowest pretension level, tension increases of less than ±3% need to be accounted for. For the *DF* values, the dynamic factor for fatigue calculations remains constant and very close to one, which confirms that the quasi-static calculation is sufficient for any of the considered pretension levels.

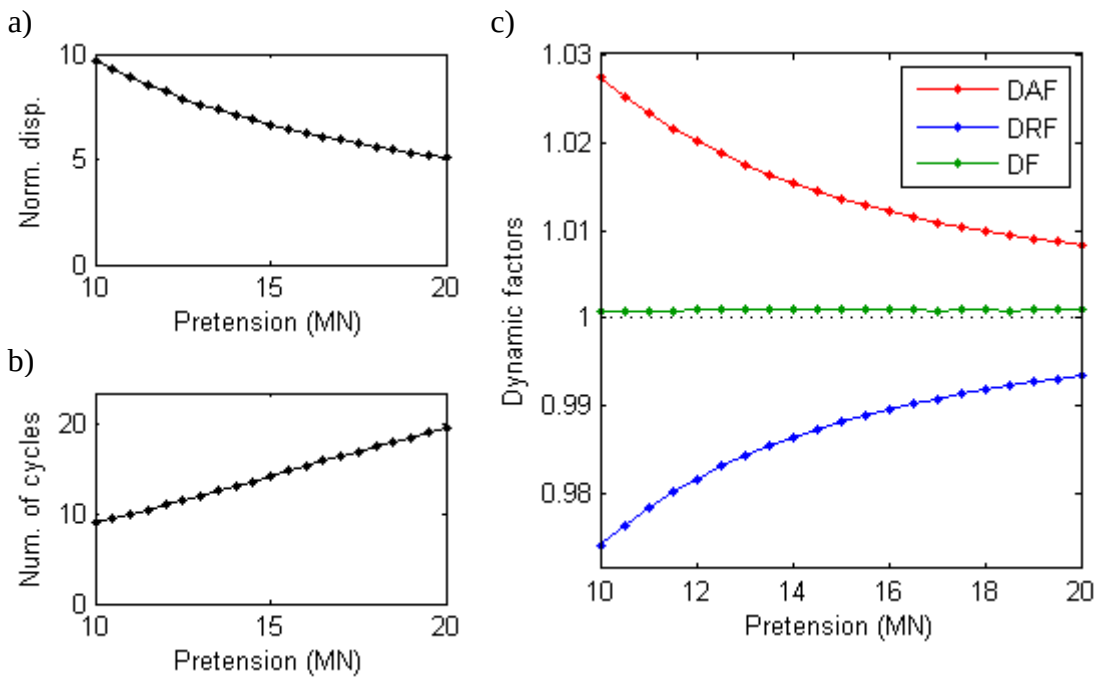

Figure 18: Influence of pretension: a) Normalized lateral displacement at mid-span; b) Number of cycles to initiate parametric resonance; c) Dynamic factors

5.7 Influence of tether length

The length of the tether clearly depends on the depth of the seabed. The distance between the floating construction (either bridge tower or submerged tunnel) and the anchoring point of the mooring line varies significantly along the length of the structure. This study evaluates the influence of parametric resonance on tethers with different lengths. All the cases are simulated for a support motion with the same amplitude of 0.1 m. Thus, the extreme static tension values are greater for shorter tether lengths (Figure 19a) because the elastic stiffness of the system is inversely proportional to the length. In other words, shorter tethers are stiffer and lead to greater tension values for the same imposed support motion. As a result, the higher quasi-static tension oscillations observed in shorter tethers lead to instabilities with larger lateral displacements, as shown in Figure 19b. Similarly, the extreme total tension values also increase (or decrease) for shorter tethers (Figure 19c). However, as observed throughout this project, these dynamic factors are remarkably small. In this case, only ±5% tension variations are expected for the shortest mooring line. Nevertheless, the dynamic factor for fatigue *DF* remains nearly constant and can be approximated as equal to one.

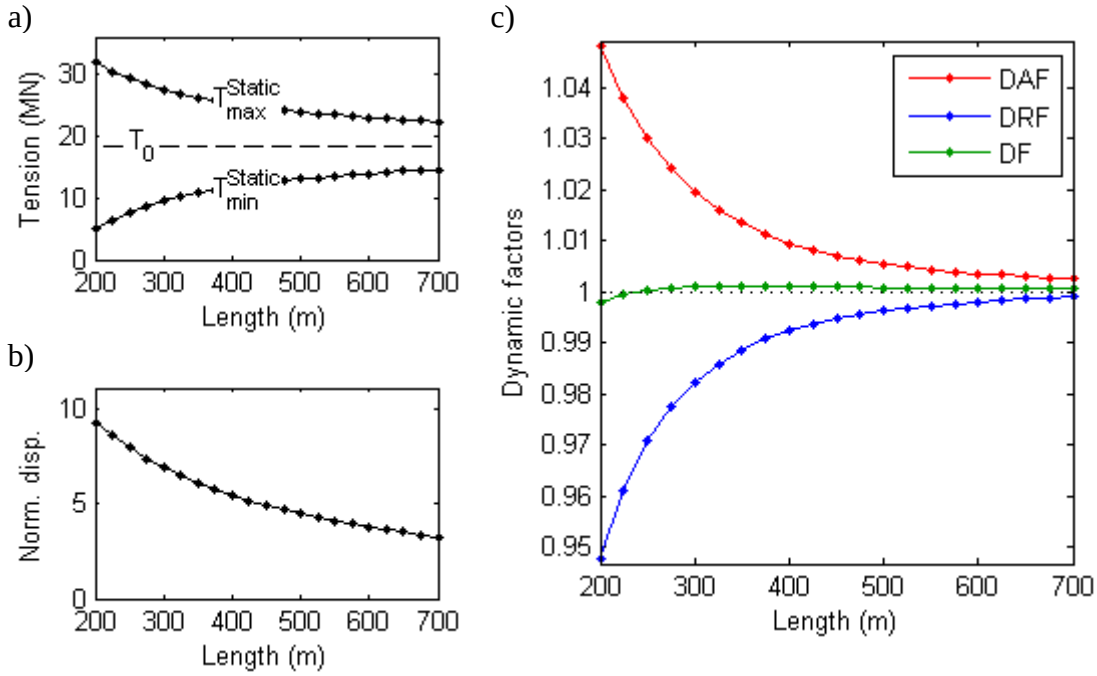

Figure 19: Influence of tether length: a) Static tension values; b) Normalized lateral displacement at mid-span; c) Dynamic factors

5.8 Influence of inclination angle

A vertical mooring system such as the one investigated in this study so far imposes little or no restraint in the horizontal plane. Therefore, large lateral motions could be induced if the floating structure is too flexible or the lateral loading is sufficiently strong. One possibility for providing additional lateral stiffness is to include pairs of inclined mooring lines in opposite configurations. This study assesses the impact of the tether inclination angle on the system's stability. According to the model definitions in Section 4, an angle of 90° corresponds to a vertical mooring line. Figure 20a shows the tether response in terms of the normalized horizontal displacement. Smaller angles are shown to give a stable response, while angles closer to vertical feature instability. This finding is supported by the results in Figure 20b that show the number of cycles needed to trigger parametric resonance. For configurations with small inclination angles, no results are shown because the parametric resonance is not triggered. In general, stability increases with a decreasing inclination angle; this can be explained by the combination of two effects. First, the actual tether length increases at smaller angles, which leads to greater system stability, as shown in Section 5.7. Second, the imposed vertical motion is effectively divided into two parts, namely, the perpendicular and tangential components. Only the tangential component parametrically excites the system, which decreases with decreasing inclination angle. The perpendicular component produces a normal external load and has a much smaller effect on the dynamics of the tether. Finally, Figure 20c shows the effect of tether inclination on the total tension dynamic factors. The stability of the system greatly influences the numerical values of the factors, obtaining higher (or lower) values in the event of unstable configurations. However, and in accordance with the previous results, the actual numerical values are very small. In this case, all the results indicate reductions smaller than ±1% compared to the static solution.

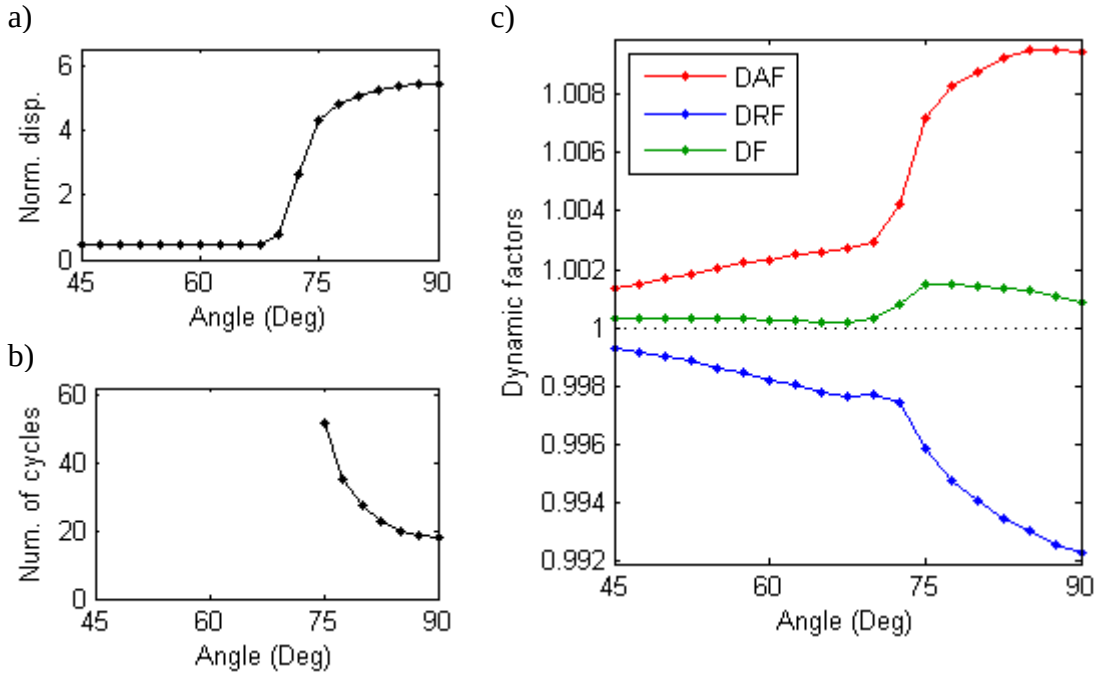

Figure 20: Influence of tether inclination: a) Normalized lateral displacement at mid-span; b) Number of cycles to initiate parametric resonance; c) Dynamic factors

5.9 Extreme bending moment values

As indicated in [37], the publications that have studied parametric excitation of cables mainly focus on lateral motion only, giving little or no attention to other load effects such as tension and bending moment values. For this reason, in [37], the authors focus on the tension values reached during parametric excitation, concluding that additional dynamic effects on tension are very small. Now, this section extends that thorough analysis to evaluate also the effects of parametric resonance on bending moments along the tether. This is achieved by numerical simulations with Abaqus [14]. In particular, some relevant case studies are investigated in detail. Maximum bending moments and tension values are compared by means of maximum sectional stress levels in terms of steel utilisation. Then multiple parametric studies are presented to evaluate the influence of different boundary conditions, excitation frequencies and excitation amplitudes.

In order to compare both load effects, namely tension and bending moment, we need to define them in terms of section stresses. Normalization of the maximum section stresses over steel's yield strength gives the utilisation of the material. Utilisation values greater than one indicate yielding of steel. When calculating utilisation values separately for each load effect, the total utilisation is the sum of all. Figure 21 shows the evolution in time of the utilisation for each load effect for the dry tether during parametric resonance. The results show that, while the tension utilisation remains approximately constant, the utilisation for bending moments varies significantly and is often greater than that of tension.

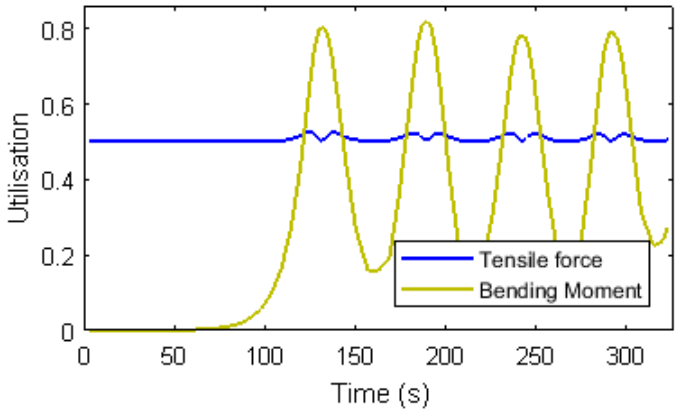

Figure 21: Utilisation of steel for a dry tether during parametric resonance

Hydrodynamic effects, such as drag force and added mass, are the greatest contributors to the damping of the system. Parametric resonance of a submerged tether can still occur, but the stresses and responses differ significantly due to the higher energy dissipation. This becomes very clear when analyzing the same tether and support motion but under water. Figure 22 shows the temporal evolution of the utilisation, now including the hydrodynamic effects. The utilisation for tensile forces remains practically constant and is of similar magnitude as for the dry tether case (Figure 21). Whereas the bending moment utilisation grows when the system arrives at the parametric instability, which occurs approximately after 140 s. However, the maximum bending moment values and so the associated maximum utilisation value is only a fraction of that observed in previous figure. While the maximum bending moment utilisation for the dry case (Figure 21) is 0.82, for the submerged case it is barely 0.10. Therefore, these results confirm that the submerged tether can also become unstable after sufficiently long excitation period. However, the effects of parametric instability are considerably smaller when including the hydrodynamic effects.

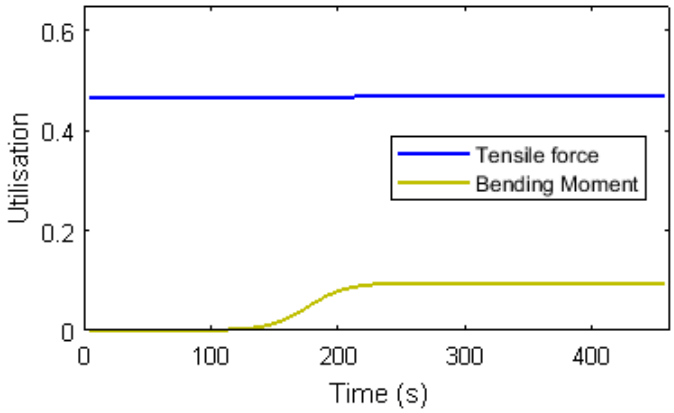

Figure 22: Utilisation of steel for a submerged tether during parametric resonance

The imposed support motion, directly related to the wave loading, can vary in amplitude and frequency. It is common to represent the system's stability for any amplitude-frequency combination in graphical form using stability maps or Strutt diagrams. The limits between stable and unstable regions are delimited by the transition curves. The regions grouping all unstable solutions are often called instability tongues. Figure 14 shows the stability map for the tether under consideration in this study. To generate this figure, 1320 separate simulations were necessary, each considering 120 cycles of imposed motion. Each simulated case is represented with a dot in Figure 14. Small black docks indicate that the corresponding amplitude-frequency combination results in a stable response of the submerged tether.

Whereas, large red dots indicate that the system is unstable, in other words, that it has reached parametric resonance.

On the other hand, the maximum utilisation due to bending moments, shown in Figure 23, is strongly related to the stability of the system. The same instability tongues observed for lateral displacements (Figure 14) can be observed on the bending moment utilisation values (Figure 23). However, the magnitude of the utilisation values due to bending moment is rather small compared to those due to tension.

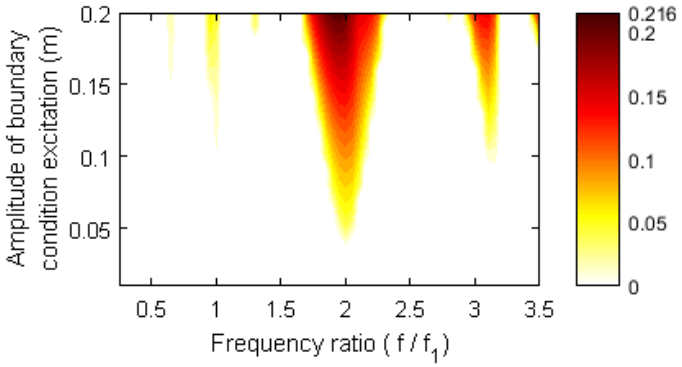

Figure 23: Maximum utilisation of steel due to bending moment

5.10 Influence of boundary conditions

The particular technological solution used to fasten the tether to the floating structure and to the seabed will determine the tether's behavior at those locations. In other words, boundary conditions of the tether are system dependent. When numerically modelling that system, it is very important to choose the correct properties of the boundary conditions. The possibilities range between free-to-rotate supports to fully restrained rotations. Therefore, this section investigates the effect of rotational stiffness (k_r) at the boundary conditions of the tether model. Figure 24 shows the fundamental frequency of the tether for various values of rotation stiffness. As expected, the stiffer the support, the higher the frequency.

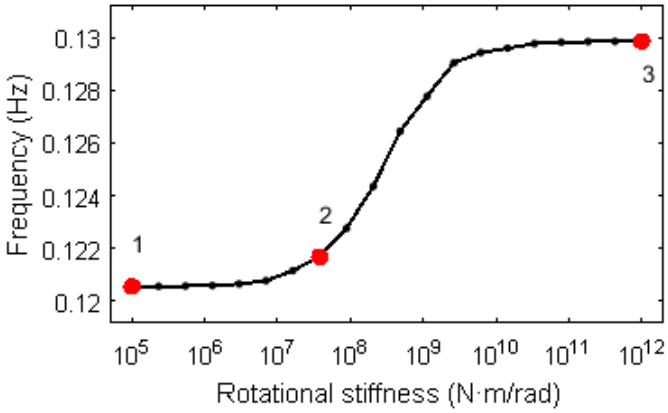

Figure 24: Tether's fundamental frequency for different rotational stiffness

Even though the frequencies change only slightly, the structural behaviour changes significantly. This is particularly pronounced for bending moments. Figure 25 shows the bending moment diagram along the tether during parametric resonance. The tethers are excited with an imposed motion with a 2:1 frequency ratio. Because the tether's fundamental frequency varies (Figure 24), the excitation frequency is different depending on the rotational stiffness

considered. Three particular rotational stiffness values are considered, which correspond to the cases marked with red dots in Figure 24. If the supports are free to rotate, the maximum bending moment is located at mid-span and there is no moment at the supports (Figure 25a). However, as soon as the rotational stiffness increases more bending moments appear at the support (Figure 25b). If the rotations are fully restrained, the bending moment diagrams are dominated by the moments near the supports (Figure 25c). However, not only the location of the maximum is of interest, it is also important to note the difference in bending moment magnitudes for each case. While for the free-to-rotate case the maximum is 0.15 MN·m (Figure 25a), for the fully restrained rotation case the maximum bending moment is 1.35 MN·m (Figure 25c). For the considered tether and depending on the rotational stiffness, the maximum bending moment can be up to one order of magnitude greater.

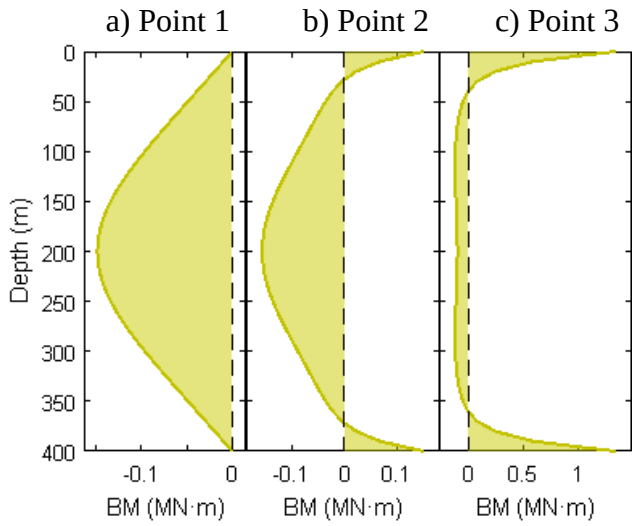

Figure 25: Bending moment diagram along the tether during parametric resonance for various rotation stiffness: a) Low stiffness (≡ free to rotate); b) Intermediate stiffness; c) High stiffness (≡ restrained rotations)

Figure 26 shows the corresponding maximum utilisation obtained during parametric resonance for each considered value of rotational stiffness. The utilisation due to tension is in practice constant, whereas for bending moment it is highest for the case with (effectively) fixed rotational supports. Therefore, to assume a high rotational stiffness is conservative and will give the highest (worst) utilisation values. A tether that allows for some rotation at the support can indeed become unstable by reaching parametric resonance, but the maximum stresses will be smaller than for the case with fully restrained rotations.

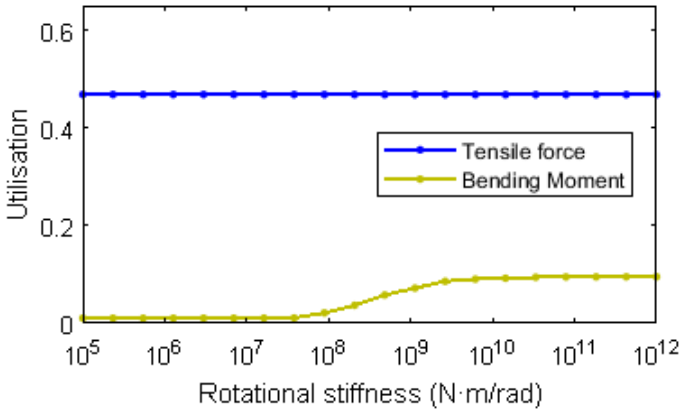

Figure 26: Maximum utilisation of steel for a submerged tether during parametric resonance for different rotational stiffness

6. Conclusions

This report has investigated the parametric excitation of taut mooring systems for floating bridges and submerged floating tunnels. It has been shown that wave loading on the floating structures lead to cyclic imposed motions that produce a parametrically excited tether. Under certain combinations of amplitude and frequency (of that imposed motion), an unstable situation might occur, which is called parametric resonance. In that case, large lateral motions can be expected on the tether. In summary, that was the existing understanding of parametric resonance in mooring systems. This report has further explored this possible instability and provided a deeper understanding of the phenomenology and the structural effects of parametric resonance. This was achieved investigating the problem in two separate but complementary approaches, namely theoretically and numerically. The analytical description of the problem is limited by the assumptions required to achieve mathematical solutions. However, they contribute to a better understanding of the key parameters of the problem and provide valuable insights. On the other hand, the numerical simulations allowed to model more complex and realistic descriptions of the mooring system and the conditions it is subjected to.

The conclusions that can be drawn from the analysis done in this report are summarized below:

- An analytical expression of the unstable configurations has been obtained by means of the Harmonic Balance Method. The obtained closed-form formulation allows for the contribution of multiple modes of vibration in situations with small sag-to-span ratios.
- The results clearly show the existence of parametric resonance that induces large lateral displacements. However, the consideration of the hydrodynamic effects greatly reduces the extent of those vibrations.
- Special emphasis is given to the cable tension. The maximum and minimum cable tensions are studied in terms of DAF (Dynamic Amplification Factor) and DRF (Dynamic Reduction factor), which are normalized dynamic factors that allow us to quickly assess the extreme tension values with respect to the static case.
- Even though the tension values show some correspondence with the instability diagrams, their numerical values are remarkably small. This is particularly evident when the hydrodynamic effects are considered in the calculations, in which case the maximum DAF raises barely above the unit value. This indicates that the maximum total tension (static + dynamic) obtained during parametric resonance are almost identical to the static prestress values in the tether. Therefore, there is no risk for cable breakage during parametric resonance due to excessive tension.

- Similar variations are observed regarding the minimum tension values. The results indicate that there is almost no reduction in the minimum cable tension compared to the static case. Therefore, there is no risk for slack cable if the static design of the mooring line is done with sufficient safety margins.
- The extreme tension values (maximum and minimum) in the tether are barely affected by the parametric resonance. This outcome is somewhat counterintuitive, indicating that unstable situations with large lateral motions feature very small dynamic tension effects.
- For stable configurations, the total tension can be correctly approximated using a quasi-static analysis. On the other hand, during parametric resonance, the dynamic effects are generally small and can be regarded as negligible. Therefore, if the design of a tether is based on the extreme tension levels, this study repeatedly shows that no dynamic analysis is needed to account for the effects of parametric resonance. Instead, a quasi-static response due to the expected vertical motion of the support is sufficiently accurate. This is applicable for calculating the extreme tension values in an ultimate limit state analysis as well as for the stress range and cycle counting needed in a fatigue limit state analysis.
- Also the maximum bending moments along the tether length are investigated and compared to extreme tension values. In order to compare both load effects, the results are expressed in terms of sectional stress values and normalized by the yield strength of the material, which gives the utilisation of steel. Tension utilisation is practically not influenced by parametric instability, whereas bending moments show only a moderate increase.
- Furthermore, the study of the influence of rotational stiffness at the supports has shown that the fully restrained rotational support leads to the highest stresses and is thus regarded as conservative.
- Finally, the analysis of multiple amplitude-frequency combinations for the support motion produced the stability diagram for the considered tether. With respect to the axial forces, the simulations confirm that the tension utilisation is practically independent of the systems stability and that it is directly proportional to the tethers elongation due to the imposed support motion. As for the bending moments, the system's stability clearly influences the results, obtaining larger utilisation values at the instability tongues. However, the magnitude of the utilisation values due to bending moment is rather small compared to those due to tension.

References

[1] Ferjefri E39 summary english jan 2012 (accessed 03.10.16) http://www.vegvesen.no/vegprosjekter/ferjefriE39/English

[2] M.M. Lwin, Floating bridges, in: W.-F. Chen, L. Duan (Eds.), Bridge Engineering Handbook, CRC Press, Boca Raton, 2000.

[3] D. Ahrens, Submerged floating tunnels – A concept whose time has arrived, Tunnelling Undergr. Space Technol. 12 (1997) 317-336. doi: 10.1016/S0886-7798(97)90022-5.

[4] C. Aage, M.M. Bernitsas, H.S. Choi, L. Crudu, A. Incecik, J.J. Murray, The Specialist Committee on Deep Water Mooring. Final report and recommendations to the 22nd ITTC. International Towing Tank Conference, Seoul, 2000.

[5] S. Weller, L. Johanning, P. Davies, Best Practice Report - Mooring of Floating Marine Renewable Energy Devices. Deliverable 3.5.3 from the MERiFIC Project, 2013.

[6] J.L. Lilien, A.P. Da Costa, Vibration amplitudes caused by parametric excitation of cable stayed structures, J. Sound Vibration 174 (1994) 69-90. doi: 10.1006/jsvi.1994.1261.

[7] M.H. El Ouni, N. Ben Kahla, A. Preumont, Numerical and experimental dynamic analysis and control of a cable stayed bridge under parametric excitation, Eng. Struct. 45 (2012) 244–256. doi: 10.1016/j.engstruct.2012.06.018.

[8] A.H. Nayfeh, D.T. Mook, P. Holmes, Nonlinear Oscillations, Wiley-VCH and Publishing House, Weinheim, Germany, 2004. doi: 10.1115/1.3153771.

[9] E.S. Caetano, Cable Vibrations in Cable-Stayed Bridges, International Association for Bridge and Structural Engineering, Zürich, Switzerland, 2007.

[10] M. Irvine. Cable Structures, The MIT Press, Cambridge, USA, 1981.

[11] MAPLE 18, Maplesoft, a division of Waterloo Maple Inc. Waterloo, Ontario.

[12] M.H. Patel, H.I. Park, Dynamics of tension leg platform tethers at low tension. part I - Mathieu stability at large parameters, Mar. Struct. 4 (1991) 257-273. doi: 10.1016/0951-8339(91)90004-U.

[13] J.A.P. Aranha, M.O. Pinto, A.J.P. Leite, Dynamic tension of cables in a random sea: analytic approximation for the envelope probability density function, Appl. Ocean. Res. 23 (2001) 93-101. doi: 10.1016/S0141-1187(01)00010-4.

[14] ABAQUS, Analysis User's Manual, Dassault Systèmes, Providence, 2011.

[15] S. Chandrasekaran, N.R. Chandak, G. Anupam, Stability analysis of TLP tethers, Ocean Eng. 33 (2006) 471–482. doi: 10.1016/j.oceaneng.2005.04.015.

[16] Det Norske Veritas, Guideline for Offshore Structural Reliability Analysis – Examples for Tension Leg Platforms, Report No. 95-3198, 1995.

[17] M.M. Gadagi, H. Benaroya, Dynamic response of an axially loaded tendon of a tension leg platform, J. Sound Vibration 293 (2006) 38–58. doi: 10.1016/j.jsv.2005.09.027.

[18] Det Norske Veritas SA, Recommended Practice DNV-RP-C205: Environmental Conditions and Environmental Loads, 2014.

[19] C. Webster, Mooring-induced damping, Ocean Eng. 22 (1995) 571-591. doi: 10.1016/0029-8018(94)00027-5.

[20] Statens Vegvesen. "Bjørnafjord submerged floating tunnel - Global dynamic response". 12149-01-OO-R-009 Rev 02

[21] D. Ahrens. "Submerged floating tunnels – A concept whose time has arrived". Chapter 10 in: Tunnelling and underground space technologies, 1997.

[22] I.K. Chatjigeorgiou, N.I. Xiros, S.A. Mavrakos, Coupling contributions and effect of Mathieu instabilities in the dynamic behaviour of vertical elastic cables and risers, WSEAS/IASME International Conference on Fluid Mechanics, Corfu, 2004.

[23] R.A. Ibrahim, Nonlinear vibrations of suspended cables—part III: Random excitation and interaction with fluid flow, Appl. Mech. Rev. 57 (2004) 515-549. doi: 10.1115/1.1804541.

[24] V.J. Papazoglou, S.A. Mavrakos, M.S. Triantafyllou, Non-linear cable response and model testing in water, J. Sound Vibration 140 (1990) 103-l 15. doi: 10.1016/0022-460X(90)90909-J.
[25] M.H. Patel, H.I. Park, Dynamics of tension leg platform tethers at low tension. part I - Mathieu stability at large parameters, Mar. Struct. 4 (1991) 257-273. doi: 10.1016/0951-8339(91)90004-U.
[26] S. Chandrasekaran, N.R. Chandak, G. Anupam, Stability analysis of TLP tethers, Ocean Eng. 33 (2006) 471–482. doi: 10.1016/j.oceaneng.2005.04.015.
[27] I.K. Chatjigeorgiou, S.A. Mavrakos, Nonlinear resonances of parametrically excited risers-numerical and analytic investigation for Ω=2ω_1, Comput. Struct. 83 (2005) 560–573. doi: 10.1016/j.compstruc.2004.11.009.
[28] G.R. Franzini, C.E.N. Mazzilli, Non-linear reduced-order model for parametric excitation analysis of an immersed vertical slender rod, Int. J. Non-Linear Mech. 80 (2016) 29–39. doi: 10.1016/j.ijnonlinmec.2015.09.019.
[29] S. Lei, W. Zhang, J. Lin, Q. Yue, D. Kennedy, F.W. Williams, Frequency domain response of a parametrically excited riser under random wave forces, J. Sound Vibration 333 (2014) 485–498. doi: 10.1016/j.jsv.2013.09.025.
[30] N. Srinil, G. Rega, S. Chucheepsakul, Three-dimensional non-linear coupling and dynamic tension in the large-amplitude free vibrations of arbitrarily sagged cables, J. Sound Vibration 269 (2004) 823–852. doi: 10.1016/S0022-460X(03)00137-8.
[31] N. Srinil, G. Rega, The effects of kinematic condensation on internally resonant forced vibrations of shallow horizontal cables, Int. J. Non-Linear Mech. 42 (2007) 180–195. doi: 10.1016/j.ijnonlinmec.2006.09.005.
[32] G. Rega, N. Srinil, R. Alaggio, Experimental and numerical studies of inclined cables: free and parametrically-forced vibrations, J. Theor. Appl. Mech. 46 (2008) 621-640.
[33] H. Yang, F. Xiao, P. Xu, Parametric instability prediction in a top-tensioned riser in irregular waves, Ocean Eng. 70 (2013) 39–50. doi: 10.1016/j.oceaneng.2013.05.002.
[34] I.K. Chatjigeorgiou, On the parametric excitation of vertical elastic slender structures and the effect of damping in marine applications, Appl. Ocean Res. 26 (2004) 23–33. doi: 10.1016/j.apor.2004.08.001.
[35] J.A.P. Aranha, M.O. Pinto, Dynamic tension in risers and mooring lines: an algebraic approximation for harmonic excitation, Appl. Ocean Res. 23 (2001) 63-81. doi: 10.1016/S0141-1187(01)00008-6.
[36] Det Norske Veritas, Fatigue Design of Offshore Steel Structures. Recommended Practice DNV-RP-C203, 2011.
[37] Cantero, D., Rønnquist, A. & Naess, A. 2017. Tension during parametric excitation in submerged vertical taut tethers. Applied Ocean Research 65: 279-289. (See Appendix D)

List of Appendices

This section contains a number of relevant appendices related to the work. First, published conference papers and journal paper in chronological order. Then, auxiliary results related to the work discussed in this report.

Appendix A: Conference paper: D. Cantero, A. Rønnquist, A. Naess. "Parametric excitation of mooring cables for submerged floating tunnels". IABSE Conference, May 2016, Guangzhou, China.

Appendix B: Conference paper: D. Cantero, A. Rønnquist, A. Naess. "Study of tension in mooring cables under parametric excitation for submerged floating tunnels". 19th Congress of IABSE, September 2016, Stockholm, Sweden.

Appendix C: Conference paper: D. Cantero, A. Rønnquist, A. Naess. "Recent studies of parametrically excited mooring cables for submerged floating tunnels". 2nd International Symposium on Submerged Floating Tunnels and Underwater Tunnel Structures, SUFTUS 2016, December 2016, Chongqing, China.

Appendix D: Journal article: D. Cantero, A. Rønnquist, A. Naess. "Tension during parametric excitation in submerged vertical taut tethers". Applied Ocean Research, Vol. 65, pp. 279-289, 2017.

Appendix E: Conference paper: D. Cantero, A. Rønnquist. "Maximum stresses in mooring lines during parametric excitation". 19th International Conference on Bridge Maintenance, Safety and management, IABMAS 2018, July 2018, Melbourne Australia.

Appendix F: Static deformation of cable.

Appendix G: Parametric excitation of Arch bridge

Appendix H: Equations of motion of inclined cable

Appendix A - Parametric excitation of mooring cables for submerged floating tunnels

Conference paper:
D. Cantero, A. Rønnquist, A. Naess. "Parametric excitation of mooring cables for submerged floating tunnels". IABSE Conference, May 2016, Guangzhou, China. DOI: 10.2749/222137816819259356

Title
Parametric excitation of mooring cables for submerged floating tunnels

Abstract:
The ferry links crossing the fjords along the west coast of Norway are going to be replaced by fixed links. Among the proposed solutions is the construction of Submerged Floating Tunnels (SFT). A mooring system should be used to restrain the movements of these floating structures. Long period waves, such as swell waves, parametrically excite the system and might result in excessive vibrations in the cable. This paper presents the equations of motion of the mooring line and derives an analytical expression, which allows for a quick identification of the system's stability. This expression is obtained through the Harmonic Balance Method (HBM) with two harmonic terms. The contribution of multiple modes of vibration is investigated for the case of small sag to span ratios. The expression is compared with the results from a numerical model, revealing the applicability of the proposed formulation.

A1. Introduction

The Norwegian government has decided to eliminate all ferries along the coastal highway E39 in order to reduce travel time and boost local economy. This route crosses several fjords and there are currently eight ferry connections in operation to cross them. These crossings are characterized by great widths (up to 5 km) and depths (up to 1 km) where non-conventional engineering solutions will be necessary. One of the proposed solutions is the construction of Submerged Floating Tunnels (SFTs), that, when built, will be the first of its kind worldwide.

An SFT is also called an Archimedes Bridge (AB) and was first proposed in 1886 [A1]. Since then, studies have investigated the feasibility of this new concept and concluded that the necessary technology is available [A2]. SFTs are essentially buoyant tunnels that float at certain depth in the water (Fig. A1). To avoid excessive movements, the structure must be moored or tethered. However, the dynamic behaviour needs special attention due to changes in water level [A2].

Tethering systems have been extensively investigated and developed for tension leg platforms in the oil industry and are based on seabed moorings designed to remain in tension throughout their operational life [A2]. The main environmental loads in such a system will be those produced by waves. The waves with longest wave periods have the potential to affect structures at greater depths [A1]. This is the case of swell waves that will affect the SFT and its mooring system even at considerable depths. This low frequency excitation produces a parametrically excited system. Small parametric excitations might lead to parametric resonance or dynamic instability that causes excessive vibrations of the mooring cable and the SFT even at frequencies away from the natural frequencies of the system.

Parametric Excitation (PE) has been extensively studied in the field of differential equations and dynamic systems, [A3] being one representative example. In bridge engineering this

phenomenon has often been reported in cable stayed bridges [A4] when girder or mast oscillations parametrically excite the cables. Similarly, in offshore platforms, parametric instability is an important aspect in the design of safe deep-water risers subjected to dynamic loads [A5] and is still a hot research topic [A6]. In the same way, in [A7] the effect of PE on moored SFTs is analysed. However, the authors believe that additional studies are necessary to characterize the phenomenon of parametrically excited mooring systems for SFT.

a) b)

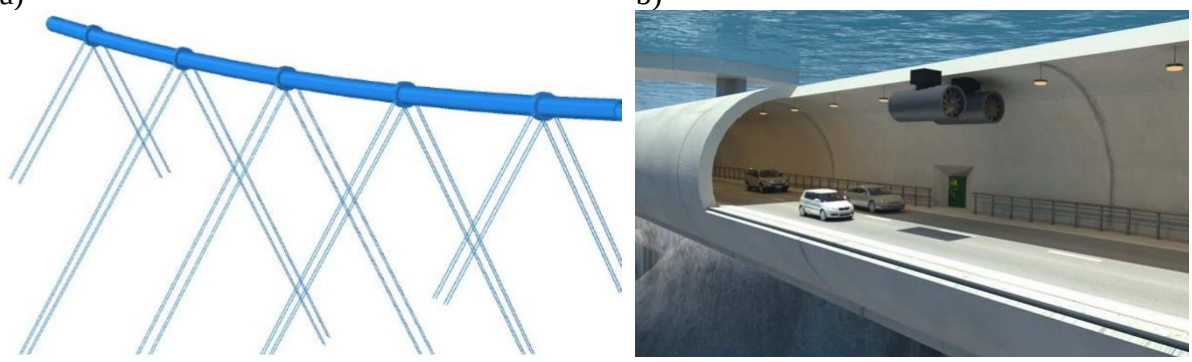

Fig. A1: Submerged floating tunnel; a) Tunnel and mooring lines; b) Tunnel detail (Illustration: Statens vegvesen/Vianova)

The aim of this paper is to derive an analytical expression for quickly checking the design of a mooring cable under parametric excitation. Section A2 derives the equations of motion of a cable excited by changes in the boundary condition position and derives the analytical expression of the instability regions. This is followed by a discussion on the effect of nonlinearities and drag forces. Finally, the formulation is compared to a numerical solution of the system

A2. Theoretical Analysis

A2.1 Equations of motion

Each cable in the mooring system of an SFT can be modelled as a cable suspended between two points. The wave loading produces oscillations of one of the cable ends and is represented as a cyclic displacement of one of the boundary conditions (Fig. A2). The equation of motion can be derived looking at the differential element of the cable and establishing the dynamic equilibrium and using D'Alembert's principle:

$$m\frac{\partial^2 y}{\partial t^2} + c\frac{\partial y}{\partial t} - \big(N + \Delta N(t)\big)\frac{\partial^2 y}{\partial x^2} - \Delta N(t)\frac{\partial^2 y_0}{\partial x^2} = 0 \qquad \text{(A1)}$$

where:
m = mass per unit length
$y(x,t)$ = cable displacement
c = cable internal damping
N = axial force at the initial configuration
$\Delta N(t)$ = variation of the axial force
$y_0(x)$ = initial static deformation of cable

The equation can be solved by separation of variables, where it is assumed that the solution is in the form of (Eq. (A2)), where $Y_j(t)$ are the generalized coordinates and the $\Phi_j(x)$ the modes of vibration.

$$y(x,t) = \sum_{j=1}^{n} Y_j(t)\phi_j(x);\ \ \phi_j(x) = \sin\left(\frac{j\pi x}{L}\right) \tag{A2}$$

The variation of the axial force in the cable is proportional to the cable length increment, which is equal to the combined contribution of three terms (Eq. (A3)). First, cable length increment is equal to the displacement of the boundary condition along the cable chord. For displacements perpendicular to cable chord it can be approximated using a Taylor expansion and including the terms up to second degree. Similarly, increment in length due to the cable dynamic deformation is approximated upon Taylor expansion and discarding higher order terms.

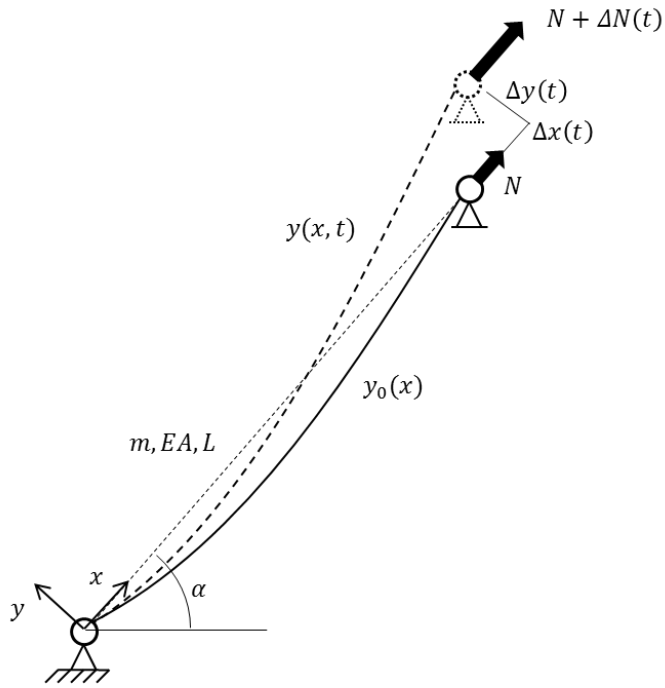

Fig. A2: Sketch of mooring line model

$$\Delta N(t) = \frac{EA}{L}\left(\Delta x(t) + \frac{\Delta y(t)^2}{2L} + \sum_{j=1}^{n} \frac{j^2\pi^2 Y_j(t)^2}{4L^2}\right) \tag{A3}$$

The partial differential equation (Eq. (A1)) can be transformed into a system of second order differential equations applying Galerkin's method [A4]. The general case is a set of coupled Mathieu equations. However, the coupling terms are small when the relation between sag and span is small [A4]. This condition can be expressed in terms of Irvine's parameter λ^2 [A8] that quantifies the relative importance of elastic and geometric effects. When $\lambda^2 < 0.1$, the system of equations can be uncoupled, obtaining a second order differential equation for each mode j (See Eq. (A4)).

$$mL^2\ddot{Y}_j + cL^2\dot{Y}_j + \frac{j^4\pi^4 EA}{4L^2}{Y_j}^3 + j^2\pi^2\left(N + \frac{EA\,\Delta x}{L} + \frac{EA\,\Delta y^2}{2L^2}\right)Y_j = 0 \tag{A4}$$

The support's displacement in time is assumed to be harmonic with frequency Ω and amplitude A, which can be written in terms of the cable's inclination angle α as follows:

$$\Delta x(t) = A\sin(\alpha)\cos(\Omega t);\ \Delta y(t) = A\cos(\alpha)\cos(\Omega t) \tag{A5}$$

A2.2 Instability analysis

Eq. (A4) is the non-linear Mathieu equation where the excitation appears as time-varying coefficients [A3] or parameters, thus called parametric excitation. A small parametric excitation can generate an unbounded solution (unstable solution). It is of great importance to identify when instability might occur. The boundaries that separate the stable from unstable solutions are termed Transition Curves (TC). One possibility to calculate the TC is through the Harmonic Balance Method (HBM) that essentially approximates the solution to Eq. (A4) as a Fourier series (Eq. (A6)). Because the phase shift is unknown, both sin and cos must be included [A4].

$$Y_j(t) = \sum_{n=0}^{N} \Upsilon_{(2n-1)}\sin(n\Omega t) + \Upsilon_{2n}\cos(n\Omega t) \tag{A6}$$

Substituting Eq. (A6) into Eq. (A4), multiplying the result by the basis $\{\sin(\Omega t), \cos(\Omega t), \ldots, \sin(n\Omega t), \cos(n\Omega t)\}$, integrating over one full cycle and balancing harmonic terms gives a system of equations with the Fourier coefficients Υ_i as the unknowns. Solutions of the system provide the Fourier coefficients that define periodic solutions for Eq. (A4). The transition curves are thus defined when the determinant of the coefficient matrix of the system is zero.

A2.3 Analytical solution

It has been shown that two sets of solutions exist depending on the period considered, either 2π and 4π, which correspond respectively to the sum of all even and odd n values in Eq. (A6). The number of harmonic terms considered N defines the accuracy of the solution. In the literature only one term is generally considered. However, here two terms are considered ($N = 2$) because there is a significant increase in accuracy. Analytical expressions for the TC are obtained with the aid of symbolic calculation software [A9]. Two separate expression are defined in Eq. (A7) and Eq. (A8), corresponding to periods 2π and 4π respectively. See the appendix for complete definition of the auxiliary expressions B_i and C_i.

$$A = \pm B_1\left(2L\sqrt{B_2(B_3 \pm \sqrt{B_4})}\right)\ \ for\ T = 2\pi \tag{A7}$$

$$A = \pm C_1\left(L\sqrt{2}\sqrt{C_2 \pm \sqrt{C_3}}\right)\ \ for\ T = 4\pi \tag{A8}$$

The expressions of the TC can be used to calculate the stability regions associated to any mode of vibration j. Fig. A3 shows the stability chart derived from the analytical expressions for mode j without damping.

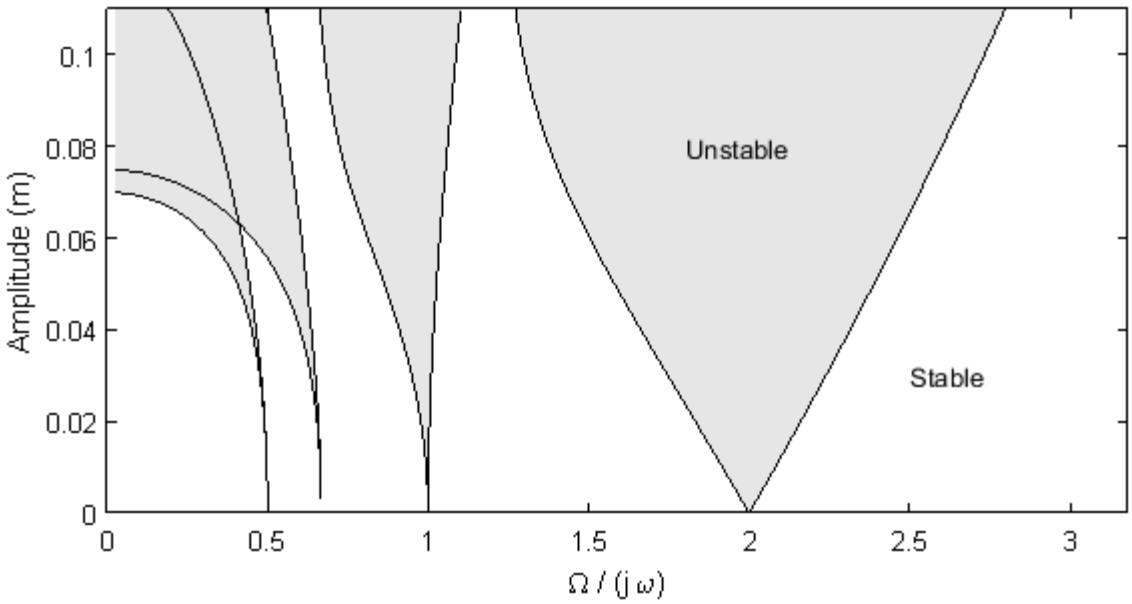

Fig. A3: Stability chart for mode-j

In order to find the stability map for our model it is necessary to consider the contribution of several modes. This can be achieved by superimposing as many modes as deemed necessary. Fig. A4 shows the stability chart for one particular cable example considering 3 modes and 5% damping. The formulation allows us to easily include the contribution of higher modes of vibration. In particular it is important to include the first and second instability regions of each mode.

A3. Numerical solution

The expressions derived in previous section allow us to identify situations that would produce large displacements in the mooring line due to harmonic movements of one of the boundary conditions. However, the analytical expression is only an approximation that needs to be validated against a numerical solution of the problem at hand. Therefore, a mooring line was modelled with ABAQUS [A10] considering geometric nonlinearities. The cable is submerged in water and is thus influenced by drag forces and additional mass effects. These effects have been included by means of the Morison Equation using the toolbox AQUA provided by the software.

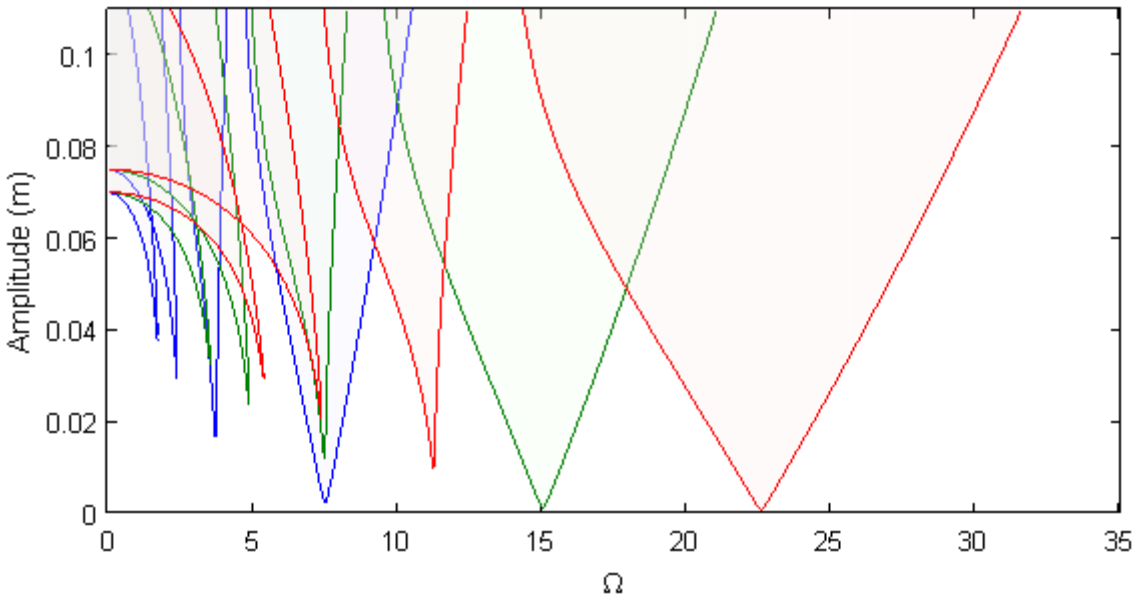

Fig. A4: Stability chart for case study. Blue = mode-1; Green = mode-2; Red = mode-3

A3.1 Nonlinearities and hydrodynamic effects

A cable modelled as in Fig. A2 and parametrically excited at a critical frequency has an unbounded solution. The result is the classic parametric resonance of the linear Mathieu equation that features an exponential growth, as can be seen in Fig. A5a. In a truly linear system the amplitude grows until the system is destroyed [A3]. The same situation is studied in Fig. A5b including the nonlinear effects. The displacements grow up to an upper bound that corresponds to the limit cycle of the nonlinear response. Real physical systems do not exhibit unbounded responses. By including the nonlinear effects, a more realistic model is obtained. In parametric resonance the nonlinearities will limit the oscillation amplitudes and are almost independent of the cable internal damping [A4].

For a submerged slender structure, the most important nonlinear contributions are the hydrodynamic effects [A11]. These effects are drag, inertia and added mass that are included in the system with the Morison Equation, which has been widely used in ocean engineering problems giving reasonable results [A12]. When the hydrodynamic effects are taken into account the cable displacements are reduced considerably, as seen in Fig. A5c.

The responses in Fig. A5 are significantly different. However, they all correspond to the same excitation and responses should be regarded as unstable. Thus, the stability criterion needs to be redefined when considering nonlinear and hydrodynamic effects. Now, a solution is regarded as unstable when the displacements in the cable are greater than those of the boundary condition. Following this definition, it was found that the inclusion of the nonlinear and hydrodynamic terms does not affect the stability of the system, they only affect the limit value. Therefore, the formulation derived in Section A2 can be used to identify unstable configurations.

A3.2 Numerical validation

The analytical expression derived in Section A2 is compared against the numerical solution for a range of excitation frequencies and amplitudes in Fig. A6. It can be seen that there is a good

match between the stability predictions derived from the Harmonic Balance Method and the numerical solution.

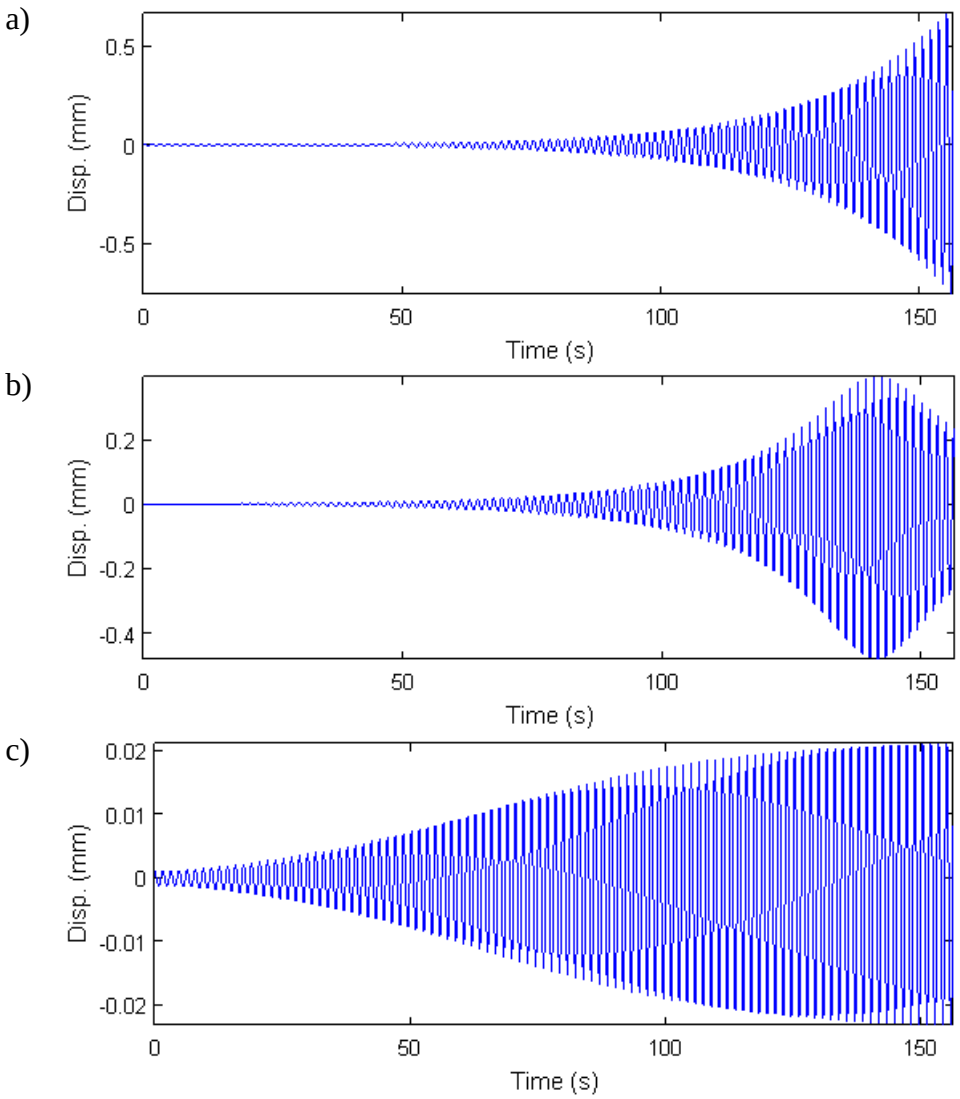

Fig. A5: Cable displacement under parametric resonance for A = 0.01 m; a) linear case; b) with nonlinear effects; c) including nonlinear and hydrodynamic effects

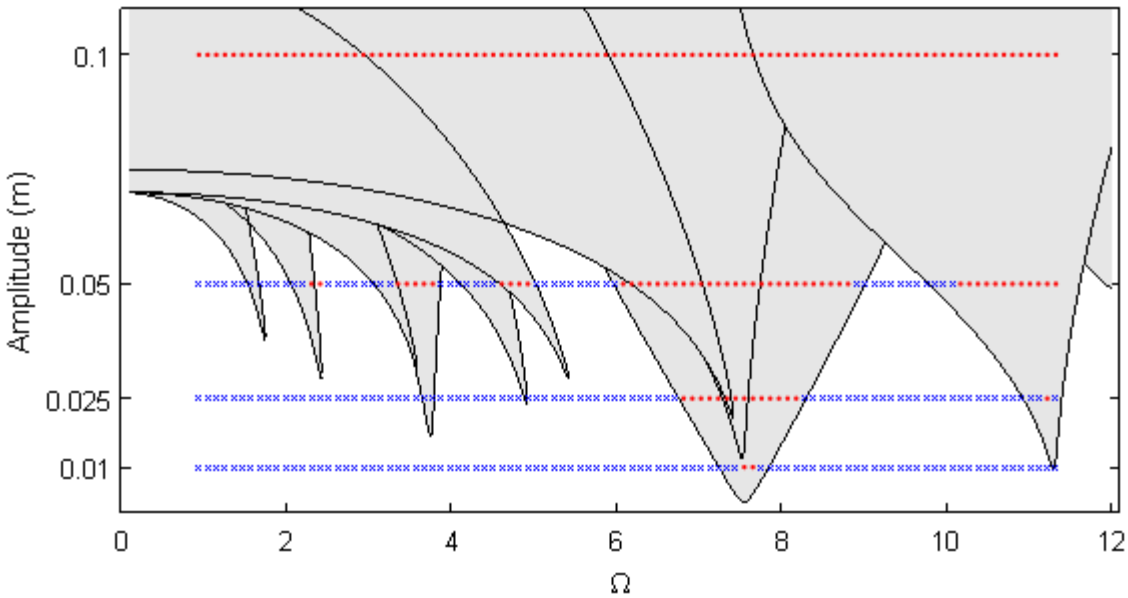

Fig. A6: Stability chart for 3 modes of vibration (shaded areas). Numerical solutions: blue cross = stable; red dot = unstable

Conclusions

This paper has presented a new type of structure, namely the Submerged Floating Tunnel. One critical aspect in its dynamic behaviour is the parametric excitation of the mooring system due to long period waves. By means of the Harmonic Balance Method an analytical expression of the unstable configurations has been obtained. The formulation allows for the contribution of multiple modes of vibration in situations with small sag to span ratios. The effects of nonlinearities and hydrodynamic effects have been discussed. The formulation is then validated against the results from a numerical model. The analytical expression can easily be integrated in the design process to avoid situations that might lead to parametric excitation.

Acknowledgements

The research presented in this manuscript was possible thanks to the financial support of The Fjord Crossing research program for the Coastal Highway Route E39.

Appendix

Auxiliary expressions in Eq. (A7):

$$B_1 = \frac{1}{\pi^3 EAB_2} \tag{A.A1}$$

$$B_2 = 8L^2\Omega^2 m - 3N\pi^2 \tag{A.A2}$$

$$B_3 = 16L^6\Omega^6\pi^2 m^3 + 4L^6\Omega^4\pi^2 c^2 m - 28L^4 N\Omega^4\pi^4 m^2 - 2L^4 N\Omega^2\pi^4 c^2 + 14L^2 N^2\Omega^2\pi^6 m - 2N^3\pi^8 \tag{A.A3}$$

$$B_4 = 256L^{12}\Omega^{12}\pi^4 m^6 + 128L^{12}\Omega^{10}\pi^4 c^2 m^4 - 768L^{10}N\Omega^{10}\pi^6 m^5 + 16L^{12}\Omega^8\pi^4 c^4 m^2 - 128L^{10}N\Omega^8\pi^6 c^2 m^3 + 864L^8 N^2\Omega^8\pi^8 m^4 + 16L^{10}N\Omega^6\pi^6 c^4 m + 36L^8 N^2\Omega^6\pi^8 c^2 m^2 - 464L^6 \mathrm{N}^3\Omega^6\pi^{10} m^3 - 8L^8 N^2\Omega^4\pi^8 c^4 + 16L^6 N^3\Omega^4\pi^{10} c^2 m + 129L^4 N^4\Omega^4\pi^{12} m^2 - 7L^4 N^4\Omega^2\pi^{12} c^2 - 18L^8 N^5\Omega^2\pi^{14} m + N^6\pi^{16} \tag{A.A4}$$

Auxiliary expressions in Eq. (A.8):

$$C_1 = \frac{1}{4EA\pi^4} \tag{A.A5}$$

$$C_2 = 99L^4\Omega^4\pi^4m^2 + 12L^4\Omega^2\pi^4c^2 - 152L^2N\Omega^2\pi^6m + 48N^2\pi^8 \tag{A.A6}$$

$$\begin{aligned} C_3 = {} & 9477L^8\Omega^8\pi^8m^4 + 936L^8\Omega^6\pi^8c^2m^2 - 27216L^6N^1\Omega^6\pi^{10}m^3 \\ & -432L^8\Omega^4\pi^8c^4 - 1344L^6N\Omega^4\pi^{10}c^2m + 25056L^4N^2\Omega^4\pi^{12}m^2 \\ & -1408L^4N^2\Omega^2\pi^{12}c^2 - 9472L^2N^3\Omega^2\pi^{14}m^2 + 1280N^4\pi^{16} \end{aligned} \tag{A.A7}$$

References

[A1] JAKOBSEN B., “Design of the Submerged Floating Tunnel operating under various conditions”, *Procedia Engineering*, Vol. 4, 2010, pp. 71–79.

[A2] FERRO G. et al., “Submerged floating tunnels analysis project”, *Tunnelling and Underground Space Technology*, Vol. 12, No. 2, 1997, pp. 337-346.

[A3] NAYFEH A.H., and MOOK D.T., *Nonlinear Oscillations*. Wiley-VCH, Weinheim, Germany, 2004.

[A4] LILIEN J.L., and PINTO DA COSTA A., “Vibration Amplitudes caused by Parametric Excitation of Cable Stayed Structures”, *Journal of Sound and Vibration*, Vol. 174, No. 1, 1994, pp. 69-90.

[A5] XIAO F., and YANG H.Z., “Probabilistic Assessment of Parametric Instability of a Top Tensioned Riser in Irregular Waves”, *Journal of Marine Science and Technology*, Vol. 19, 2014, pp. 245-256.

[A6] YANG H., XIAO F., and XU P., “Parametric Instability Prediction in a Top Tensioned Riser in Irregular Waves”, *Ocean Engineering*, Vol. 70, 2013, pp. 39-50.

[A7] SUN S.N., and SU Z.B., “Parametric Vibration of Submerged floating Tunnel Tether under Random Excitation”, *China Ocean Engineering*, Vol. 25, No. 2, 2011, pp. 349-356.

[A8] IRVINE M., *Cable Structures*, The MIT Press, Cambridge, 1981.

[A9] MAPLE 18, Maplesoft, a division of Waterloo Maple Inc., Waterloo, Ontario.

[A10] ABAQUS, *Analysis user’s manual*, Dassault Systèmes, Providence, 2011.

[A11] CHATJIGEORGIOU I.K., XIROS N.I., and MAVRAKOS S.A., “Coupling Contributions and Effect of Mathieu Instabilities in the Dynamic Behaviour of Vertical Elastic Cables and Risers”, *Proceedings of WSEAS and IASME conference on Fluid Mechanics*, Corfu, 2004.

[A12] KIM M.H., “Hydrodynamics of Offshore Structures” in Eds: HERBICH J.B. et al. *Developments of Offshore Engineering*, Elsevier, 1999, pp. 336-381.

Appendix B - Study of tension in mooring cables under parametric excitation for submerged floating tunnels

Conference paper:
D. Cantero, A. Rønnquist, A. Naess. "Study of tension in mooring cables under parametric excitation for submerged floating tunnels". 19th Congress of IABSE, September 2016, Stockholm, Sweden.

Title:
Study of tension in mooring cables under parametric excitation for submerged floating tunnels

Abstract:
The coastal highway E39 project in Norway is considering the construction a Submerged Floating Tunnel (SFT). Some of the preliminary designs use a mooring system to maintain the structure in the prescribed position. The main environmental load in such a system will be long period swell waves. This low frequency excitation produces a parametrically excited system. Certain situations might lead to parametric resonance or dynamic instability that causes excessive vibrations of the cable and the SFT. However, it is unclear how parametric excitation affects the cable tension of a mooring system. Correct design should avoid excessive forces that might break the line or very small forces that lead to momentarily slack cables. The aim of this paper is to assess the validity of using the stability charts for the design of mooring lines with respect to safe levels of cable forces. This is achieved through the numerical analysis of a cable model using Abaqus. Cable vibrations and cable forces are analysed and compared for a range of amplitudes and frequencies of the support motions. In addition, the dry and submerged cases are compared, clearly exposing the repercussion of the hydrodynamic effects.

B1. Introduction

The coastal highway E39 project in Norway plans to replace several ferry connections crossing the fjords with fixed links. These crossings are characterized by great widths (up to 5 km) and depths (up to 1 km) where non-conventional engineering solutions will be necessary. One of the proposed solutions is the construction of a Submerged Floating Tunnel (SFT), which essentially consists of at watertight tube that is floating at a certain depth in the water. This type of structure has also been called submerged floating tube bridge or Archimedes bridge. Depending on the floatability of the tunnel, the position of the tube in the water has to be fixed either using pontoons or by mooring it to the seabed. In this paper, the vertically moored tunnel variety is studied. This typology has no visual impact and reduces the risks of ship collisions by placing the tube at a sufficient depth below the sea level. See an example of an SFT fixed by vertical mooring lines in Figure B1.

The idea of an SFT was first theoretically proposed already over one century ago. Since then, there have been a few attempts to materialize it. However, to this day, no such structure has been built. Thus, when finally built in Norway, it will be the first of its kind. Even if the engineering knowledge and the technology are available, there is an evident lack of experience designing, building and operating such a structure. For this reason, it is necessary to carefully review and adapt every aspect in this new structural typology. One of the identified issues is the possibility of having parametric excitation in the mooring lines due to periodic changes in height of the water level. In particular, there are concerns with the effect of long period waves (swell) that generate in the open sea. These waves are characterized by a low frequency

component, can last for several hours and its effects decrease only linearly with water depth. Consequently, they would induce some long lasting harmonic loading on the submerged tunnel that translate to imposed support motions in the mooring lines.

a)

b)

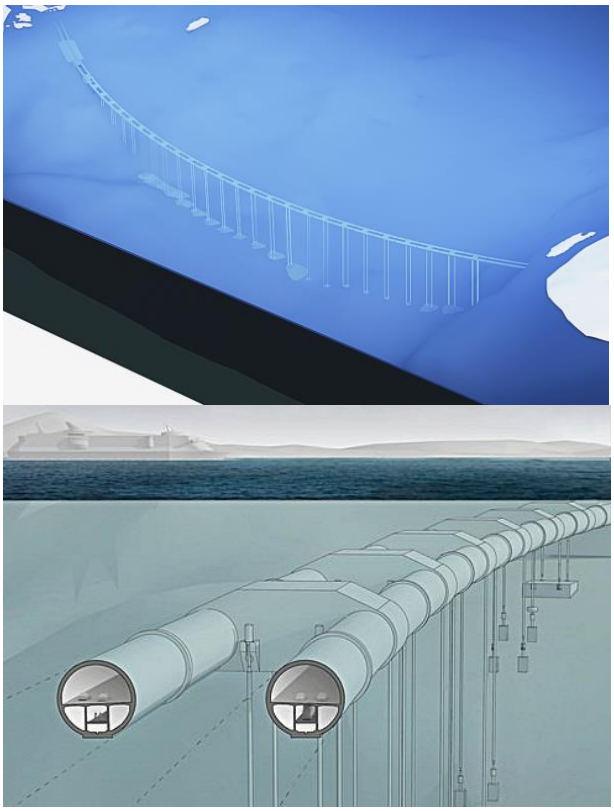

Figure B1. Submerged Floating Tunnel (SFT); a) General view; b) Cross-section; (Source: Snøhetta)

A cable excited by harmonically varying imposed displacements of one of its ends is a parametrically excited system. Under certain conditions, parametric excitation leads to parametric resonance, which is an unstable situation that produces excessive lateral displacements in the cable. The principal parametric resonance occurs when the frequency of the support motion is twice the fundamental frequency of the system. However, there are many more frequencies that induce instability in the system. Furthermore, the greater the amplitude of the support motion the larger the number of frequencies that lead to unstable motion. Parametric excitation has been studied extensively in the literature, [B1] being a seminal example. The authors have investigated this phenomenon also in a previous IABSE conference [B2], in which simplified analytical expressions are derived to readily identify when parametric resonance might occur.

The main characteristic of parametric resonance is the development of very large deformations in the cable. In a perfectly linear system the amplitudes of these deformations grow exponentially. However, in reality, the non-linear effects limit these deformations to a large but bounded value. Furthermore, the displacements of a submerged cable are significantly different to those of a dry one. The hydrodynamic effects play an essential role, being the most important non-linear contribution [B3] as an additional line damping component [B4].

Most of the published studies on parametric excitation in cables investigate exclusively the lateral displacements. However, only a few of them examine also the cable tension. A very

good example is [B5] that provides qualitative explanations of various parametric resonances in a dry cable based on numerical simulation results. The relation between lateral displacements and cable tension under parametric resonance is not straightforward, particularly when considering non-linear effects. However, to the best of the authors' knowledge there is no study that explicitly investigates the tension of cables under parametric resonance including hydrodynamic effects. It is particularly interesting to evaluate the extreme cable stresses developed during parametric resonance. Very high cable tension might produce cable breakage. On the other hand, very small or no cable tension might result in momentarily slack cables, which might induce large impulse forces on the moored structure when it changes back to a taught line. Furthermore, the difference between the maximum and the minimum stresses defines the amplitude of the load cycle which is a fundamental parameter in correct assessment of the fatigue life.

This paper revisits the problem of parametric excitation of mooring lines with special emphasis on the cable tension and considering the influence of hydrodynamic effects. Section B2 describes the numerical model that represents the parametrically excited mooring line. Then, Section B3 investigates the dry cable in order to give a clear overview of what parametric excitation is and how it affects the internal tension of the cable. In particular, the maximum and minimum of the cable tensions are studied in terms of normalized dynamic factors that allow us to quickly assess the extreme tension values with respect to the static case. Next, the same analysis is done but considering the influence of the hydrodynamic effects. Finally, some interesting conclusions are extracted from the comparison between dry and submerged mooring lines under parametric excitation.

B2. Numerical model

The studied mooring line is modelled as a vertical cable of length L with pin supports at both ends. The upper support is the one that would be connected to the floating structure. The cable is modelled including an initial internal tension T_0 that would be present in the static equilibrium of a taught mooring line. The effect of the changes in water level is represented by imposing a support motion at the upper end. This has been represented with a harmonic motion with amplitude A and frequency f. Figure B2 shows a schematic of the model.

This model is first studied without any hydrodynamic effect (dry) in Section B3. The results highlight the parametric resonance phenomenon and give some insights on the relation between displacements and cable tension. Then, in Section B4, the submerged cable is studied. Hydrodynamic effects are taken into account using the Morison's equation [B6], which is a well-established approximation for the kind of calculations carried out in this paper. Two important parameters are necessary, namely the added mass coefficient C_A and the drag coefficient C_D whose numerical values are 1 and 1.5 respectively as recommended in [B7].

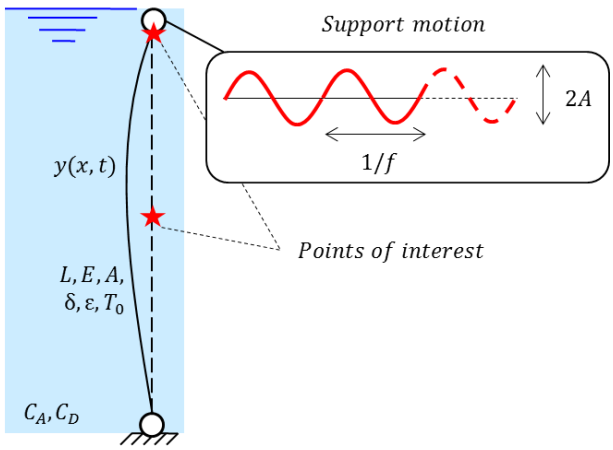

Figure B2. Sketch of mooring line model

Two particularly representative points in the model are the mid-span of the cable and the upper support, as shown in Figure B2. In terms of displacement, when parametric resonance occurs, large displacements are expected at the mid-span point, while the displacements at the upper point are imposed and defined by a harmonic function in terms of A and f. On the other hand, for the tension, both points are important. The tension distribution along the cable is not constant when dynamically loaded. It is necessary to calculate the tension at mid-span to assess how loose or tight the cable becomes. It is also necessary to calculate the tension at the upper support because it is the force that will be transmitted to the tunnel. Therefore, the current analysis of tension is focused on these two representative points. However, for simplicity, no distinction is made in the analysis. Maximum (or minimum) tension values are calculated as the maximum (or minimum) values among both locations.

The numerical model is developed in ABAQUS [B8] using 40 beam elements (B21) including geometric non-linear effects. The contribution of the hydrodynamic effects is included using the Aqua toolbox of the software. For each simulated case, 100 cycles of the support motion is considered, which is more than sufficient time to develop parametric resonance or to reach the steady state situation. The numerical time integration of the solution is done with ABAQUS using a sufficiently small time step that gives a minimum sampling rate of 100Hz. The particular cable properties used in this study are listed in Table B1.

Table B1: Numerical values of model properties

Symbol	Description	Value	Unit
L	Length	100	m
E	Young's modulus	$210 \cdot 10^9$	N/m^2
A	Area	785.40	cm^2
δ	Density	7800	kg/m^3
ε	Damping	0.1	%
T_0	Initial tension	$2 \cdot 10^6$	N
f_1^d	Fundamental frequency (dry)	0.9034	Hz
f_1	Fundamental frequency	0.8493	Hz

B3. Cable tension vs deformation

This section introduces the phenomenon of parametric resonance for a dry mooring line, i.e. without considering the hydrodynamic effects. This allows us to clearly identify parametric

resonance and define some convenient ways to study it. The main focus is to study the relation between two load effects, namely the lateral displacements and internal tension.

First, one particular situation is shown in Figure B3 that corresponds to the mooring line with a support motion with a Frequency Ratio (*FR*) of 2 and an amplitude *A* of 0.03 m. Note that *FR* is defined as the ratio of the excitation frequency to the fundamental frequency. Similar results have been reported in previous publications, being a very good example [B5]. Figure B3a shows the lateral displacements at the mid-span of the cable. For graphical reference, the maximum and minimum static vertical displacements are shown (u_{max}^{Static} *and* u_{min}^{Static}), which correspond to *A* and -*A*. Note that the time-history corresponds to lateral displacements, whereas the references are for vertical displacements. Even though the results are for different directions it is still useful to compare how much bigger the displacements are compared to the support motions in a parametric resonant situation. The time-history shows the typical response for such a system under parametric resonance which is termed beating phenomenon [B5]. The displacements grow exponentially over time until a certain maximum (or minimum) value is reached. Then the displacement decay just to repeat the exponential growth again. For this particular case the maximum displacement is 1.59 m while the amplitude of the support motion is only 0.03 m, this is 53 times greater.

Intuition would suggest that the internal cable tension should have a similar evolution in time, or at least feature some maximum values at the same time as those reported for the displacements. But this is not the case. Figure B3b shows the time-history of the total tension at the upper support. For reference, the initial cable tension T_0 is shown, also the static tension for situations with the maximum and minimum support displacements, indicated respectively as T_{max}^{Static} and T_{min}^{Static}. The results show that generally the tension values oscillate around the initial tension except when the maximum displacements are reported. Then, there is a slight increase in maximum tension that surpasses the static value. On the other hand, the minimum tension value grows, even above the initial static tension, against all intuition. This was also reported in [B5] and termed band narrowing, and is typical behaviour for the tension in parametric resonance.

It has to be noted that relatively high (and low) values of tension are obtained at the very beginning of each of the simulations. This is due to the sudden start of the support motion, which produces a small temporary increase of the tension and Indicated as T_{max}^{Start} and T_{min}^{Start} in Figure B3b. These extreme tension values are not really interesting for our analysis and are only a consequence of the way of modelling the problem. In reality, the amplitude of the support motion will grow gradually. For this reason, the first 10 cycles of each simulation are neglected when calculating the maximum (and minimum) tension values.

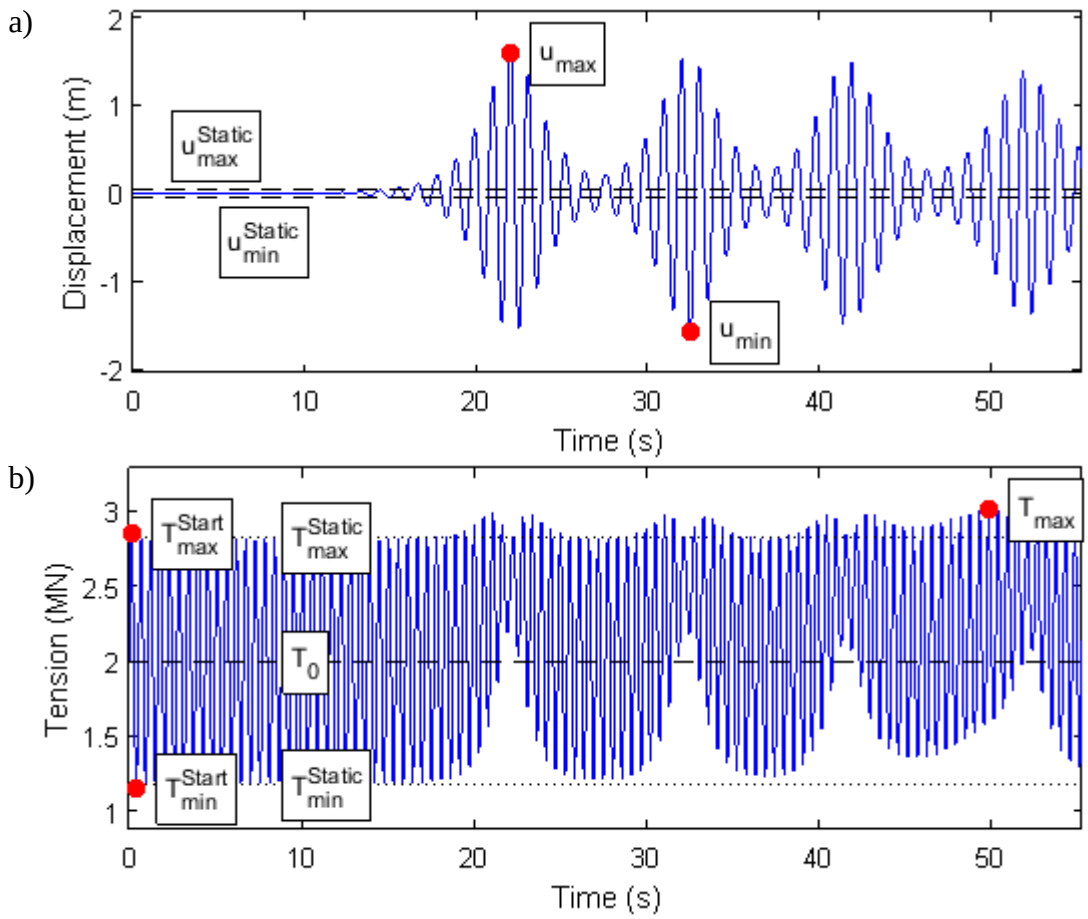

Figure B3. Results for harmonic support motion (FR = 2; A = 0.03 m); a) Lateral displacement at mid-span; b) Tension at support

To analyse the changes in tension it is convenient to define them in terms of dynamic factors. Here two distinct factors are used to clearly differentiate the results between maximum tension and minimum tension. The factor is a normalization of the extreme values of the tension with respect to the calculated extreme static response corresponding to the extreme support motions. We define Dynamic Amplification Factor (DAF) in Eq. (B1) and Dynamic Reduction Factor (DRF) in Eq. (B2). For the maximum tension DAF is greater than or equal to one. Conversely, the factor for the minimum (DRF) is smaller than or equal to one. These factors allow us to study the problem from the static design perspective. The mooring line can be studied statically based on the expected support motion amplitude and then factored to obtain the maximum and minimum tension values.

$$DAF = \frac{T_{max}}{T_{max}^{Static}} \geq 1 \qquad \text{(B1)}$$

$$DRF = \frac{T_{min}}{T_{min}^{Static}} \leq 1 \qquad \text{(B2)}$$

Now, the same analysis is performed but for a wide range of Frequency Ratios and Amplitudes of the support motion. In particular, the *FR* is varied in a discrete space with values from 0.25 to 3.5 in increments of 0.05, whereas the considered amplitudes are from 0.005m to 0.1m in 0.005m increments. Figure B4 shows the instability diagram based on the lateral displacements of the cable at mid-span. Each of the studied *FR* and A combinations is represented as a dot. If the particular case renders a stable solution it is depicted as a small black dot. But, when a particular *FR* and *A* combination leads to an unstable result it is represented with a larger red

dot. Note that the criterion used to identify instability is when the displacements at mid-span are greater than the support motion. As expected, the results clearly feature distinct areas with parametric resonance, which are usually called instability tongues. There are two distinct tongues emanating from the FR 1 and 2. There are also many other tongues that are due to the contribution of higher modes and combination of harmonics.

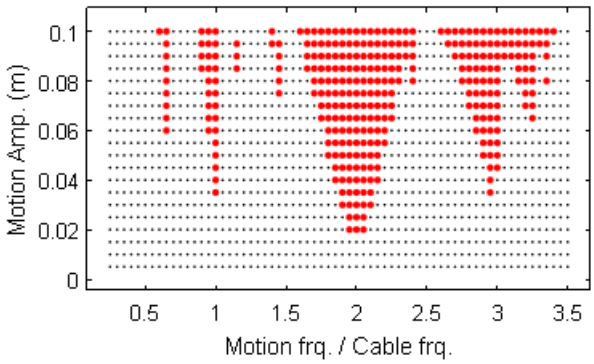

Figure B4. Instability diagram for dry cable

It is interesting to explore how this instability diagram for lateral displacements relates to the maximum and minimum cable tensions. Figure B5a shows the maximum cable tension in terms of DAF. Some of the instability tongues reported in Figure B4 can also be seen here. However, the maximum DAF for any *FR* and *A* combination is 1.38, which means that the maximum total tension (static + dynamic) is only 38% greater than the maximum static. But it is even more interesting to study the DRF as presented in Figure B5b. The minimum tension in the cable is either equal to the minimum static or just slightly smaller. This is reflected in the DRF values that have an absolute minimum value of 0.99. This is, the minimum tension is 99% of the minimum static, or in other words, there is only a 1% reduction of the total tension when compared to the static one. The instability tongues in Figure B4 can also be seen in Figure B5b but, in this case, the values of DRF during parametric resonance are equal to one. As seen before in Figure B3b, during parametric resonance the minimum tension grows above the minimum static value, hence achieving a value of 1 for the DRF.

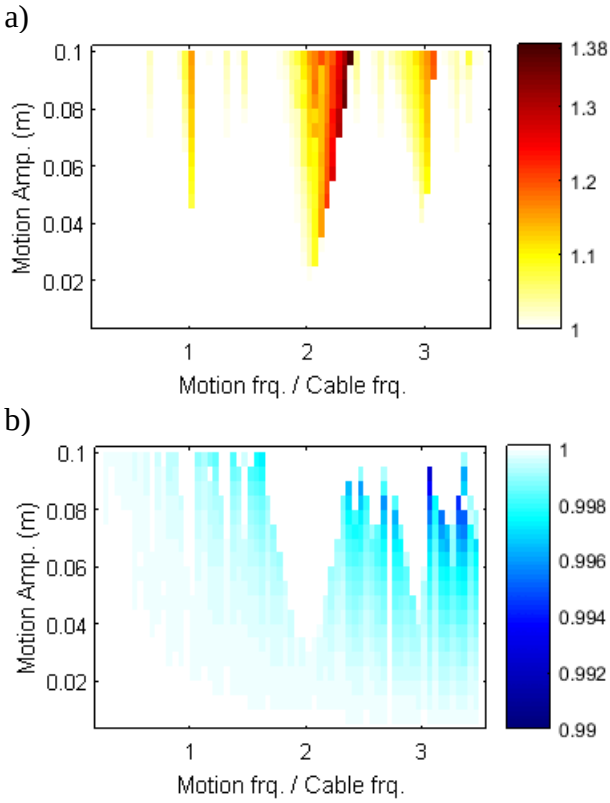

Figure B5. Normalized extreme tension for dry cable; a) Maximum (DAF); b) Minimum (DRF)

B4. Including hydrodynamic effects

As mentioned in the introduction, the hydrodynamic effects are the greatest contributors to the damping of the system. Parametric resonance of the submerged cable can still occur but the tensions and displacements are significantly smaller. This section studies the same simulations as in Section B3 but now including the hydrodynamic effects.

First, let us revisit the same situation as presented in Figure B3. The time-history response of the lateral displacement is given in Figure B6a, now including the hydrodynamic effects. Parametric resonance plays an important role again, leading to a rapid growth and achieving maximum displacements of 0.26 m. In terms of displacements it can be seen that in an unstable situation the maximum is much smaller since now it is only 8.5 times greater than the amplitude of the support motion. Furthermore, no beating phenomenon is observed. Now the extreme values of the lateral displacements grow up to a certain value and remain constant. As for the tension, the values in Figure B6b are barely affected by the parametric resonance. There is only a slight increase in both, maximum and minimum tensions which translate to DAF and DRF values of 1.009 and 1 respectively.

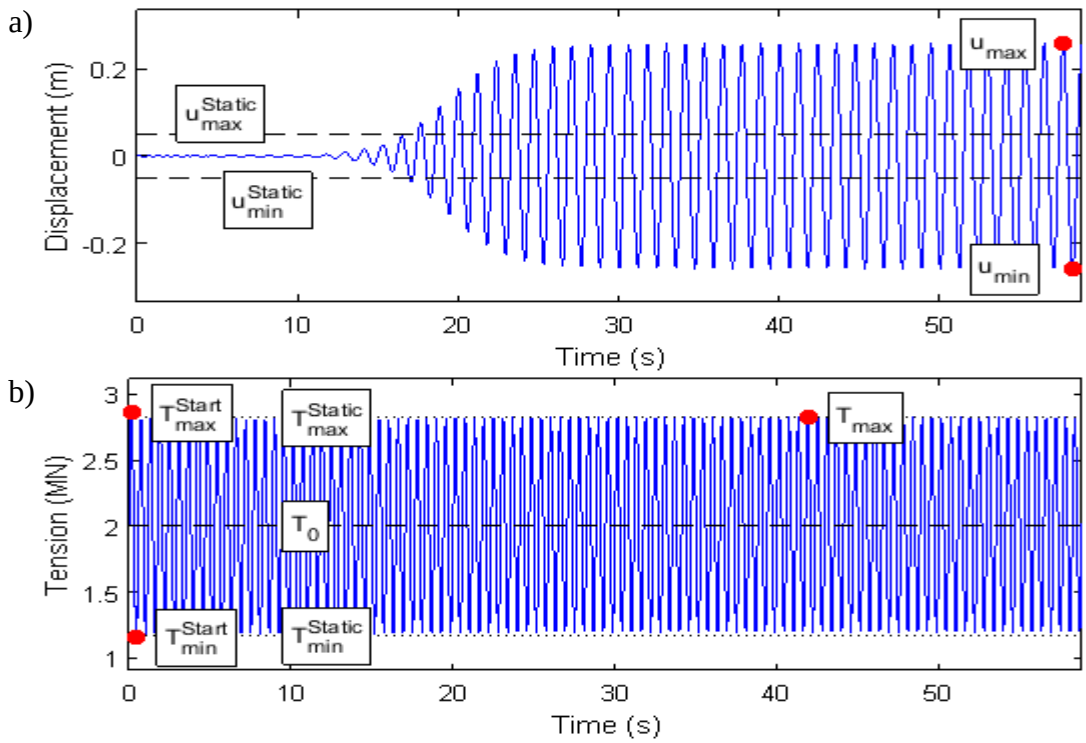

Figure B6. Results for harmonic support motion (FR = 2; A = 0.03 m) including hydrodynamic effects; a) Lateral displacement at mid-span; b) Tension at support

Figure B7 shows the instability diagram of the submerged cable in terms of lateral displacements. Compared to Figure B4 the area of the instability tongues is smaller. In other words, more *FR* and *A* combinations give a stable solution and can be attributed to the additional energy dissipation of the hydrodynamic effects. Having said this, there are still some very significant instability regions that lead to excessive lateral vibrations of the cable.

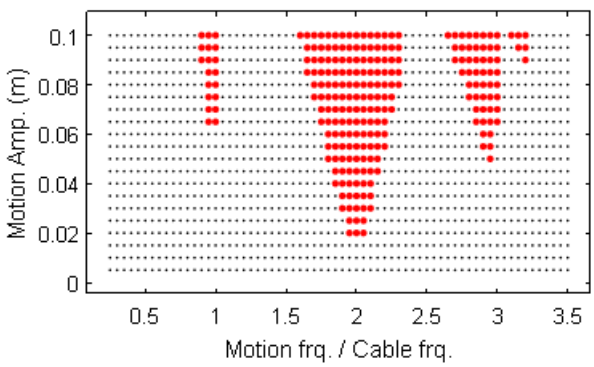

Figure B7. Instability diagram for submerged cable

The effects on tension are evaluated in Figure B8. There is a clear correlation between instability tongues from Figure B7 and DAF values in Figure B8a. However, the maximum DAF for all amplitudes and excitation frequencies considered is very small, reaching a value of only 1.015. This means that the maximum tension is only 1.5% greater than that of the static case. On the other hand, the DRF in Figure B8b are very similar to those reported in Figure B5b for the dry cable. But this is due to the fact that in general DRF are very close to the unity.

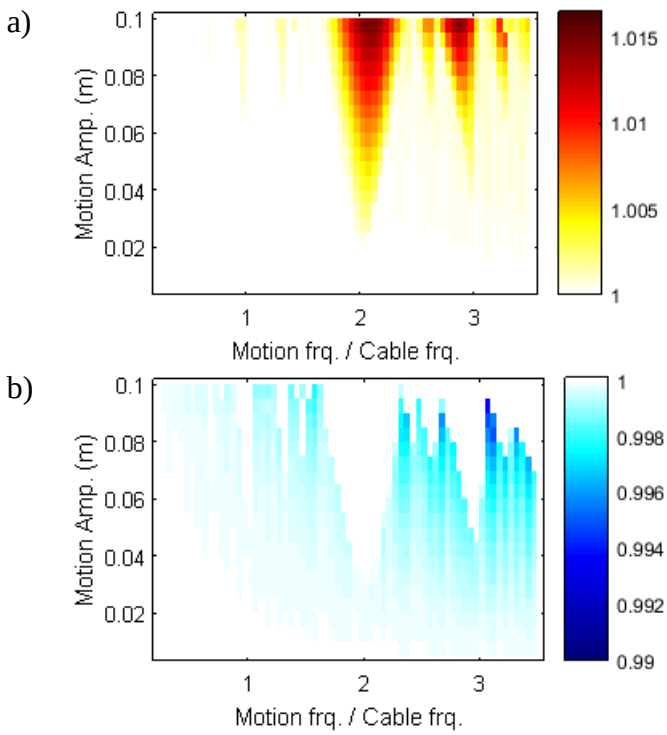

Figure B8. Normalized extreme tension for submerged cable; a) Maximum (DAF); b) Minimum (DRF)

B5. Conclusions

This paper revisits the problem of parametric excitation of mooring lines with special emphasis on the cable tension and considering the influence of hydrodynamic effects. A numerical model of a mooring line is used and a harmonic support motion is imposed. A wide range of excitation amplitudes and frequencies are considered. The results clearly show the existence of parametric resonance that induces large lateral displacements. However, the consideration of the hydrodynamic effects greatly reduces the extent of those vibrations. The maximum and minimum cable tensions are studied in terms of DAF and DRF, which are normalized dynamic factors that allow us to quickly assess the extreme tension values with respect to the static case. Even though the tension values show some correspondence with the instability diagrams, their numerical values are remarkably small. The maximum DAF value is 1.38 for the dry cable and reduces to a barely significant value of 1.015 when including the hydrodynamic effects. As for DRF, similar values are obtained for either the dry or the submerged cable, obtaining a minimum value of 0.99. This indicates that there is almost no reduction in the minimum cable tension compared to the static case. Therefore, there is no risk for cable breakage or slack cable if the static design of the mooring line is done with sufficient safety margins.

Acknowledgements

The research presented in this manuscript was possible thanks to the financial support of The Fjord Crossing research program for the Coastal Highway Route E39.

References

[B1] Nayfeh A.H. and Mook D.T. *Nonlinear Oscillations*. Weinheim : Wiley-VCH; 2004.

[B2] Cantero D., Rønnquist A. and Naess A. Parametric Excitation of Mooring Cables for Submerged Floating Tunnels. *Proceedings of IABSE Conference*, Guangzhou; 2016.

[B3] Chatjigeorgiou I.K., Xiros N.I. and Mavrakos S.A. Coupling Contributions and Effect of Mathieu Instabilities in the Dynamic Behaviour of Vertical Elastic Cables and Risers. *Proceedings of the WSEAS conference*, Corfu; 2004.

[B4] Brown D.T. and Mavrakos S. Comparative Study on Mooring Line Dynamic Loading. *Marine Structures*. 1999; **12**: 131-151.

[B5] Lilien J.L. and Pinto Da Costa A. Vibration Amplitudes caused by Parametric Excitation of Cable Stayed Structures. *Journal of Sound and Vibration*. 1994; **174**(1): 96-90.

[B6] Journée J.M.J. and Massie W.W. *Offshore Hydromechanics*. Delft: Delft University of Technology; 2001.

[B7] Det Norske Veritas SA. *Recommended Practice DNV-RP-C205: Environmental Conditions and Environmental Loads*. 2014.

[B8] ABAQUS. *Analysis user's manual*. Providence: Dassault Systèmes; 2011.

Appendix C - Recent Studies of Parametrically Excited Mooring Cables for Submerged Floating Tunnels

Conference paper:
D. Cantero, A. Rønnquist, A. Naess. "Recent studies of parametrically excited mooring cables for submerged floating tunnels". 2nd International Symposium on Submerged Floating Tunnels and Underwater Tunnel Structures, SUFTUS 2016, December 2016, Chongqing, China. DOI: 10.1016/j.proeng.2016.11.571

Title:
Recent Studies of Parametrically Excited Mooring Cables for Submerged Floating Tunnels

Abstract:
Most current designs for Submerged Floating Tunnels (SFT) include a mooring system to fix the position of these floating structures. Long period waves, such as swell waves, parametrically excite the system and might result in excessive vibrations in the cable. This paper presents two distinct studies. First, an analytical investigation of the system's stability is performed to derive a closed-form expression, which allows for a quick evaluation of the system's stability. This expression is obtained through the Harmonic Balance Method (HBM) with two harmonic terms. The contribution of multiple modes of vibration is investigated for the case of small sag to span ratios. The expression is compared with the results from a numerical model, revealing the applicability of the proposed formulation. The second study investigates the tension in the mooring line during parametric excitation. Correct design should avoid excessive forces that might break the line or very small forces that lead to momentarily slack cables. Thus, the aim of this study is to assess the validity of using the stability charts for the design of mooring lines with respect to safe levels of cable forces. This is achieved through the numerical analysis of a cable model using Abaqus. Cable vibrations and cable forces are compared for a range of amplitudes and frequencies of the support motions.

Nomenclature

A	support motion amplitude	T	support motion period
B_i	auxiliary expression	TC	Transition Curve
c	cable internal damping	$y(x,t)$	cable displacement
C_i	auxiliary expression	$y_0(x)$	static deformation of cable
DAF	Dynamic Amplification Factor	$Y_j(t)$	generalized coordinate
DRF	Dynamic Reduction Factor	α	cable inclination angle
E	material Young's modulus	$\Delta N(t)$	variation in cable tension
L	Length of cable	λ^2	Irvine's parameter
m	mass per unit length	$\Phi_j(x)$	mode of vibration
N	cable tension	ω	fundamental frequency of cable
SFT	Submerged Floating Tunnel	Ω	support motion frequency

C1. Introduction

The Norwegian government has decided to eliminate all ferries along the coastal highway E39 in order to reduce travel time and boost local economy. This route crosses several fjords and there are currently eight ferry connections in operation to cross them. There are 5 fjord crossings where fixed links are to be built with widths over 2 km (up to 5 km) and depths over

500 m (up to 5 km), where non-conventional engineering solutions will be necessary. One of the proposed solutions is the construction of a submerged floating tunnel (SFT), that, when built, will be the first of its kind worldwide. The preliminary studies have suggested a variety of possibilities with different cross sections and floating devices. However, any viable solution will need a mooring system to maintain the structure in the prescribed position (Fig. C1). The main environmental load in such a system will be the long period swell waves. This low frequency excitation produces a parametrically excited system. Certain situations might lead to parametric resonance or dynamic instability that causes excessive vibrations of the cable and the SFT.

a b

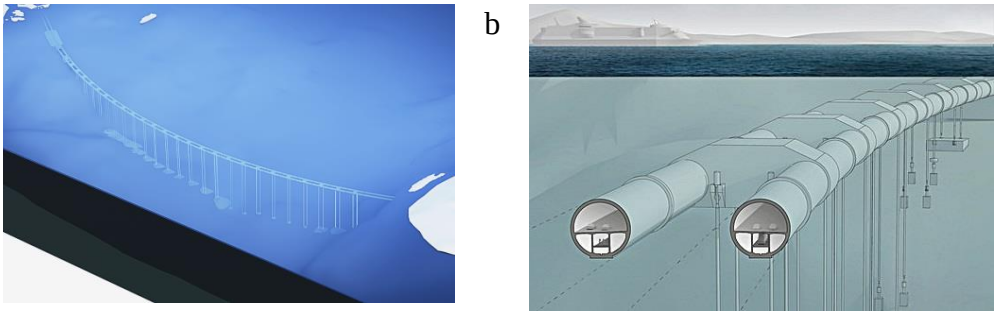

Fig. C1. Submerged Floating Tunnel; (a) General view; (b) Cross-section; (Source: Snøhetta).

Parametric Excitation (PE) has been extensively studied in the field of differential equations and dynamic systems, [C1] being one representative example. In bridge engineering this phenomenon has often been reported in cable stayed bridges [C2] when girder or mast oscillations parametrically excite the cables. Similarly, in offshore platforms, parametric instability is an important aspect in the design of safe deep-water risers subjected to dynamic loads [C3] and is still a hot research topic [C4]. In the same way, in [C5] the effect of PE on moored SFTs is analyzed. However, most of the published studies on parametric excitation in cables investigate exclusively the lateral displacements. Only a few of them examine also the cable tension. A very good example is [C2] that provides qualitative explanations of various parametric resonances in a dry cable based on numerical simulation results. The relation between lateral displacements and cable tension under parametric resonance is not straightforward, particularly when considering non-linear effects. To the best of the authors' knowledge there is no study that explicitly investigates the tension of cables under parametric resonance including hydrodynamic effects. It is particularly interesting to evaluate the extreme cable stresses developed during parametric resonance. Very high cable tension might produce cable breakage. On the other hand, very small or no cable tension might result in momentarily slack cables, which might induce large impulse forces on the moored structure when it changes back to a taught line. Furthermore, the difference between the maximum and the minimum stresses defines the amplitude of the load cycle which is a fundamental parameter in correct assessment of the fatigue life.

The aim of this paper is to introduce the studies currently being performed by the structural dynamics group at the Norwegian University of Science and Technology (NTNU). A summary of the most important findings published in [C6, C7] is provided. Two distinct studies are reported in this document. The first study shows the derived analytical expression of the transition curves, which allows for a quick identification of the system's stability. This expression is obtained through the Harmonic Balance Method (HBM) with two harmonic terms. The contribution of multiple modes of vibration is investigated for the case of small sag to span ratios. The expression is compared with the results from a numerical model, revealing the applicability of the proposed formulation. The second study focuses on the cable tension of

the mooring system during parametric excitation. The validity of using the stability charts for the design of mooring lines with respect to safe levels of cable forces is assessed. This is achieved through the numerical analysis of a cable model. Cable vibrations and cable forces compared for a range of amplitudes and frequencies of the support motion.

C2. Instability analysis

This section derives the analytical expression of the Transition Curves (TC), which define the boundaries between stable and unstable solutions of a cable under parametric excitation. Then the expression is compared to the results obtained from a numerical model.

C2.1 Equations of motion

A mooring line of an SFT can be modelled as a cable suspended between two points. The wave loading excites the submerged structure inducing oscillations on one of the cable ends. This is represented as a cyclic imposed displacement of the upper boundary condition (Fig. C2a). The equation of motion can be derived considering a differential element of the cable, establishing the dynamic equilibrium and using D'Alembert's principle:

$$m\frac{\partial^2 y}{\partial t^2} + c\frac{\partial y}{\partial t} - \left(N + \Delta N(t)\right)\frac{\partial^2 y}{\partial x^2} - \Delta N(t)\frac{\partial^2 y_0}{\partial x^2} = 0 \tag{C1}$$

The equation can be solved by separation of variables, in which it is assumed that the solution is in the form of Eq. (C2), where $Y_j(t)$ are the generalized coordinates and the $\Phi_j(x)$ the modes of vibration.

$$y(x,t) = \sum_{j=1}^{n} Y_j(t)\phi_j(x); \qquad \phi_j(x) = sin\left(\frac{j\pi x}{L}\right) \tag{C2}$$

The variation of the tension in the cable is proportional to the cable length increment, which is equal to the combined contribution of three terms, as seen in Eq. (C3). First, the cable length increment is equal to the displacement of the boundary condition along the cable chord. For displacements perpendicular to cable chord it can be approximated using a Taylor expansion and including the terms up to second degree. Similarly, the increment in length due to the cable dynamic deformation is approximated upon Taylor expansion and discarding higher order terms.

$$\Delta N(t) = \frac{EA}{L}\left(\Delta x(t) + \frac{\Delta y(t)^2}{2L} + \sum_{j=1}^{n}\frac{j^2\pi^2 Y_j(t)^2}{4L^2}\right) \tag{C3}$$

Applying Galerkin's method [C2], the partial differential equation (Eq. (C1)) is transformed into a system of second order differential equations. The general case is a set of coupled Mathieu equations. However, the coupling terms are small when the relation between sag and span is small [C2]. This condition can be expressed in terms of Irvine's parameter λ^2 [C8] that quantifies the relative importance of elastic and geometric effects. When $\lambda^2 < 0.1$, the system of equations can be uncoupled, obtaining a second order differential equation for each mode-*j*:

$$mL^2\ddot{Y}_j + cL^2\dot{Y}_j + \frac{j^4\pi^4 EA}{4L^2}{Y_j}^3 + j^2\pi^2\left(N + \frac{EA\,\Delta x}{L} + \frac{EA\,\Delta y^2}{2L^2}\right)Y_j = 0 \tag{C4}$$

The support's displacement in time is assumed to be harmonic with frequency Ω and amplitude A, which can be written in terms of the cable's inclination angle α as follows:

$$\Delta x(t) = A\, sin(\alpha)\, cos(\Omega t); \qquad \Delta y(t) = A\, cos(\alpha)\, cos(\Omega t) \tag{C5}$$

C2.2 Analytical solution

Eq. (C4) is the non-linear Mathieu equation where the excitation appears as time-varying coefficients [C1] or parameters, thus called parametric excitation. A small parametric excitation can generate an unbounded solution (unstable solution). It is of great importance to identify when instability might occur. The boundaries that separate the stable from unstable solutions are termed Transition Curves (TC). One possibility to calculate the TC is through the Harmonic Balance Method (HBM) that essentially approximates the solution to Eq. (C4) as a Fourier series (Eq. (C6)). Because the phase shift is unknown, both *sin* and *cos* must be included [C2].

$$Y_j(t) = \sum_{n=0}^{M} \Upsilon_{(2n-1)}\, sin(n\Omega t) + \Upsilon_{2n}\, cos(n\Omega t) \tag{C6}$$

Substituting Eq. (C6) into Eq. (C4), multiplying the result by the basis $\{\sin(\Omega t), \cos(\Omega t), \ldots, \sin(n\Omega t), \cos(n\Omega t)\}$, integrating over one full cycle and balancing harmonic terms gives a system of equations with the Fourier coefficients Υ_i as the unknowns. Solutions of the system provide the Fourier coefficients that define periodic solutions for Eq. (C4). The transition curves are thus defined when the determinant of the coefficient matrix of the system is zero. The number of harmonic terms considered M defines the accuracy of the solution. In the literature only one term is generally considered. However, here two terms are considered ($N = 2$) because there is a significant increase in accuracy. Analytical expressions for the TC are obtained with the aid of symbolic calculation software [C9]. Two separate expressions are defined in Eq. (C7) and Eq. (C8), corresponding to periods 2π and 4π, which correspond respectively to the sum of all even and odd n values in Eq. (C6) respectively. See the Appendix for complete definition of the auxiliary expressions B_i and C_i.

$$A = \pm B_1 \left(2L\sqrt{B_2(B_3 \pm \sqrt{B_4})} \right) \; for\; T = 2\pi \tag{C7}$$

$$A = \pm C_1 \left(L\sqrt{2}\sqrt{C_2 \pm \sqrt{C_3}} \right) \; for\; T = 4\pi \tag{C8}$$

The expressions of the TC can be used to calculate the stability regions associated to any mode of vibration j. Fig. C2b shows the stability chart derived from the analytical expressions for mode-j without damping.

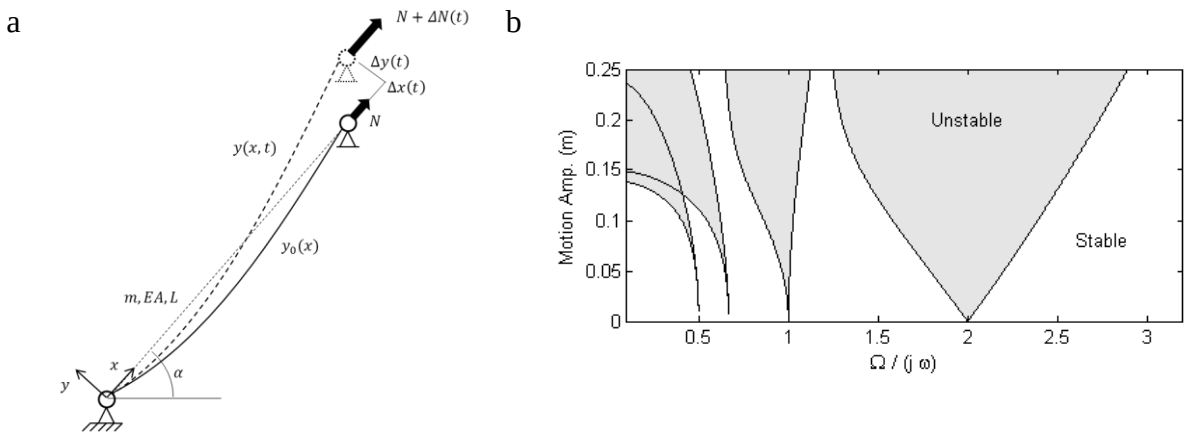

Fig. C2. (a) Sketch of mooring line model; (b) Analytical stability tongues for mode-j.

C2.3 Numerical validation

The expressions derived in previous section allow us to identify situations that would produce large displacements in the mooring line due to harmonic movements of one of the boundary conditions. However, the analytical expression is only an approximation that needs to be compared against a numerical solution of the problem at hand. Therefore, a mooring line was modelled with ABAQUS [C10] considering geometric nonlinearities. The cable is submerged in water and is thus influenced by drag forces and additional mass effects. These effects have been included by means of the Morison Equation using the toolbox AQUA provided by the software. Two important parameters are necessary, namely the added mass coefficient C_A and the drag coefficient C_D whose numerical values are 1 and 1.5 respectively as recommended in [C11]. The particular cable properties used in this study are provided in Table C1.

Table C1. Numerical values of cable properties.

Symbol	Description	Value	Unit
L	Length	100	m
E	Young's modulus	$210 \cdot 10^9$	N/m^2
A	Area	785.40	cm^2
δ	Density	7800	kg/m^3
ε	Damping	0.1	%
N	Initial tension	$2 \cdot 10^6$	N
f_1	Fundamental frequency	0.8493	Hz

The analytical expression derived in Section C2.2 is compared against the numerical solution in Fig. C3. In order to find the analytical stability map for our model it is necessary to consider the contribution of several modes. This can be achieved by superimposing as many modes as deemed necessary. Fig. C3 shows the stability chart for the particular cable defined in Table C1 considering 7 modes and 5% damping. The formulation allows us to easily include the contribution of higher modes of vibration. In particular it is important to include the first and second instability regions of each mode. The numerical stability map is obtained analyzing the results from 1320 separate simulations for a range of excitation frequencies and amplitudes. In particular, the ratio Ω/ω is varied in a discrete space with values from 0.25 to 3.5 in increments of 0.05, whereas the considered amplitudes are from 0.005m to 0.1m in 0.005m increments. It can be seen that there is a good match between the stability predictions derived from the closed-form expressions and the numerical solution.

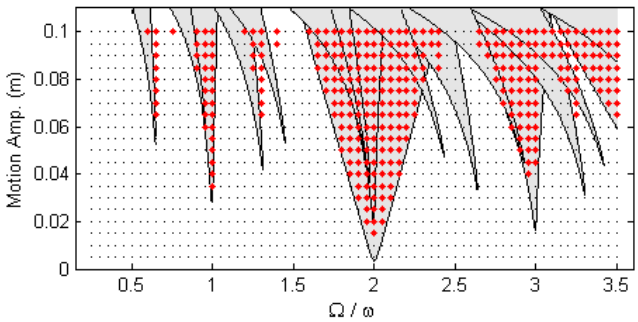

Fig. C3. Stability chart for 7 modes of vibration (shaded areas). Numerical solutions: small black dot = stable; big red dot = unstable.

C3. Mooring line tension

This section analyzes the tension of the mooring line during parametric excitation. First, one particular example is shown to illustrate the different effect of parametric resonance on different load effects, namely lateral displacements and total cable tension. Then the extreme values of tension are investigated for the same range of motion amplitudes and frequencies as in Section C2.3.

C3.1 Tension during parametric resonance

One particular situation is shown in Fig. C4 that corresponds to the mooring line with a support motion with a frequency ratio (Ω/ω) of 2 and an amplitude A of 0.1 m. Fig. C4a shows the lateral displacements at the mid-span of the cable. For graphical reference, the maximum and minimum static vertical displacements are shown (u_{max}^{Static} and u_{min}^{Static}), which correspond to A and -A. Note that the time-history corresponds to lateral displacements, whereas the references are for vertical displacements. Even though the results are for different directions it is still useful to compare how much bigger the displacements are compared to the support motions in a parametric resonant situation. The time-history shows the typical response for such a system under parametric resonance. The displacements grow exponentially over time until a certain maximum (or minimum) value is reached. For this particular case the maximum displacement is 0.5068 m while the amplitude of the support motion is only 0.1 m, this is more than 5 times greater.

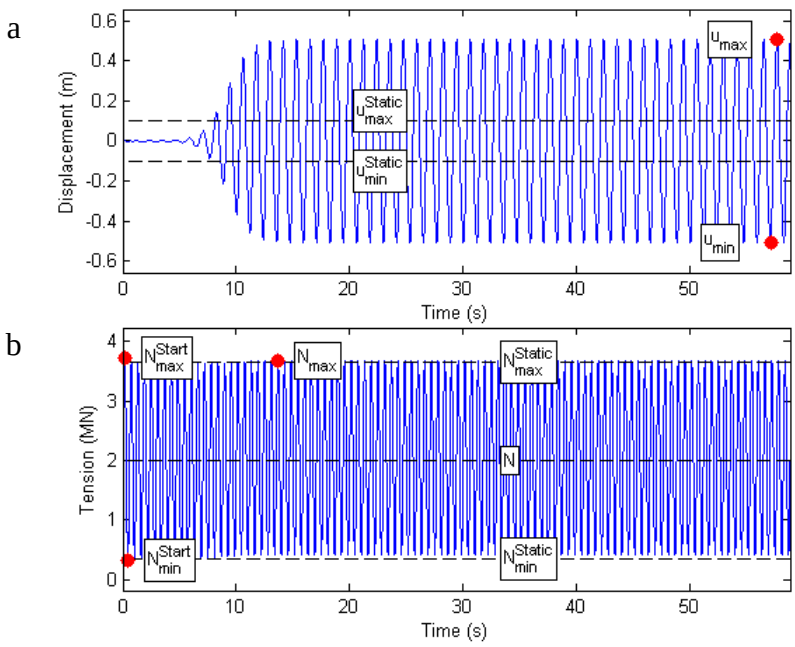

Fig. C4. Results for harmonic support motion (Ω/ω= 2; A = 0.1 m) a) Lateral displacement at mid-span; b) Tension at support.

Intuition would suggest that the internal cable tension should have a similar evolution in time, or at least feature some significant growth at the same time as those reported for the displacements. But this is not the case. Fig. C4b shows the time-history of the total tension at the upper support. For reference, the initial cable tension N is shown, also the static tension for situations with the maximum and minimum support displacements are indicated respectively as N_{max}^{Static} and N_{min}^{Static}. It can be seen that the tension values are barely affected by the parametric resonance. There is only a slight increase of the maximum tension. At the same time, the minimum tension values are greater than N_{min}^{Static} during steady-state. This means that during parametric resonance the possibility of reaching a slack cable situation actually reduce. It has to be noted that higher (and lower) values of tension are obtained at the very beginning of each of the simulations. This is due to the sudden start of the support motion, which produces a small temporary increase of the tension and indicated as N_{max}^{Start} and N_{min}^{Start} in Fig. C4b. These extreme tension values are not really interesting for our analysis and are only a consequence of the way of modelling the problem. In reality, the amplitude of the support motion will grow gradually. For this reason, the first 10 cycles of each simulation are neglected when calculating the maximum (and minimum) tension values.

C3.2 Parametric study

To analyze the changes in tension it is convenient to define them in terms of dynamic factors. Here two distinct factors are used to clearly differentiate the results between maximum tension and minimum tension. The factor is a normalization of the extreme values of the tension with respect to the calculated extreme static response corresponding to the extreme support motions. We define Dynamic Amplification Factor (DAF) and Dynamic Reduction Factor (DRF) in Eq. (C9). For the maximum tension DAF is greater than or equal to one. Conversely, the factor for the minimum (DRF) is smaller than or equal to one. These factors allow us to study the problem from the static design perspective. The mooring line can be studied statically based on the expected support motion amplitude and then factored to obtain the maximum and minimum tension values.

$$DAF = \frac{N_{max}}{N_{max}^{Static}} \geq 1; \qquad DRF = \frac{N_{min}}{N_{min}^{Static}} \leq 1 \tag{C9}$$

It is interesting to explore how the instability diagram for lateral displacements (Fig. C3) relates to the maximum and minimum cable tensions. Fig. C5a shows the maximum cable tension in terms of DAF. Some of the instability tongues reported in Fig. C3 can also be seen here. However, the maximum DAF for any Ω/ω and A combination is 1.0165, which means that the maximum total tension (static + dynamic) is only 1.65% greater than the maximum static. But it is even more interesting to study the DRF as presented in Fig. C5b. The minimum tension in the cable is either equal to the minimum static or just slightly smaller. This is reflected in the DRF values that have an absolute minimum value of 0.9937. This is, the minimum tension is 99.37% of the minimum static, or in other words, there is only a 0.67% reduction of the total tension when compared to the static one. The instability tongues in Fig. C3 can also be seen in Fig. C5b but, in this case, the values of DRF during parametric resonance are equal to one. As seen before in Fig. C4b, during parametric resonance the minimum tension grows above the minimum static value, hence achieving a value of 1 for the DRF.

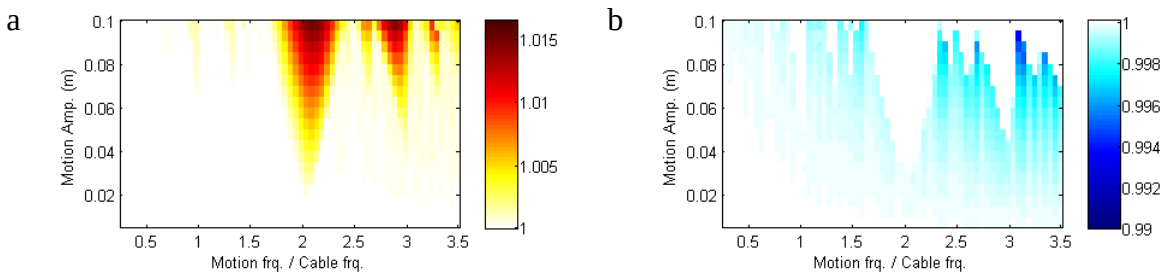

Fig. C5. Normalized extreme tension for submerged cable; (a) Maximum (DAF); (b) Minimum (DRF).

C4. Conclusion

This paper revisits the problem of parametric excitation of mooring lines. First, by means of the Harmonic Balance Method, an analytical expression of the unstable configurations has been obtained. The formulation allows for the contribution of multiple modes of vibration in situations with small sag to span ratios. The formulation is then validated against the results from a numerical model. The analytical expression can easily be integrated in the design process to avoid situations that might lead to parametric excitation.

The second study investigated the cable for a wide range of excitation amplitudes and frequencies. The maximum and minimum cable tensions are studied in terms of DAF and DRF, which are normalized dynamic factors that allow us to quickly assess the extreme tension values with respect to the static case. Even though the tension values show some correspondence with the instability diagrams, their numerical values are remarkably small. The results clearly show small increase/reduction in the maximum/minimum cable tension compared to the static case. Therefore, there is no risk for cable breakage or slack cable if the static design of the mooring line is done with sufficient safety margins.

Acknowledgements

The research presented in this manuscript was possible thanks to the financial support of The Fjord Crossing research program for the Coastal Highway Route E39.

C. Appendix

Auxiliary expressions in Eq. (C7):

$$B_1 = \frac{1}{\pi^3 E A B_2} \tag{C.A1}$$

$$B_2 = 8L^2\Omega^2 m - 3N\pi^2 \tag{C.A2}$$

$$\begin{aligned} B_3 = {} & 16L^6\Omega^6\pi^2 m^3 + 4L^6\Omega^4\pi^2 c^2 m - 28L^4 N\Omega^4\pi^4 m^2 \\ & -2L^4 N\Omega^2\pi^4 c^2 + 14L^2 N^2\Omega^2\pi^6 m - 2N^3\pi^8 \end{aligned} \tag{C.A3}$$

$$\begin{aligned} B_4 = {} & 256L^{12}\Omega^{12}\pi^4 m^6 + 128L^{12}\Omega^{10}\pi^4 c^2 m^4 - 768L^{10}N\Omega^{10}\pi^6 m^5 \\ & +16L^{12}\Omega^8\pi^4 c^4 m^2 - 128L^{10}N\Omega^8\pi^6 c^2 m^3 + 864L^8 N^2\Omega^8\pi^8 m^4 \\ & +16L^{10}N\Omega^6\pi^6 c^4 m + 36L^8 N^2\Omega^6\pi^8 c^2 m^2 - 464L^6 N^3\Omega^6\pi^{10} m^3 \\ & -8L^8 N^2\Omega^4\pi^8 c^4 + 16L^6 N^3\Omega^4\pi^{10} c^2 m + 129L^4 N^4\Omega^4\pi^{12} m^2 \\ & -7L^4 N^4\Omega^2\pi^{12} c^2 - 18L^8 N^5\Omega^2\pi^{14} m + N^6\pi^{16} \end{aligned} \tag{C.A4}$$

Auxiliary expressions in Eq. (C8):

$$C_1 = \frac{1}{4EA\pi^4} \tag{C.A5}$$

$$C_2 = 99L^4\Omega^4\pi^4 m^2 + 12L^4\Omega^2\pi^4 c^2 - 152L^2 N\Omega^2\pi^6 m + 48N^2\pi^8 \tag{C.A6}$$

$$\begin{aligned} C_3 = {} & 9477L^8\Omega^8\pi^8 m^4 + 936L^8\Omega^6\pi^8 c^2 m^2 - 27216L^6 N^1\Omega^6\pi^{10} m^3 \\ & -432L^8\Omega^4\pi^8 c^4 - 1344L^6 N\Omega^4\pi^{10} c^2 m + 25056L^4 N^2\Omega^4\pi^{12} m^2 \\ & -1408L^4 N^2\Omega^2\pi^{12} c^2 - 9472L^2 N^3\Omega^2\pi^{14} m^2 + 1280N^4\pi^{16} \end{aligned} \tag{C.A7}$$

References

[C1] A.H. Nayfeh, D.T. Mook,Nonlinear Oscillations, Wiley-VCH, Germany, 2004.

[C2] J.L. Lilien, A. Pinto Da Costa, Vibration amplitudes caused by parametric excitation of cable stayed structures, J. Sound Vib. 174 (1994) 69-90.

[C3] F. Xiao, H.Z. Yang, Probabilistic assessment of parametric instability of a top tensioned riser in irregular waves, J. Marine Sci. Tech. 19 (2014) 245-256.

[C4] H. Yang, F. Xiao, P. Xu, Parametric instability prediction in a top tensioned riser in irregular waves. Ocean Eng. 70 (2013) 39-50.

[C5] S.N. Sun, Z.B. Su, Parametric vibration of submerged floating tunnel tether under random excitation. China Ocean Eng. 25 (2011) 349-356.

[C6] D. Cantero, A. Rønnquist, A. Naess, Parametric excitation of mooring cables for submerged floating tunnels, IABSE conference, May 2016, Guangzhou, China.

[C7] D. Cantero, A. Rønnquist, A. Naess, Study of tension in mooring cables under parametric excitation for submerged floating tunnels, 19th IABSE Congress, September 2016, Stockholm, Sweden.

[C8] M. Irvine. Cable Structures, The MIT Press, Cambridge, USA, 1981.

[C9] MAPLE 18, Maplesoft, a division of Waterloo Maple Inc. Waterloo, Ontario.

[C10] ABAQUS, Analysis user’s manual, Dassult Systemes, Providence, 2011.

[C11] Det Norske Veritas SA, Recommended Practice DNV-RP-C205: Environmental Conditions and Environmental Loads, 2014.

Appendix D - Tension during parametric excitation in submerged vertical taut tethers

Journal article:
D. Cantero, A. Rønnquist, A. Naess. “Tension during parametric excitation in submerged vertical taut tethers”. Applied Ocean Research, Vol. 65, pp. 279-289, 2017. DOI: 10.1016/j.apor.2017.05.002

Title
Tension during parametric excitation in submerged vertical taut tethers

Abstract
The construction of a suspension bridge with floating pylons or a submerged floating tunnel requires the installation of a mooring system. The option of taut vertical tethers, similar to those used in tension-leg platforms, has been suggested in preliminary designs. The environmental loading on the tether, mainly due to wind waves and swell, results in a parametrically excited system. Certain loading conditions develop instabilities that translate into large horizontal motion. However, the effects of parametric resonance on the tension values have rarely been investigated. This paper aims to clarify the relation between lateral displacement and tether tension and to quantify the extreme tension values in the event of parametric resonance. The presented analysis is based on a full numerical model of the tether that includes geometric and hydrodynamic nonlinear effects. This model is used to investigate a representative example that illustrates parametric resonance and multiple parametric studies to assess the effects of the excitation frequency, amplitude, initial pretension, tether length and inclination angle on the tether’s response. The results reported here provide the basis for a recommendation on designing a tether under parametric resonance regarding the ultimate extreme values and fatigue life.

D1. Introduction

The National Roads Authority (NRA) in Norway is planning to cross several fjords along the west coast of the country as part of the “Ferry-free E39” project [D1]. These crossings are characterized by large widths (up to 5 km) and depths (up to 1 km) that require unconventional engineering solutions. The preliminary designs suggest the construction of floating suspension bridges and submerged floating tunnels, as illustrated in Figure D1. A floating bridge is not a new idea and several examples can be found worldwide [D2]. However, no precedent exists of a suspension bridge with multiple floating towers. A submerged floating tunnel is a structural concept that has been considered several times during the last century [D3]; this tunnel essentially consists of a watertight buoyant tube at a certain depth underwater. To date, no such structure has ever been built. Both a long floating bridge and a submerged floating tunnel require a mooring system (Figure D1) to position these floating structures and to resist any imposed motion due to environmental loading. Since these structures would be located near the end of the fjord next to the sea, they would be exposed to sea states with wind waves and swell. In particular, swells have a long period and can last for several hours with effects that decrease linearly with water depth. There are concerns that these environmental loads can parametrically excite the tethers of the mooring system, leading to parametric resonance or Mathieu instability.

a) b)

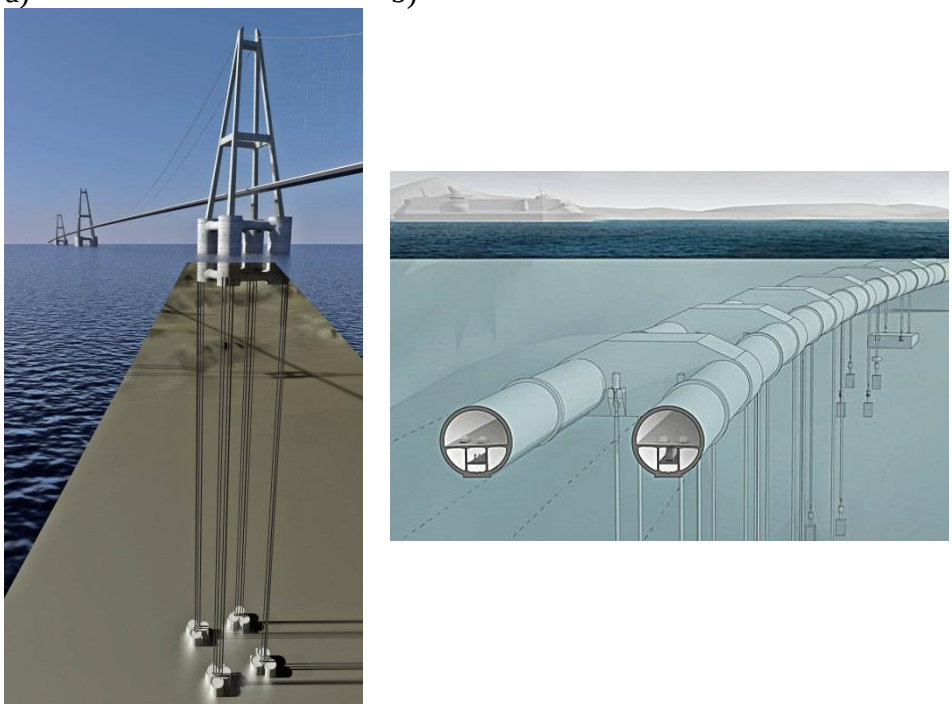

Figure D1: a) Floating cable-stayed bridge (Source: The Norwegian Public Roads Administration; https://flic.kr/p/pcgEt3); b) Submerged floating tunnel (Source: Snøhetta; https://flic.kr/p/yGeftB)

The taut mooring systems proposed in Figure D1 are similar to those used in Tension-Leg Platforms (TLP), which are usually made of steel tubes [D4]. These tension pipes or tethers are designed to avoid slack cable configurations while also considering the peak and fatigue loading conditions [D5]. As a result, these tethers have high pretension levels, zero net buoyancy and such massive dimensions that they cannot be considered to be compliant in the axial direction [D4]. The environmental loads on the bridge towers or the submerged tunnel lead to varying tension levels and imposed motions on the tether that define a parametrically excited system.

A tether excited by harmonically varying imposed displacements of one of its ends is a parametrically excited system. Under certain conditions, parametric excitation leads to parametric resonance, which is an unstable situation that produces excessive lateral motion. The principal parametric resonance occurs when the frequency of the upper support motion is twice the fundamental frequency of the tether, i.e., a 2:1 frequency ratio. However, there are many more frequencies that induce instability in the system. Reasonably small amplitudes of anchorage oscillations may lead to important steady-state tether responses [D6,D7]. Furthermore, the greater the amplitude of the support motion is, the more frequencies there are that lead to unstable motion. Parametric excitation has been extensively studied in the field of differential equations and dynamic systems [D8] and is generally described by the nonlinear Mathieu equation, where the excitation appears as time-varying coefficients. In bridge engineering, this phenomenon has been theoretically studied [D6], investigated in laboratory experiments [D7] and examined in cable-stayed bridges [D9] where girder or mast oscillations have parametrically excited the stay cables.

The response of a submerged tether differs significantly to that of a dry tether because of the influence of hydrodynamic drag, which is the most important nonlinear contribution [D10] and

acts as an additional line damping component. Moreover, it has been shown [D11,D12] that the out-of-plane motion can be neglected when calculating the response of submerged slender structures. For a tether in an unstable condition, the quadratic fluid damping force limits the amplitude of the lateral motion [D13]. An example of instability analysis for TLP tethers is given in [D14]. Reference [D15] derives an approximate analytical expression of tether displacements including hydrodynamic effects for principal parametric resonance. Additional literature reviews of the instabilities of risers and immersed slender structures can be found in [D16,D17].

The majority of the publications that have studied the parametric excitation of cables (either dry or submerged) mainly focus on lateral motion. As indicated in [D18], tension has been overlooked in many studies. However, displacement is not the most important load effect. In fact, tension and stress values are of greater relevance when designing a taut mooring line. Some publications have specifically investigated tension to some extent. For example, reference [D6] numerically shows how tension values develop on a dry cable during parametric excitation. In addition, [D19] studies numerically tension using an experimentally validated model, while [D18] shows that to achieve correct tension values, the model must account for spatiotemporal variations of tension along the cable. Moreover, [D20] shows that the difference in magnitude (in spatial distribution) between the maximum and minimum tensions increases for a cable with significant sag. Furthermore, [D21] concludes that the increase in pretension is ultimately equivalent to the increase in damping. In addition, [D22] includes tension in the numerical analysis and states the need for understanding the impacts of parametric excitation. In [D12], the dynamic tension values are measured for a submerged cable with sag in a scaled laboratory experiment, and recommendations are provided for the scaling and the support's boundary conditions. Other examples in the literature study the cable tension, but they do not consider the particular case of parametric excitation. For instance, [D23] derives an approximate analytical expression of dynamic cable tension, and [D24] obtains an analytical approximation of the probability distribution of the dynamic tension envelope for a random sea state. Therefore, even though some investigations have considered tether tension, additional studies are needed to characterize parametrically excited taut mooring systems.

Correct tether design should include the fatigue limit state [D25] to avoid failure due to crack growth initiated from a welded joint in the tether. Detailed fatigue design recommendations can be found in [D26]. The magnitude of the stress cycle and the number of load cycles are the key parameters that determine the accumulated fatigue damage of the studied member. However, based on the studies published to date, it is not possible to assess correctly the stress values of a taut mooring line with parametric resonance or its effects on the tether's fatigue life. The total stress in a tether is the combined result of several load effects, namely the axial load, bending moments and hydrostatic pressures. In most parts of the tether's length, the main contributor to the stress is the total (static + dynamic) tension, whereas bending moment has only a marginal effect [D25]. On the other hand, bending moments can be very important near the tether ends. It is important to note, that this study does not evaluate all the aspects required for the design of a tether. The scope of this study is limited to the study of tension.

Therefore, the goal of this paper is to provide a clear description of parametric excitation on taut mooring lines with an emphasis on tension values; additionally, special attention is given to extreme tether tension values. Very high cable tension could produce tether breakage, while very small or no tether tension could result in a momentarily slack member, which might induce large impulse forces on the moored structure when the cable becomes a taut line again. Moreover, a better understanding of the difference between the maximum and the minimum

tension will allow us to suggest appropriate design procedures with respect to the tether's fatigue life. This paper also aims to clarify the relation between lateral displacement and tether tension in the event of parametric resonance. The presented analysis is based on a full numerical model of the tether that includes geometric and hydrodynamic nonlinear effects, which are difficult to include in an analytical study. In addition, realistic tether properties are used that are taken from preliminary designs of floating bridges and submerged floating tunnels.

The rest of the document starts with a description of the numerical model used in the study in Section D2. Then, based on the results from an example with a 2:1 frequency ratio, Section D3 clearly presents how parametric excitation originates and provides important comments on several aspects of the problem. Next (Section D4), a stability analysis for a wide range of frequency ratios and amplitudes is performed in terms of lateral displacements, total tension values and fatigue life calculations. The last section (Section D5) is a parametric study on three of the main design variables, namely, initial pretension, tether length and inclination angle.

D2. Numerical model

Each tether of a mooring system can be modelled as a submerged beam. In addition, the wave loading on the bridge towers or the tube of the tunnel depends on the random sea state. However, due to the transfer function from wave action to structural movements, this random process leads to a narrow banded excitation of the mooring line [D13,D24]. Thus, the wave-induced motion is represented as a sinusoidal imposed vertical displacement of the upper beam support. Figure D2 shows a schematic representation of the tether and its support motion. Specifically, the numerical model is developed in ABAQUS [D27] using 40 beam elements (B21) including nonlinear geometric effects. Each element consists of in-plane slender beam elements with two nodes and linear interpolation that translates to two degrees of freedom per node The type and number of elements was decided based on a convergence study (not reported here) that ensured accuracy and stability of the numerical results. Since large deformations are expected in the model, equilibrium is formulated in the deformed state, i.e. considering nonlinear geometric effects. The same configuration is used throughout this study. The contribution of the hydrodynamic effects (drag and added mass) is represented by the Morison equation using the Aqua toolbox in ABAQUS. A beam of total length L is assumed to have an initial pretension T_0 and supports that are free to rotate (pin), while the upper support also follows a prescribed motion. The fundamental frequency f_1 is calculated considering the beam's self-weight and the added mass contribution of the surrounding water. The imposed cyclic motion of the upper support is defined by its amplitude A and frequency f. This numerical model is used to calculate the displacement and tension of several points of interest along the tether's length. This analysis in ABAQUS was done with a direct numerical integration of the equations of motions, in order to correctly account for the nonlinear effects.

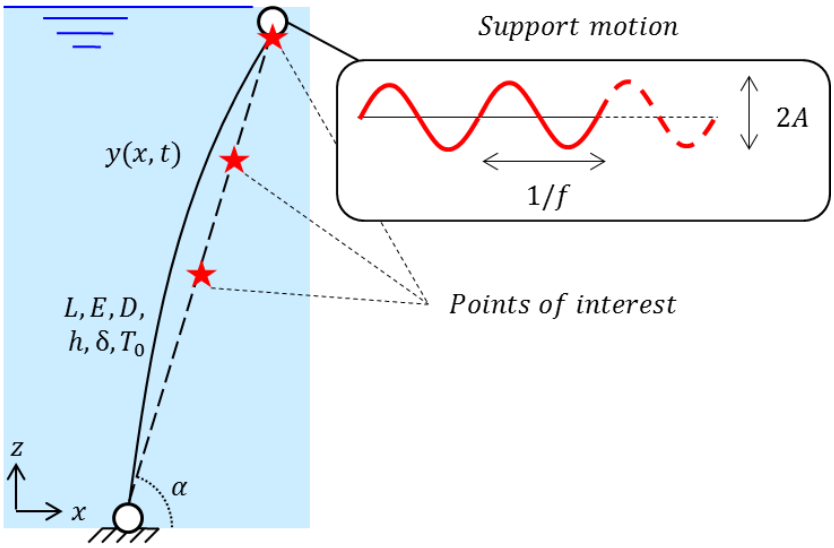

Figure D2: Sketch of tether and support motion

The particular tether properties used in this study are listed in Table D1 and are used throughout the paper unless otherwise specified in the text. The values in Table D1 correspond to those suggested in the preliminary design of the mooring system for the floating bridge and submerged tunnel of the Bjørnafjord crossing, which is part of the "Ferry-free E39" project [D1]. Moreover, similar tether dimensions and pretensions can be found in [D14,D25,D28]. To correctly account for the hydrodynamic effects, two important parameters are needed, namely, the added mass coefficient C_A and the drag coefficient C_D. The numerical values of these coefficients are listed in Table D1 and they are taken from the recommendations in [D29]. Furthermore, a small internal damping of only 0.1% is assumed to avoid any spurious numerical effects. Mooring system damping is difficult to assess precisely [D30], but a higher internal damping can be expected. Therefore, the results presented here can be considered conservative. In the numerical simulation, 120 loading cycles of the upper support motion are computed for every simulated case presented here; this is more than sufficient for developing parametric resonance and/or reaching a steady-state situation. The numerical time integration of the solution is performed using a sufficiently small time step that gives a minimum sampling rate of 100 Hz. The numerical stability and accuracy of the solution was assessed in a preliminary convergence study that is not shown here.

Table D1: Tether properties

Description	Symbol	Value	Unit
Length	L	400	m
Young's modulus	E	$2.1 \cdot 10^{11}$	N/m^2
Diameter	D	1.119	m
Thickness	h	38	mm
Density	δ	7800	kg/m^3
Initial pretension	T_0	$18.5 \cdot 10^6$	N
Inclination angle	α	90	degrees
Fundamental frequency	f_1	0.1299	Hz
2nd frequency	f_2	0.2648	Hz
3rd frequency	f_3	0.4096	Hz
Added mass coefficient	C_A	1	-
Drag coefficient	C_D	1.5	-

D3. Tension during parametric excitation

This section aims to clarify what parametric excitation is based on a particular example that features a frequency ratio (support motion frequency f to tether's fundamental f_1) of 2:1. Special attention is given to the tension values and their relation with the lateral displacements of the tether. The numerical model presented in Section D2 is computed for the tether with the properties listed in Table D1. The results from the example considered in this section are dissected to examine different aspects of the problem in detail, which are each presented in a different subsection. First, the influence of hydrodynamic effects is assessed by comparing the response of a dry tether to a submerged tether. Then, the parametric excitation phenomenology is explained graphically, providing clear insight into why instability occurs. In addition, the following subsections discuss the spatial distribution of the tension values, how to define a stability criterion and the definition of dynamic factors to assess the magnitude of extreme tension values.

D3.1 Dry tether

A tether modelled as a linear system and parametrically excited at a critical frequency has an unbounded solution. The result is the classic parametric resonance of the linear Mathieu equation featuring exponential growth. In a truly linear system, the amplitude increases until the system is destroyed [D8]. However, real physical systems do not exhibit unbounded responses. By including the nonlinear effects, a more realistic model is obtained. During parametric resonance, the nonlinearities limit the oscillation amplitudes. Therefore, the tether is modelled to include nonlinear geometric effects. Figure D3a shows the time-history of the mid-span lateral displacements, which exhibit exponential growth over time until a certain maximum (or minimum) value is reached. Then, the displacements decay and repeat the exponential growth again. For this particular example, the maximum displacement is 4.47 m, while the amplitude of the upper support motion is only 0.10 m. This beating-like behaviour during parametric resonance is also reported in [D6,D15,D20].

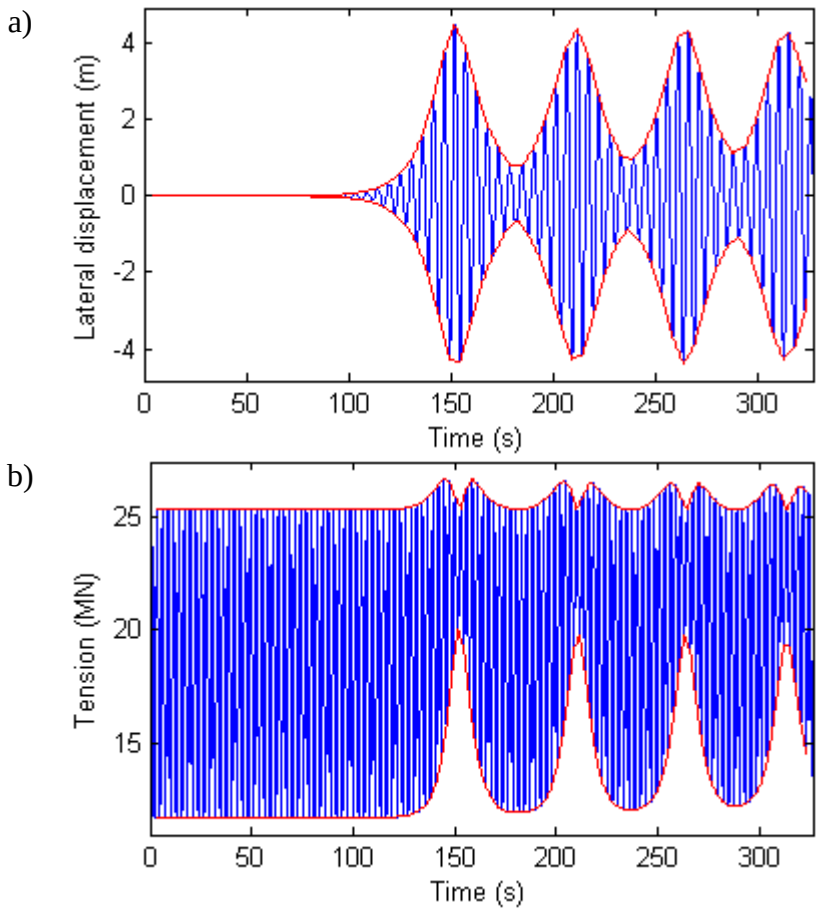

Figure D3: Dry tether response at the mid-span for a 2:1 frequency ratio: a) Horizontal displacement; b) Total tension (red lines = outer envelopes to response)

Intuition suggests that the internal tether tension should have a similar evolution over time or should at least feature some extreme values at the same times as those reported for the displacements in Figure D3a; however, this is not the case. Figure D3b shows the time-history of the total tension at the upper support. Before instability is triggered, the tension values oscillate according to the imposed motion of the support. After parametric resonance has started, both the maximum tension values and the minimum tension values increase. Moreover, the difference between the tension extremes is lowest exactly when the maximum displacements occur. This counterintuitive behaviour of the tension was also reported in [D6] and explained as the synchronous compensation of the tension oscillations by the support motions.

D3.2 Submerged tether

As mentioned in the introduction, the hydrodynamic effects are the greatest contributors to the damping of the system. Parametric resonance of the submerged tether can still occur, but the displacement and tension responses differ significantly. The time-history response of the lateral displacement is given in Figure D4a, which also includes the hydrodynamic effects. The figure shows that the lateral displacement of the tether starts to increase rapidly after 100 s of excitation and reaches steady-state conditions after 220 s. This increase is mainly limited by the dissipative effects of the hydrodynamic contributions. The extreme lateral displacement values at mid-span are indicated by the labels $u_{x,max}^{mid}$ and $u_{x,min}^{mid}$. For reference, the figure shows the amplitude of the vertical motion (±0.1 m) of the upper support in dashed black lines;

in addition, the envelopes of the time series are indicated with a solid red line. Parametric resonance plays an important role in the rapid growth. However, compared to the dry tether example (Section D3.1), the extreme displacements only reach 0.55 m, and more interestingly, no beating phenomenon is observed. These differences between dry tether (Figure D3a) and submerged tether (Figure D4a) can only be attributed to the additional damping of the hydrodynamic effects.

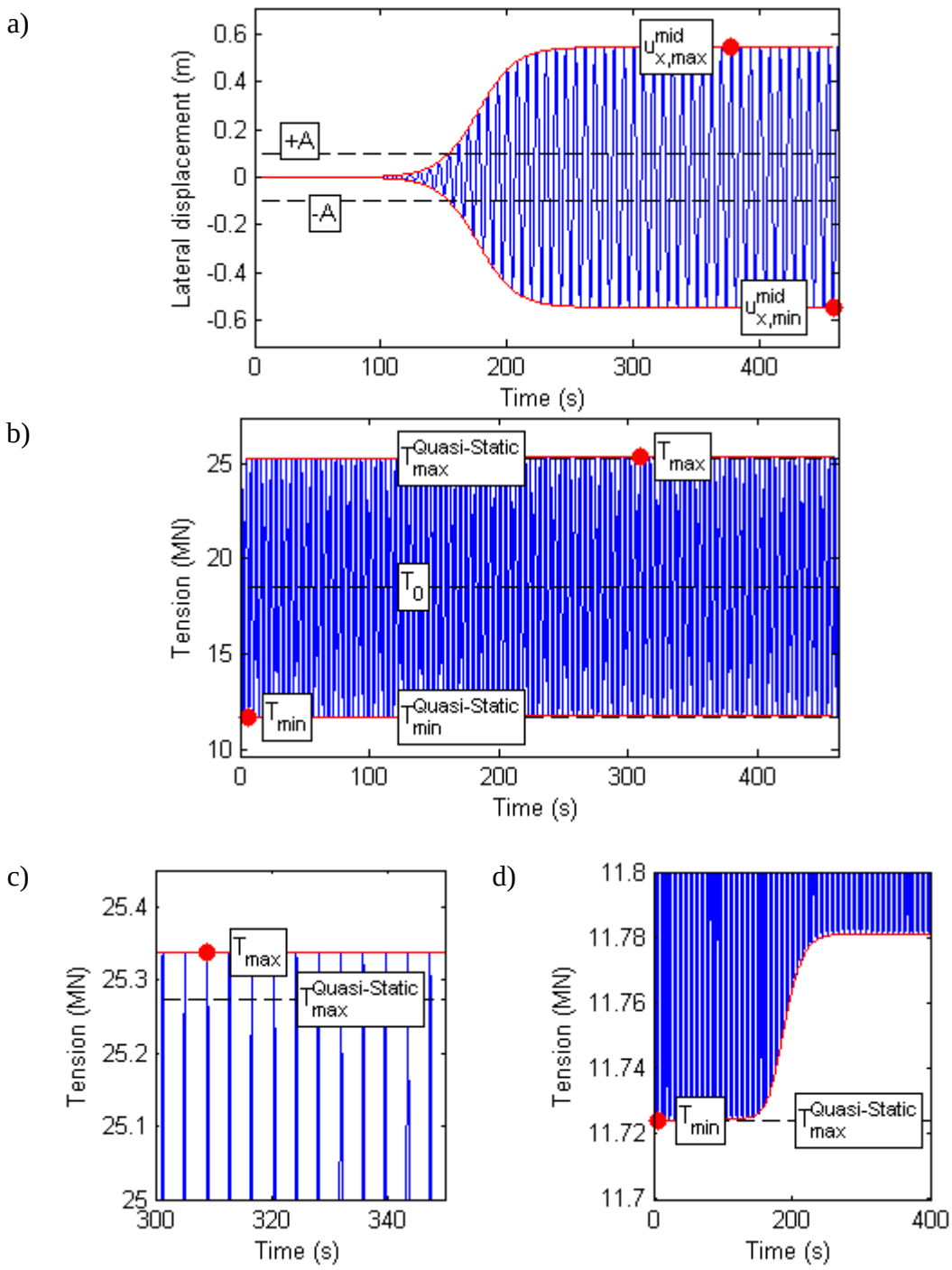

Figure D4: Submerged tether response at the mid-span for a 2:1 frequency ratio: a) Horizontal displacement; b) Total tension; c) Zoomed view near T_{max}; d) Zoomed view near T_{min} (red lines = outer envelopes to response)

Figure D4b presents the total tension of the submerged tether at the mid-span; this figure shows that the tension values are barely affected by the parametric resonance. For reference, the initial tether tension T_0 is indicated in the figure. The horizontal dashed black lines labelled $T_{max}^{Quasi-Static}$ and $T_{min}^{Quasi-Static}$ reveal the extreme quasi-static tension values expected due to the imposed cyclic motion ($A = 0.1\ m$). While the system response is stable ($t < 100\ s$), the tension values oscillate following the expected quasi-static response due to the imposed motion. However, when parametric resonance starts, only a small change can be observed. Then, the maximum tension values slowly increase to T_{max}, which is only slightly greater than $T_{max}^{Quasi-Static}$ (Figure D4c). On the other hand, the minimum tension value T_{min} occurs at the beginning of the time series because the minimum tension values actually increase over time, even if only marginally (Figure D4d). Therefore, the effect of parametric excitation on the dynamic tension is very small. This result is somewhat counterintuitive: a situation that has large lateral motion (Figure D4a) features only very small dynamic tension effects (Figure D4b). This can be explained analysing the lateral displacement response. Even though the parametric resonance has been triggered, the steady-state response features constant amplitude due to the energy dissipation effects of the hydrodynamic contribution. In addition, this amplitude is an order of magnitude smaller for the submerged tether (Figure D4a), compared to the dry example in Figure D3a. These smaller and stationary lateral motions are not big enough to induce significant changes in the tension variation compared to the quasi-static response (Figure D4b).

D3.3 Phenomenology

To better understand parametric excitation, the response of the tether can be illustrated using a 3D graphical representation. The time-histories of the horizontal displacement at mid-span (u_x^{mid}) and the vertical motion at the upper support (u_y^{upper}) are plotted together in Figure D5 for the 2:1 frequency ratio example. Both displacements are presented at the same scale to clearly visualize the large magnification observed during parametric resonance. Here, the colour code is proportional to the system's energy content, where blue values indicate low energy levels and red values indicate high energy levels. Figure D5 shows only the part of the response that has a rapid growth due to parametric instability. First, due to the boundary condition motion, only vertical displacements with small energy values are observed. However, as soon as the parametric resonance is triggered, the horizontal displacements quickly increase to several times greater than the imposed vertical motion. While the vertical motion ranges between ±0.1 m, the lateral displacement ranges between ±0.5 m.

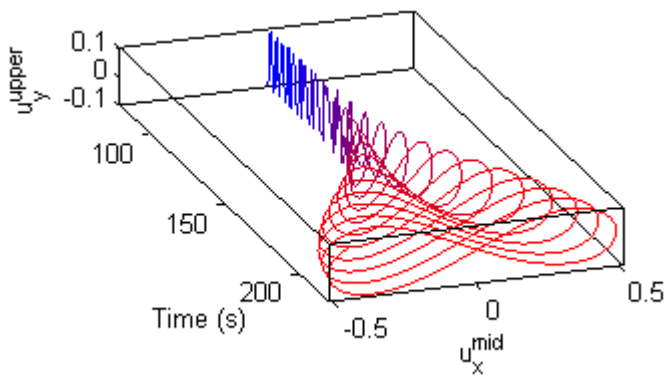

Figure D5: 3D plot of the tether response at the mid-span

The physical explanation of why the lateral displacements of the tether increase so much is illustrated in Figure D6. The figure shows several instances (A-E) of one full cycle of the tether's lateral motion. Because of the 2:1 frequency ratio, during a single cycle, the upper support moves vertically two full cycles. Every time that the tether is fully bent and is returning to its static equilibrium position (instances A, C and, E in Figure D6), the upper support is moving upwards. This positive vertical movement makes the tether move faster. For every repetition of this cycle, the imposed motion adds more energy to the system until it eventually becomes unstable. Section D4 shows that other frequency ratios can also lead to unstable responses, and that the instability mechanism for those cases is similar to the one presented in Figure D6. However, the 2:1 frequency ratio provides the most intuitive example and reaches instability more quickly (requires fewer cycles); therefore, this example is generally called principal parametric resonance.

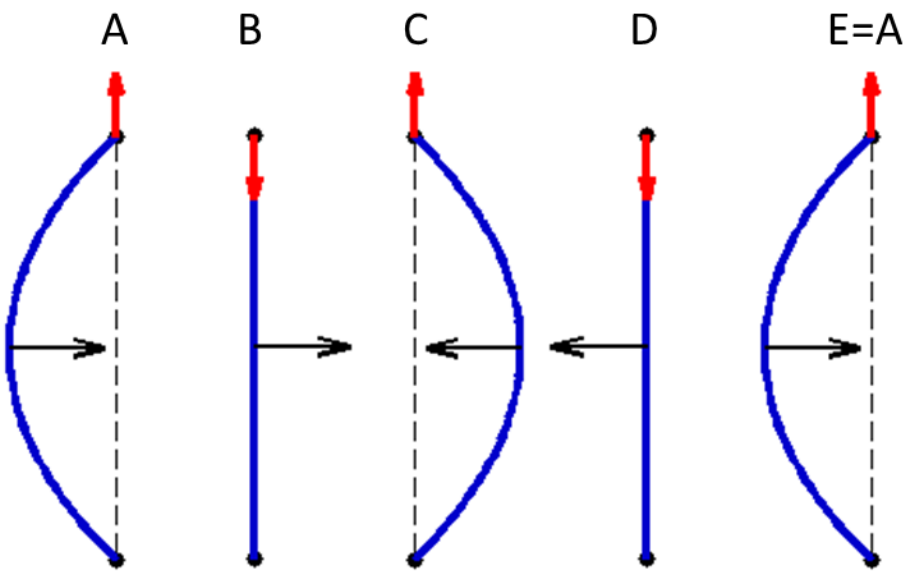

Figure D6: Multiple instances of one full cycle of tether lateral displacement for the 2:1 frequency ratio (blue lines = tether lateral deformation; black dashed lines = static equilibrium position; black horizontal arrow = direction of movement; and red vertical arrow = imposed vertical motion)

D3.4 Spatial distribution

Because of the contribution of higher modes of vibration, it can be argued that extreme load effects can be found anywhere along the tether. Generally, the maximum lateral displacement occurs at the mid-span, but this is not necessarily always the case. For instance, an ideal situation that excites only the 2nd mode of the tether would lead to maximum motion at the quarter-span, while the mid-span section featured no lateral vibration. For this reason, every simulation in this study calculates the response of several points of interest along the tether length. The conclusions are based on the simultaneous analysis of multiple locations, thus including the effects of higher vibration modes.

As noted in the introduction, to correctly evaluate the total tension, it is important to consider its spatial distribution along the tether, as verified by the results obtained for the 2:1 frequency ratio example. The tension time-histories for all the elements in the model are extracted, and Figure D7 shows the instantaneous maximum and minimum tension values along the tether in

two separate curves. In other words, Figure D7 shows the envelope of maximum and minimum tension along the tether. At the beginning of the simulation (Figure D7a), some differences exist between the extreme values during the initial transient vibration phase because the sudden application of the imposed motion at the upper support produces additional vibrations that travel as compressive waves but vanish rapidly. In the remaining duration of the example, the maximum and minimum tension values anywhere along the tether are practically identical. This is also true when parametric resonance occurs and the system has reached its steady-state response (Figure D7b). This indicates that tension is constant along the tether length at any given time instant. Nevertheless, in subsequent simulations, a range of selected points of interest along the tether length is examined, similar to the lateral displacement.

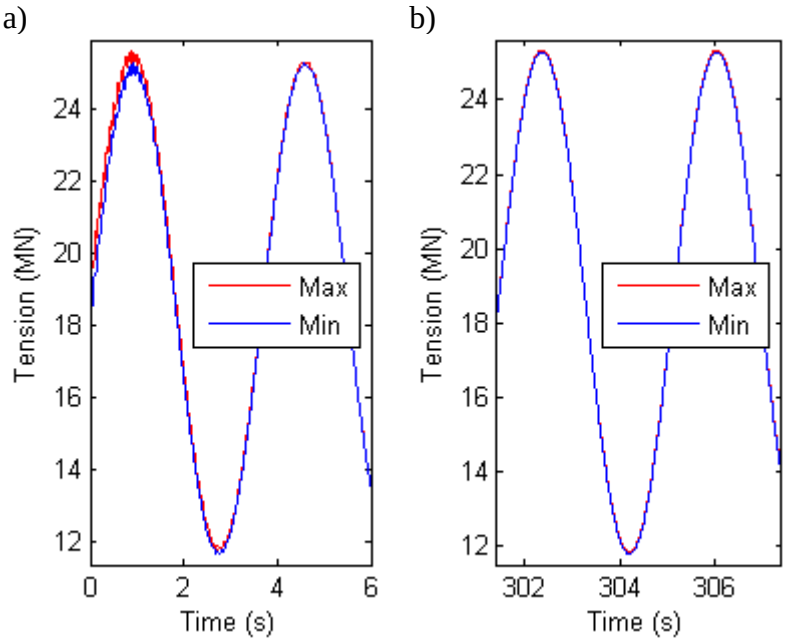

Figure D7: Instantaneous maximum and minimum tension along the tether during: a) Initial transient vibration; b) Parametric resonance

D3.5 Stability criteria

In parametric excitation studies, identifying when the system is unstable or has reached parametric resonance is of paramount importance. In theoretical studies that work directly on a mathematical description of the problem, instability can be defined as a mathematical condition [D8]. However, when dealing with measurements or, as in this study, with simulated results, it is not trivial to clearly flag instability, and procedures to do so are generally not well documented. One possibility is using the Lyapunov exponents [D31], as reported in [D32] and [D33]; however, in practice, this is not without problems and it can be computationally time consuming. Therefore, this study uses a ratio based on the Root Mean Square (RMS) values of the response. For instance, the horizontal displacement response of the tether in Figure D4a corresponds to an unstable situation. A convenient way to identify instability is by comparing the RMS (proportional to the energy content) of the signal to the RMS of the first few cycles. Ratios close to one indicate that the dynamic behaviour has not changed considerable and that the response is stable. However, as the RMS ratio increases, the system can be considered unstable. This definition of stability in relative terms allows us to easily apply the criterion to any point along the tether without previous knowledge of its expected stable behaviour. Here, the stability criterion is defined for a RMS ratio > 1.1 to allow for small spurious increases

that do not correspond to instability. For the particular case shown in Figure D4a, comparing the last four cycles to the first four cycles of the response gives a ratio of 10.73.

D3.6 Extremes evaluation

To characterize the effects of parametric resonance on the total tension values of the tether, it is necessary to quantify both extremes, i.e., maximum and minimum tension values, which are convenient to analyse in terms of dynamic factors. Here, we introduce the Dynamic Amplification Factor (*DAF*) and the Dynamic Reduction Factor (*DRF*), which are defined in Eq. (D1) and Eq. (D2) respectively using the notation presented in Figure D4b. In essence, these factors are the normalizations of the dynamic tension increments with respect to the quasi-static tension increments due to the imposed upper support motions. For the particular case shown in Figure D4b, *DAF* is 1.0094, which means that the quasi-static increment $\Delta T_{max}^{Quasi-Static}$ has to be increased by only 0.94% to account for the dynamic effects. On the other hand, *DRF* is 0.9923, which is equivalent to decreasing $\Delta T_{min}^{Quasi-Static}$ by 0.77%. Values of *DRF* that are less than one indicate that the total minimum tension is larger than the quasi-static minimum, as shown in Figure D4b.

$$DAF = \frac{\Delta T_{max}}{\Delta T_{max}^{Quasi-Static}} = \frac{T_{max} - T_0}{T_{max}^{Quasi-Static} - T_0} \qquad \text{Eq. (D1)}$$

$$DRF = \frac{\Delta T_{min}}{\Delta T_{min}^{Quasi-Static}} = \frac{T_{min} - T_0}{T_{min}^{Quasi-Static} - T_0} \qquad \text{Eq. (D2)}$$

D4. Stability study and fatigue

So far, this paper has presented results for a particular example where the imposed support motion has a 2:1 frequency ratio and a specific amplitude (0.1 m). However, in addition to occurring for multiple frequency ratios, parametric resonance is also strongly dependent on the amplitude of the imposed motion. Therefore, this section performs stability analysis for a wide range of frequency ratios (f/f_1) and amplitudes (A) of the upper support motion. In particular, the frequency ratio is varied in a discrete space from 0.25 to 3.5 in increments of 0.05, while the amplitude varies from 0.005 m to 0.1 m in 0.005 m increments, providing a total of 1320 simulated cases. The stability is studied first in terms of lateral displacement, then it is compared to the results of tether tension and finally the consequences on fatigue life calculation are evaluated.

D4.1 Lateral displacement

Figure D8a shows the instability diagram based on the lateral displacement of the tether at the mid-span. Each of the studied f/f_1 and A combinations is represented as a dot. If the particular case renders a stable solution, it is depicted as a small black dot; when the combination leads to an unstable result, it is represented by a larger dot. As expected, the results clearly feature distinct areas with parametric resonance, which are usually called instability tongues. The biggest tongue emanates from the 2:1 frequency ratio and corresponds to the principal parametric resonance. In addition, several other tongues correspond to other frequency ratios, higher vibration modes and/or a combination of harmonics. Figure D8a also shows the theoretical tongues associated to the Mathieu equation. These theoretical instability regions are

drawn based on the analytical expressions reported in the Appendix. These analytical expressions derive from the theoretical analysis of a taut simply supported cable using the harmonic balance method considering two harmonic terms. The direct comparison of the numerical and theoretical instability regions shows a good agreement.

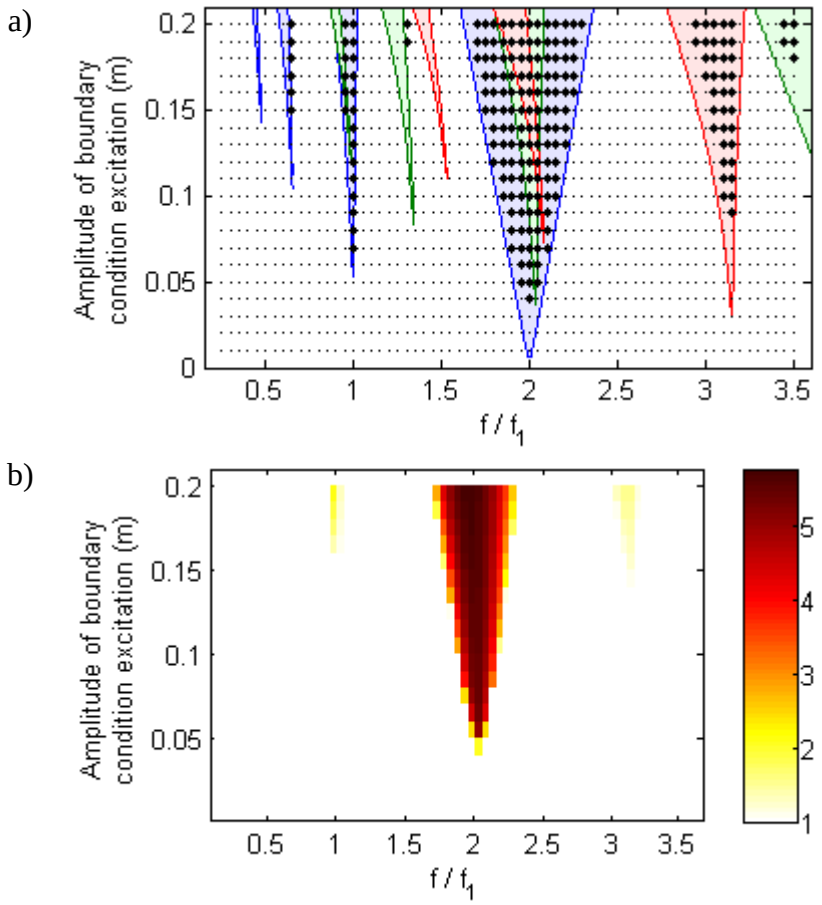

Figure D8: a) Instability map for numerical results (stable = small dot, unstable = large dot) and theoretical instability tongues (see Appendix) associated to tether's 1st mode (Blue), 2nd mode (Green) and 3rd (Red) mode; b) Normalized lateral displacement values

Figure D8a is the standard stability map, which is also called a Strut diagram. This map allows us to clearly identify the instability regions of the problem. However, it is difficult to assess the relative importance of each of the tongues. In theory, for infinitely long excitations, all unstable cases will reach steady-state and similar extreme displacement values. However, in practice, it is interesting to examine the maximum displacements achieved during parametric resonance for a finite duration of excitation. Figure D8b shows the maximum lateral displacements normalized by the amplitude of the support motion. In all the simulated cases, the excitation lasted for 120 cycles. The results clearly show that the 2:1 frequency ratio tongue has the highest values, indicating a quicker instability and confirming its importance compared to the other tongues.

D4.2 Tether tension

The effect of tether instability is evaluated in Figure D9 for the extreme tension values in terms of the dynamic factors *DAF* and *DRF* defined in Section D3.6. There is a clear correlation between the instability tongues shown in Figure D8 and the results in Figure D9. However, the

actual numerical values of the factors are remarkably small. In the case of *DAF* in Figure D9a, the overall maximum value is 1.019, meaning that the maximum total tension (static + dynamic) is only 1.9% greater than that in the static case. The results in Figure D9b show that the minimum tension in the tether is either equal to or slightly less than the minimum static tension. In particular, the absolute minimum *DRF* value is 0.977, which corresponds to a 2.3% decrease in the static tension.

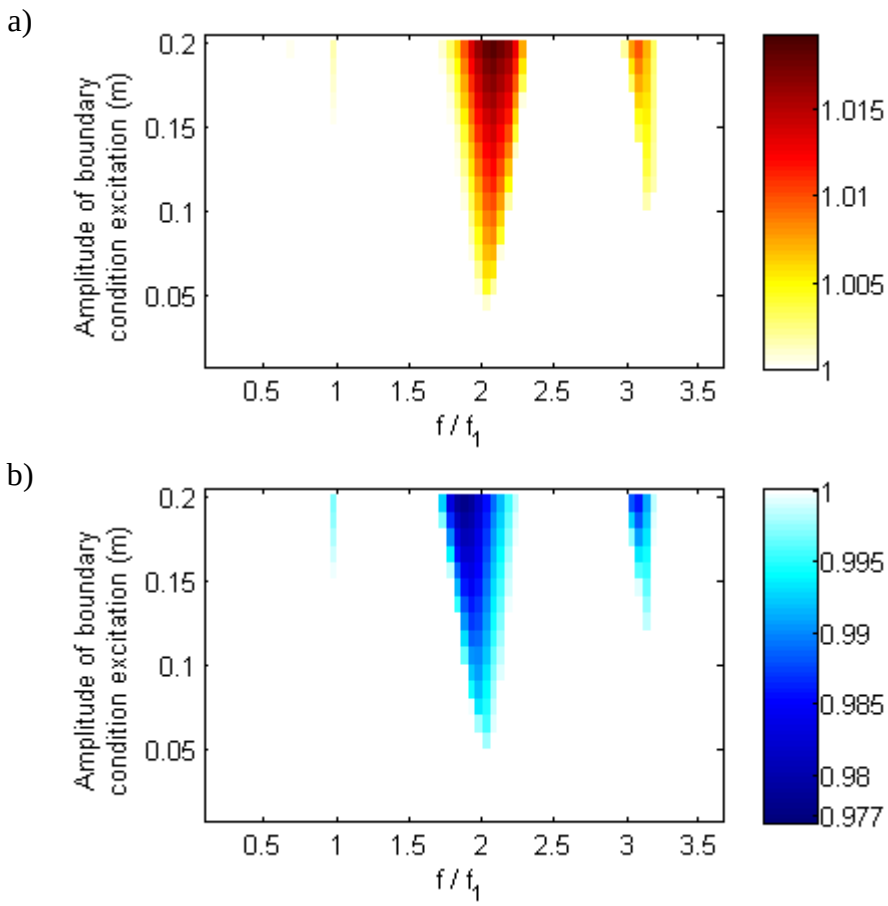

Figure D9: Tension dynamic factors: a) *DAF*; b) *DRF*

The main conclusion drawn from the results in Figure D9 is that the dynamic tension contribution during parametric resonance is very small. It is also interesting to note that outside of the instability tongues, the dynamic factors are virtually equal to one. In other words, the total tension during stable conditions is the same as the total tension due to quasi-static loading. Therefore, if the design of a tether is based on a maximum displacement criterion, the results in Figure D8 suggest that any possibility of parametric resonance should be avoided. However, in reality, a tether is designed with respect to the maximum stress levels. According to the results in Figure D9, the extreme tension levels are either close to or identical to the tension based on a quasi-static response, indicating that the dynamic effects of parametric resonance are very small. Furthermore, this conclusion can be refined when directly exploring the consequences on fatigue calculations.

D4.3 Fatigue

This section evaluates the effect of parametric excitation on the fatigue life calculations of tethers by introducing a new factor that facilities this analysis. The main parameter in any

fatigue calculation is the stress range *S*; this range is directly proportional to the tension increment ΔT, which can be written as:

$$\Delta T = T_{max} - T_{min} \qquad \text{Eq. (D3)}$$

Using the definitions of *DAF* and *DRF* given in Eq. (D1) and Eq. (D2):

$$\Delta T = DAF \cdot \Delta T_{max}^{Quasi-Static} - DRF \cdot \Delta T_{min}^{Quasi-Static} \qquad \text{Eq. (D4)}$$

In the case of taut tethers, it can generally be assumed that the static tension increment (ΔT_{max}^{Static}) due to positive vertical displacement of the support is of the same magnitude but opposite sign as the static tension increment (ΔT_{min}^{Static}) due to lowering the support motion. Thus, representing both tension increments as $\frac{1}{2}\Delta T^{Static}$, we can rewrite expression Eq. (D4) as:

$$\Delta T = \frac{(DAF + DRF)}{2} \cdot \Delta T^{Quasi-Static} = DF \cdot \Delta T^{Quasi-Static} \qquad \text{Eq. (D5)}$$

Eq. (D5) introduces the Dynamic Factor (*DF*) and can be used to easily determine the total tension increment (including static and dynamic effects) by simply factoring the tension increment obtained from quasi-static analysis. Moreover, *DF* is the average of the *DAF* and *DRF* values. Figure D10 gives the numerical values of this new factor for the same frequency ratios and amplitudes studied in the previous subsections. Similarly, the results show the presence of multiple instability tongues, and the tongue emerging near the 2:1 frequency ratio shows the highest values. In particular, the maximum value in Figure D10 is 1.006, and the minimum value is 0.987, which are equivalent to 0.6% and -1.3% changes in the tension increment, respectively. The *DF* values for a given critical frequency ratio (say 2:1) may be either negative or positive depending on its excitation frequency with respect to the centre of the corresponding instability tongue. Therefore, the stress range *S* obtained from a quasi-static analysis should be decreased or increased, effectively increasing or decreasing the calculated fatigue life of the member, respectively. However, the *DF* values are very small regardless of their sign, which supports the assertion that it is safe to perform only quasi-static simulations for the fatigue calculations of a tether. Even if parametric resonance occurs, the dynamic effects on tension are sufficiently small to be covered by the general safety factors of the design process.

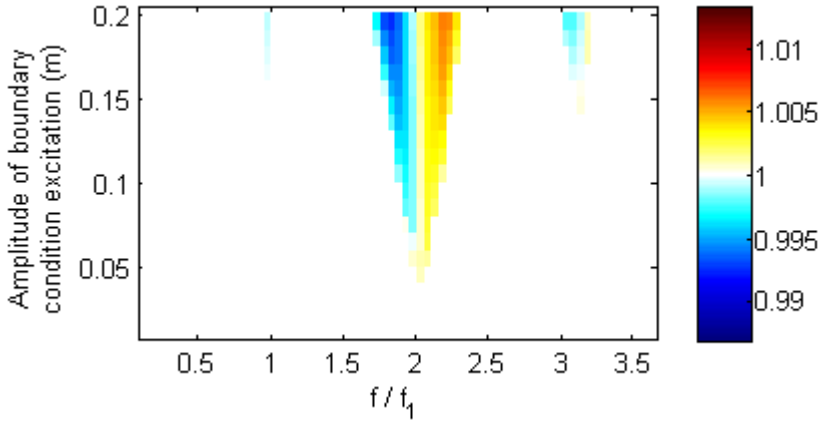

Figure D10: Tension Dynamic Factor (*DF*)

D5. Parametric studies

The tether properties used in the previous sections and listed in Table D1 correspond to a representative example of the tethers to be used in the construction of a floating bridge and a submerged floating tunnel. However, these properties are derived from preliminary designs, and some variations can be expected. This section evaluates the influence of three of the main design variables faced in the project. In particular, the following subsections investigate the effect of the initial pretension, tether length and inclination angle. The studies evaluate their influence on system stability and, most importantly, its effect on the total tension. For these analyses, the frequency ratio is set to 2:1, and the amplitude *A* is 0.1 m. The fundamental frequency of the tether changes in each study and needs to be recalculated for each new tether configuration.

D5.1 Pretension

The influence of pretension is first evaluated in terms of the normalized mid-span tether displacement in Figure D11a, which clearly shows a decrease with increasing pretension. That is, the system's stability increases with increasing pretension. This fact is also shown as an increase in the number of cycles needed to trigger parametric resonance, as plotted in Figure D11b. Similarly, the dynamic factors that quantify extreme tension increments (*DAF* for maximum and *DRF* for minimum) also decrease with increasing pretension. Nevertheless, the numerical values of these factors are still quite small. Even for the lowest pretension level, tension increases of less than ±3% need to be accounted for. For the *DF* values, the dynamic factor for fatigue calculations remains constant and very close to one, which confirms that the quasi-static calculation is sufficient for any of the considered pretension levels.

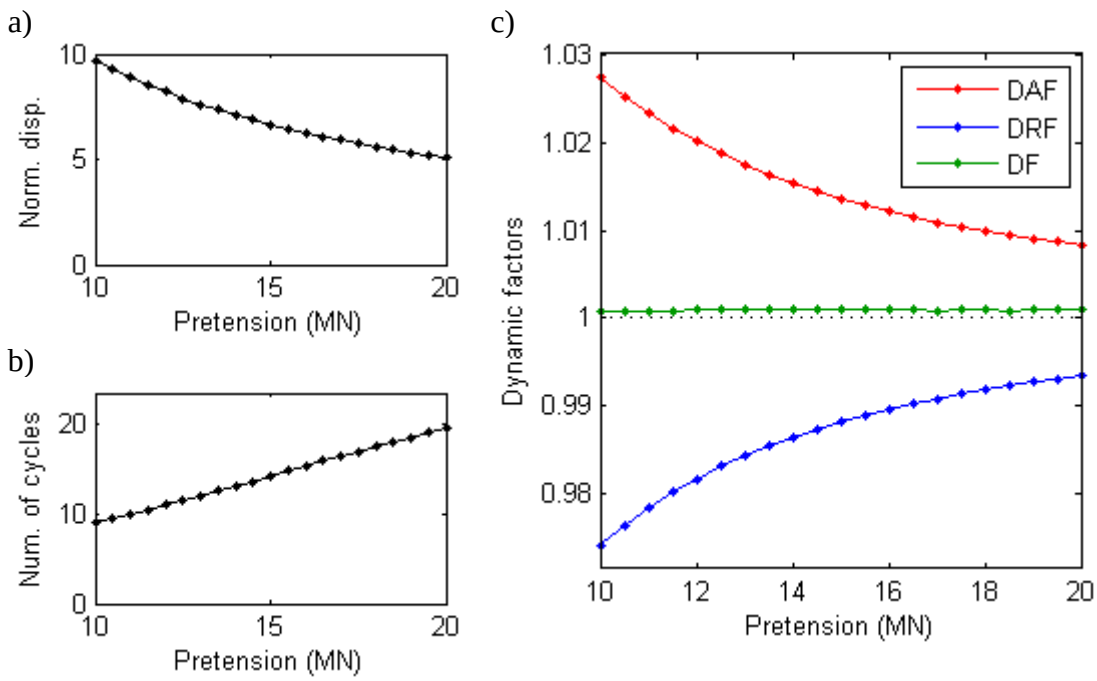

Figure D11: Influence of pretension: a) Normalized lateral displacement at mid-span; b) Number of cycles to initiate parametric resonance; c) Dynamic factors

D5.2 Length

The length of the tether clearly depends on the depth of the seabed. The distance between the floating construction (either bridge tower or submerged tunnel) and the anchoring point of the mooring line varies significantly along the length of the structure. This study evaluates the influence of parametric resonance on tethers with different lengths. All the cases are simulated for a support motion with the same amplitude of 0.1 m. Thus, the extreme static tension values are greater for shorter tether lengths (Figure D12a) because the elastic stiffness of the system is inversely proportional to the length. In other words, shorter tethers are stiffer and lead to greater tension values for the same imposed support motion. As a result, the higher quasi-static tension oscillations observed in shorter tethers lead to instabilities with larger lateral displacements, as shown in Figure D12b. Similarly, the extreme total tension values also increase (or decrease) for shorter tethers (Figure D12c). However, as observed throughout this paper, these dynamic factors are remarkably small. In this case, only ±5% tension variations are expected for the shortest mooring line. Nevertheless, the dynamic factor for fatigue *DF* remains nearly constant and can be approximated as equal to one.

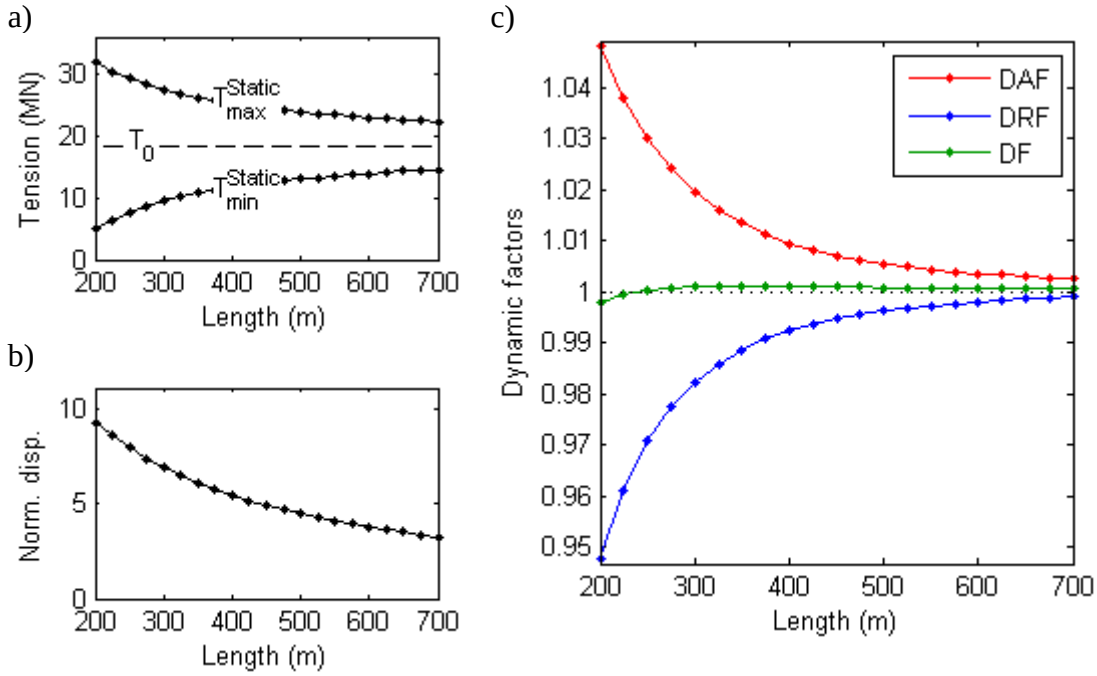

Figure D12: Influence of tether length: a) Static tension values; b) Normalized lateral displacement at mid-span; c) Dynamic factors

D5.3 Inclination angle

A vertical mooring system such as the one investigated in this study so far imposes little or no restraint in the horizontal plane. Therefore, large lateral motions could be induced if the floating structure is too flexible or the lateral loading is sufficiently strong. One possibility for providing additional lateral stiffness is to include pairs of inclined mooring lines in opposite configurations. This study assesses the impact of the tether inclination angle on the system's stability. According to the definitions in Section D2, an angle of 90° corresponds to a vertical mooring line. Figure D13a shows the tether response in terms of the normalized horizontal displacement. Smaller angles are shown to give a stable response, while angles closer to vertical feature instability. This finding is supported by the results in Figure D13b that show the number of cycles needed to trigger parametric resonance. For configurations with small inclination angles, no results are shown because the parametric resonance is not triggered. In general, stability increases with a decreasing inclination angle; this can be explained by the combination of two effects. First, the actual tether length increases at smaller angles, which leads to greater system stability, as shown in Section D5.2. Second, the imposed vertical motion is effectively divided into two parts, namely, the perpendicular and tangential components. Only the tangential component parametrically excites the system, which decreases with decreasing inclination angle. The perpendicular component produces a normal external load and has a much smaller effect on the dynamics of the tether. Finally, Figure D13c shows the effect of tether inclination on the total tension dynamic factors. The stability of the system greatly influences the numerical values of the factors, obtaining higher (or lower) values in the event of unstable configurations. However, and in accordance with the previous results, the actual numerical values are very small. In this case, all the results indicate reductions smaller than ±1% compared to the static solution.

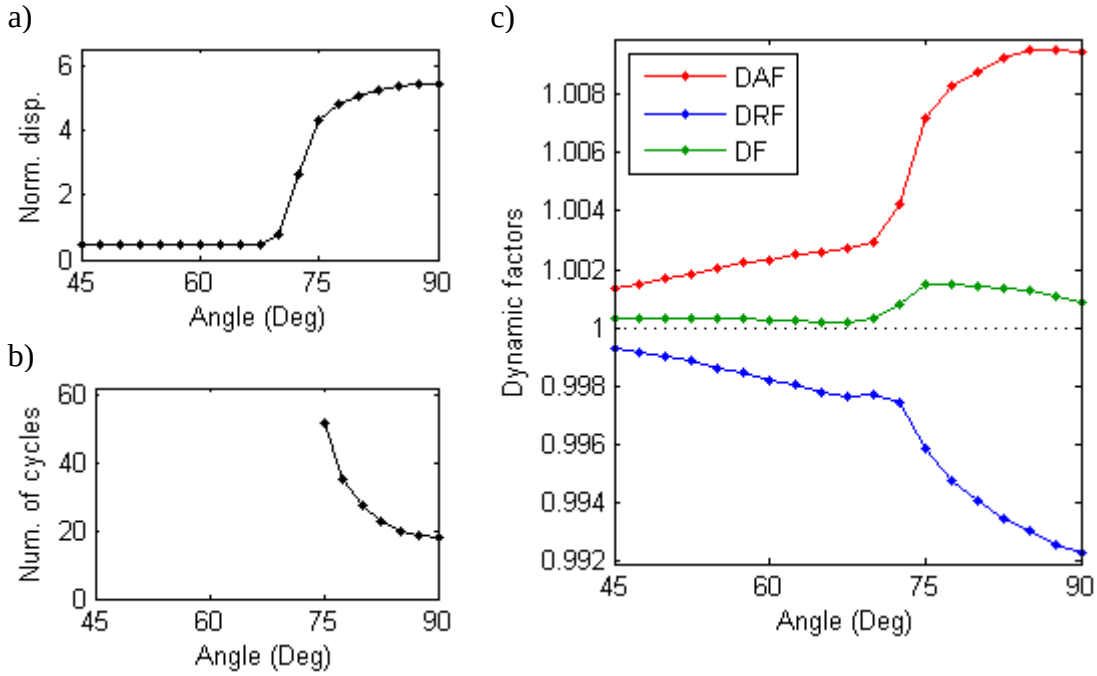

Figure D13: Influence of tether inclination: a) Normalized lateral displacement at mid-span; b) Number of cycles to initiate parametric resonance; c) Dynamic factors

Conclusions

This document has investigated the effect of parametric excitation on the response of taut mooring lines. Particular emphasis is given to the total tension values in the tether. The analysis is done using a nonlinear numerical model of a tether based on preliminary designs of floating bridges and submerged floating tunnels. The results from a 2:1 frequency ratio example show that the tension values are barely affected by the parametric resonance. This outcome is somewhat counterintuitive, indicating that unstable situations with large lateral motions feature very small dynamic tension effects. This conclusion is also confirmed by an investigation that considers a wide range of frequency ratios and amplitudes. Despite the clear correlation between instability tongues (due to lateral displacements) and extreme total tension values, the actual increment in tension due to parametric resonance is remarkably small. The results are expressed in terms of dynamic factors to evaluate the extreme (maximum and minimum) tension values and the effects on the fatigue life calculations. For stable configurations, the total tension can be correctly approximated using a quasi-static analysis. On the other hand, during parametric resonance, the dynamic effects are generally small and can be regarded as negligible. Therefore, if the design of a tether is based on the extreme tension levels, this study repeatedly shows that no dynamic analysis is needed to account for the effects of parametric resonance. Instead, a quasi-static response due to the expected vertical motion of the support is sufficiently accurate. This is applicable for calculating the extreme tension values in an ultimate limit state analysis as well as for the stress range and cycle counting needed in a fatigue limit state analysis.

D. Appendix. Analytical expressions of transition curves

This appendix provides the analytical expressions of the transition curves for a taut cable parametrically excited by inline harmonic support motion. Note that the final expressions reported here correspond to adapted and improved versions of the equations published by the authors in [D34], where additional details on the derivation can be found. In particular, the

derivation outlined below corresponds to a simply supported cable of length L, with an initial axial force N and a support motion $\Delta x(t) = A\cos(\Omega t)$, where A is the amplitude and Ω is the frequency of the motion. The lateral displacements $u(x,t)$ of such a cable can be described by the equation of motion Eq. (D.A1), where m and c are respectively the mass and viscous damping per unit length and $\Delta N(t)$ is the variation of the axial force due to the support motion.

$$m\frac{\partial^2 u}{\partial t^2} + c\frac{\partial u}{\partial t} - \big(N + \Delta N(t)\big)\frac{\partial^2 u}{\partial x^2} = 0 \qquad \text{Eq. (D.A1)}$$

The solution can be expressed as the sum of n modes of vibration Φ_j factored by the generalized coordinates U_j:

$$u(x,t) = \sum_{j=1}^{n} U_j(t)\phi_j(x); \qquad \phi_j(x) = \sin\left(\frac{j\pi x}{L}\right) \qquad \text{Eq. (D.A2)}$$

The variation in axial force $\Delta N(t)$ can be written as the sum of two contributions (Eq. (D.A3)), namely the tension changes due to cable length increment and due to lateral displacements, which can be approximated using a Taylor expansion.

$$\Delta N(t) = \frac{EA}{L}\left(\Delta x(t) + \sum_{j=1}^{n}\frac{j^2\pi^2 U_j(t)^2}{4L^2}\right) \qquad \text{Eq. (D.A3)}$$

Substituting Eq. (D.A3) into Eq. (D.A1) and performing a Garlerkin projection on the partial differential equation gives a set of uncoupled Mathieu equations, one for each mode considered. The final equation for mode-*j* is:

$$mL^2\ddot{U}_j + cL^2\dot{U}_j + \frac{j^4\pi^4 EA}{4L^2}{U_j}^3 + j^2\pi^2\left(N + \frac{EA\,\Delta x}{L}\right)U_j = 0 \qquad \text{Eq. (D.A4)}$$

The transition curves define the boundaries that separate stable from unstable solutions of Eq. (D.A4). It is possible to derive expressions of these transition curves using the harmonic balance method. This method essentially approximates the solution as a Fourier series (Eq. (D.A5)) considering N harmonic terms. Substituting Eq. (D.A5) into Eq. (D.A4), multiplying the result by the basis $\{\sin(\Omega t), \cos(\Omega t), \ldots, \sin(n\Omega t), \cos(n\Omega t)\}$, integrating over one full cycle and balancing harmonic terms gives a system of equations with the Fourier coefficients Υ_i as the unknowns. Solutions of the system provide the Fourier coefficients that define periodic solutions for Eq. (D.4). The transition curves are thus defined when the determinant of the coefficient matrix of the system is zero [D34].

$$U_j(t) = \sum_{n=0}^{N}\Upsilon_{(2n-1)}\sin(n\Omega t) + \Upsilon_{2n}\cos(n\Omega t) \qquad \text{Eq. (D.A5)}$$

The analytical expression of the transition curves in the amplitude-frequency plane (A,Ω) is given by Eq. (D.A6) and Eq. (D.A7), which is expressed in terms of auxiliary variables defined in Eq. (D.A8) to Eq. (D.A17). Depending on the considered period T (either 2π or 4π) there

exist two sets of solutions that correspond respectively to the sum of all even and odd *n* values in Eq. (D.A5). The number of harmonic terms considered is two ($N = 2$).

$$A(\Omega) = \pm B_1\sqrt{B_2(B_3 \pm \sqrt{B_4})}\ \ for\ T = 2\pi \qquad \text{Eq. (D.A6)}$$

$$A(\Omega) = \pm C_1\sqrt{C_2 \pm \sqrt{C_3}}\ \ for\ T = 4\pi \qquad \text{Eq. (D.A7)}$$

The auxiliary variables are defined below.

$$A_1 = m\,L^2\Omega^2 \qquad \text{Eq. (D.A8)}$$

$$A_2 = N\,j^2\pi^2 \qquad \text{Eq. (D.A9)}$$

$$A_3 = c\,\Omega\,L^2 \qquad \text{Eq. (D.A10)}$$

$$B_1 = \frac{2L}{EAB_2\pi^2 j^2} \qquad \text{Eq. (D.A11)}$$

$$B_2 = 8A_1 - 3A_2 \qquad \text{Eq. (D.A12)}$$

$$B_3 = 2(2A_1 - A_2)(A_3^2 + (A_1 - A_2)(4A_1 - A_2)) \qquad \text{Eq. (D.A13)}$$

$$\begin{gathered} B_4 = 8(2A_1^2 + 2A_1A_2 - A_2^2)A_3^4 \\ +(128A_1^4 - 128A_1^3A_2 + 36A_1^2A_2^2 + 16A_1A_2^3 - 7A_2^4)A_3^2 \\ +(A_1 - A_2)^2(4A_1 - A_2)^4 \end{gathered} \qquad \text{Eq. (D.A14)}$$

$$C_1 = \frac{L\sqrt{2}}{4EA\pi^2 j^2} \qquad \text{Eq. (D.A15)}$$

$$C_2 = 12A_3^2 + (9A_1 - 4A_2)(11A_1 - 12A_2) \qquad \text{Eq. (D.A16)}$$

$$\begin{gathered} C_3 = -432A_3^4 + 8(117A_1^2 - 168A_1A_2 - 176A_2^2)A_3^2 \\ +(13A_1 - 20A_2)(9A_1 - 4A_2)^3 \end{gathered} \qquad \text{Eq. (D.A17)}$$

Acknowledgements

The research presented in this manuscript was possible thanks to the financial support of The Fjord Crossing research program for the Coastal Highway Route E39.

References

[D1] Ferjefri E39 summary english jan 2012 http://www.vegvesen.no/vegprosjekter/ferjefriE39/English (accessed 03.10.16).

[D2] M.M. Lwin, Floating bridges, in: W.-F. Chen, L. Duan (Eds.), Bridge Engineering Handbook, CRC Press, Boca Raton, 2000.

[D3] D. Ahrens, Submerged floating tunnels – A concept whose time has arrived, Tunnelling Undergr. Space Technol. 12 (1997) 317-336. doi: 10.1016/S0886-7798(97)90022-5.

[D4] C. Aage, M.M. Bernitsas, H.S. Choi, L. Crudu, A. Incecik, J.J. Murray, The Specialist Committee on Deep Water Mooring. Final report and recommendations to the 22nd ITTC. International Towing Tank Conference, Seoul, 2000.
[D5] S. Weller, L. Johanning, P. Davies, Best Practice Report - Mooring of Floating Marine Renewable Energy Devices. Deliverable 3.5.3 from the MERiFIC Project, 2013.
[D6] J.L. Lilien, A.P. Da Costa, Vibration amplitudes caused by parametric excitation of cable stayed structures, J. Sound Vibration 174 (1994) 69-90. doi: 10.1006/jsvi.1994.1261.
[D7] M.H. El Ouni, N. Ben Kahla, A. Preumont, Numerical and experimental dynamic analysis and control of a cable stayed bridge under parametric excitation, Eng. Struct. 45 (2012) 244–256. doi: 10.1016/j.engstruct.2012.06.018.
[D8] A.H. Nayfeh, D.T. Mook, P. Holmes, Nonlinear Oscillations, Wiley-VCH and Publishing House, Weinheim, Germany, 2004. doi: 10.1115/1.3153771.
[D9] E.S. Caetano, Cable Vibrations in Cable-Stayed Bridges, International Association for Bridge and Structural Engineering, Zürich, Switzerland, 2007.
[D10] I.K. Chatjigeorgiou, N.I. Xiros, S.A. Mavrakos, Coupling contributions and effect of Mathieu instabilities in the dynamic behaviour of vertical elastic cables and risers, WSEAS/IASME International Conference on Fluid Mechanics, Corfu, 2004.
[D11] R.A. Ibrahim, Nonlinear vibrations of suspended cables—part III: Random excitation and interaction with fluid flow, Appl. Mech. Rev. 57 (2004) 515-549. doi: 10.1115/1.1804541.
[D12] V.J. Papazoglou, S.A. Mavrakos, M.S. Triantafyllou, Non-linear cable response and model testing in water, J. Sound Vibration 140 (1990) 103-l 15. doi: 10.1016/0022-460X(90)90909-J.
[D13] M.H. Patel, H.I. Park, Dynamics of tension leg platform tethers at low tension. part I - Mathieu stability at large parameters, Mar. Struct. 4 (1991) 257-273. doi: 10.1016/0951-8339(91)90004-U.
[D14] S. Chandrasekaran, N.R. Chandak, G. Anupam, Stability analysis of TLP tethers, Ocean Eng. 33 (2006) 471–482. doi: 10.1016/j.oceaneng.2005.04.015.
[D15] I.K. Chatjigeorgiou, S.A. Mavrakos, Nonlinear resonances of parametrically excited risers-numerical and analytic investigation for $\Omega = 2\omega_1$, Comput. Struct. 83 (2005) 560–573. doi: 10.1016/j.compstruc.2004.11.009.
[D16] G.R. Franzini, C.E.N. Mazzilli, Non-linear reduced-order model for parametric excitation analysis of an immersed vertical slender rod, Int. J. Non-Linear Mech. 80 (2016) 29–39. doi: 10.1016/j.ijnonlinmec.2015.09.019.
[D17] S. Lei, W. Zhang, J. Lin, Q. Yue, D. Kennedy, F.W. Williams, Frequency domain response of a parametrically excited riser under random wave forces, J. Sound Vibration 333 (2014) 485–498. doi: 10.1016/j.jsv.2013.09.025.
[D18] N. Srinil, G. Rega, The effects of kinematic condensation on internally resonant forced vibrations of shallow horizontal cables, Int. J. Non-Linear Mech. 42 (2007) 180–195. doi: 10.1016/j.ijnonlinmec.2006.09.005.
[D19] G. Rega, N. Srinil, R. Alaggio, Experimental and numerical studies of inclined cables: free and parametrically-forced vibrations, J. Theor. Appl. Mech. 46 (2008) 621-640.
[D20] N. Srinil, G. Rega, S. Chucheepsakul, Three-dimensional non-linear coupling and dynamic tension in the large-amplitude free vibrations of arbitrarily sagged cables, J. Sound Vibration 269 (2004) 823–852. doi: 10.1016/S0022-460X(03)00137-8.
[D21] H. Yang, F. Xiao, P. Xu, Parametric instability prediction in a top-tensioned riser in irregular waves, Ocean Eng. 70 (2013) 39–50. doi: 10.1016/j.oceaneng.2013.05.002.

[D22] I.K. Chatjigeorgiou, On the parametric excitation of vertical elastic slender structures and the effect of damping in marine applications, Appl. Ocean Res. 26 (2004) 23–33. doi: 10.1016/j.apor.2004.08.001.
[D23] J.A.P. Aranha, M.O. Pinto, Dynamic tension in risers and mooring lines: an algebraic approximation for harmonic excitation, Appl. Ocean Res. 23 (2001) 63-81. doi: 10.1016/S0141-1187(01)00008-6.
[D24] J.A.P. Aranha, M.O. Pinto, A.J.P. Leite, Dynamic tension of cables in a random sea: analytic approximation for the envelope probability density function, Appl. Ocean. Res. 23 (2001) 93-101. doi: 10.1016/S0141-1187(01)00010-4.
[D25] Det Norske Veritas, Guideline for Offshore Structural Reliability Analysis – Examples for Tension Leg Platforms, Report No. 95-3198, 1995.
[D26] Det Norske Veritas, Fatigue Design of Offshore Steel Structures. Recommended Practice DNV-RP-C203, 2011.
[D27] ABAQUS, Analysis User's Manual, Dassault Systèmes, Providence, 2011.
[D28] M.M. Gadagi, H. Benaroya, Dynamic response of an axially loaded tendon of a tension leg platform, J. Sound Vibration 293 (2006) 38–58. doi: 10.1016/j.jsv.2005.09.027.
[D29] Det Norske Veritas SA, Recommended Practice DNV-RP-C205: Environmental Conditions and Environmental Loads, 2014.
[D30] C. Webster, Mooring-induced damping, Ocean Eng. 22 (1995) 571-591. doi: 10.1016/0029-8018(94)00027-5.
[D31] W..-C. Xie, Dynamic Stability of Structures, Cambridge University Press, Cambridge, United Kingdom, 2006.
[D32] R.S. Zounes, R.H. Rand, Transition curves for the quasi-periodic Mathieu equation, SIAM J. Appl. Math. 58 (1998) 1094-1115. doi: 10.1137/S0036139996303877.
[D33] C.T. Georgakis, C.A. Taylor, Nonlinear dynamics of cable stays. part 1: Sinusoidal cable support excitation, J. Sound Vibration 281 (2005) 537–564. doi: 10.1016/j.jsv.2004.01.022.
[D34] D. Cantero, A. Rønnquist, A. Naess, Recent studies of parametrically excited mooring cables for submerged floating tunnels, Procedia Eng. 166 (2016) 99-106. doi: 10.1016/j.proeng.2016.11.571

Appendix E - Maximum stresses in mooring lines during parametric excitation

Conference paper:
D. Cantero, A. Rønnquist. "Maximum stresses in mooring lines during parametric excitation". 19th International Conference on Bridge Maintenance, Safety and management, IABMAS 2018, July 2018, Melbourne Australia.

Title:
Maximum stresses in mooring lines during parametric excitation

Abstract:
The ferry links crossing the fjords along the west coast of Norway are going to be replaced by fixed links. Among the proposed solutions is the construction of Submerged Floating Tunnels (SFT). A mooring system should be used to restrain the movements of these floating structures. Long period waves, such as swell waves, parametrically excite the system and might result in excessive vibrations in the cable. Relevant literature have extensively analysed the lateral motions during parametric resonance. However, it is unclear how parametric excitation affects the stresses along the mooring line. The existing studies investigating the actual stresses developed during such violent situations are limited. Additional studies are deemed necessary for the safe design of this crucial element in SFT. Maximum tension and bending moments might vary in magnitude and location during parametric resonance. Thus, this paper investigates the maximum total stresses along the tether due to the combination of both spatial- and time-varying forces. The aim of this paper is to assess the necessity of using the stability charts for the design of mooring lines with respect to safe levels of cable stresses. This is achieved through the numerical analysis of a submerged cable model using Abaqus. Cable vibrations, forces and stresses are analysed and compared for a range of amplitudes and frequencies of the support motions.

E1. Introduction

As part of the E39 ferry-free project (Vegvesen 2012), the National Roads Authority (NRA) in Norway is planning to build floating suspension bridges and submerged floating tunnels. Because of their location (near the end of the fjords and next to the sea), they are exposed to sea states with wind waves and swell. In particular, swells have a long period and can last for several hours with effects that decrease linearly with water depth. Therefore, these constructions require mooring systems to hold them in place and to resist any imposed motion. Taut mooring systems made of steel tubes have been proposed, similar to those used in Tension-Leg Platforms (TLP) (Aage et al. 2000). These tension pipes or tethers have large dimensions and high pretension levels. The environmental loads on the bridge towers or the submerged tunnel lead to varying tension levels and imposed motions on the tether that define a parametrically excited system.

Under certain circumstances, parametric excitation leads to parametric resonance, which is an unstable situation that produces excessive lateral motions on the tether. For instance, under a harmonic imposed motion of the upper support with a frequency twice the fundamental frequency of the tether. That 2:1 frequency ratio is generally called the principal parametric resonance. Parametric excitation has been extensively studied before. In particular, when considering the particularities of submerged risers and immersed slender structures, good literature reviews on the instabilities of such structures can be found in (Franzini & Mazzilli 2015, Lei et al. 2013).

As indicated in (Cantero et al. 2017), the publications that have studied parametric excitation of cables mainly focus on lateral motion only, giving little or no attention to other load effects such as tension and bending moment values. For this reason, in (Cantero et al. 2017), the authors focus on the tension values reached during parametric excitation, concluding that additional dynamic effects on tension are very small. Now, this paper extends that thorough analysis to evaluate also the effects of parametric resonance on bending moments along the tether. This is achieved by numerical simulations with Abaqus (Abaqus 2011). In particular, some relevant case studies are investigated in detail. Maximum bending moments and tension values are compared by means of maximum sectional stress levels in terms of steel utilisation. Then multiple parametric studies are presented to evaluate the influence of different boundary conditions, excitation frequencies and excitation amplitudes.

E2. Numerical model

The tether of a mooring system is modelled as a submerged beam and the wave-induced motion is represented as a sinusoidal imposed vertical displacement of the upper beam support. The beam is modelled considering rotational stiffness (k_r) at the ends. A schematic representation of the model is given in Figure E1. The model has been developed in ABAQUS (Abaqus 2011) using 40 beam elements (B21), including nonlinear geometric effects. The drag and added mass contributions of the hydrodynamic effect are included with the Morison equation. The beam, of total length L, is assumed to have an initial pretension T_0. The vertical motion of the upper support is prescribed to a harmonic motion with amplitude A and frequency f. Table E1 shows the additional model properties required and the particular values used in this study.

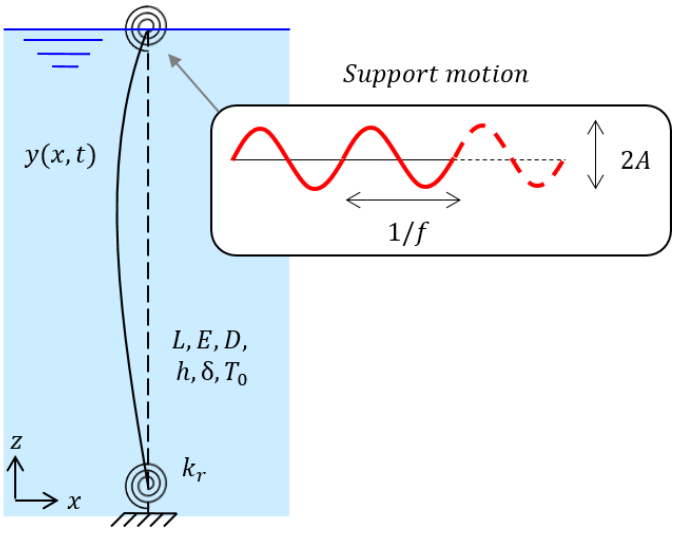

Figure E1. Sketch of tether and support motion

Table E1. Tether properties

Description	Symbol	Value	Unit
Length	L	400	m
Young's modulus	E	$2.1 \cdot 10^{11}$	N/m^2
Yield strength	R	$420 \cdot 10^6$	N/m^2
Diameter	D	1.119	m
Thickness	h	38	mm
Density	δ	7800	kg/m^3
Initial pretension	T_0	$18.5 \cdot 10^6$	N
Fundamental frequency	f_1	0.1299	Hz
2nd frequency	f_2	0.2648	Hz
3rd frequency	f_3	0.4096	Hz
Added mass coefficient	C_A	1	-
Drag coefficient	C_D	1.5	-

E3. Parametric resonance of a dry tether

This section investigates the response of a dry tether, i.e. without considering any hydrodynamic effects. The results highlight the importance of the instabilities produced by parametric excitation. In particular, the tether presented in Section E2, considering fixed rotational supports, is excited with an imposed support motion with twice the tether's fundamental frequency (2:1 frequency ratio). Figure E2a shows the time-history of the mid-span lateral displacements, featuring a maximum of 4.47 m, while the amplitude of the upper support motion is only 0.10 m. Similar beating-like behavior during parametric resonance have also been reported in (Lilien & Da Costa 1994), amongst others. However, other load effects have only rarely been investigated and additional analysis are required.

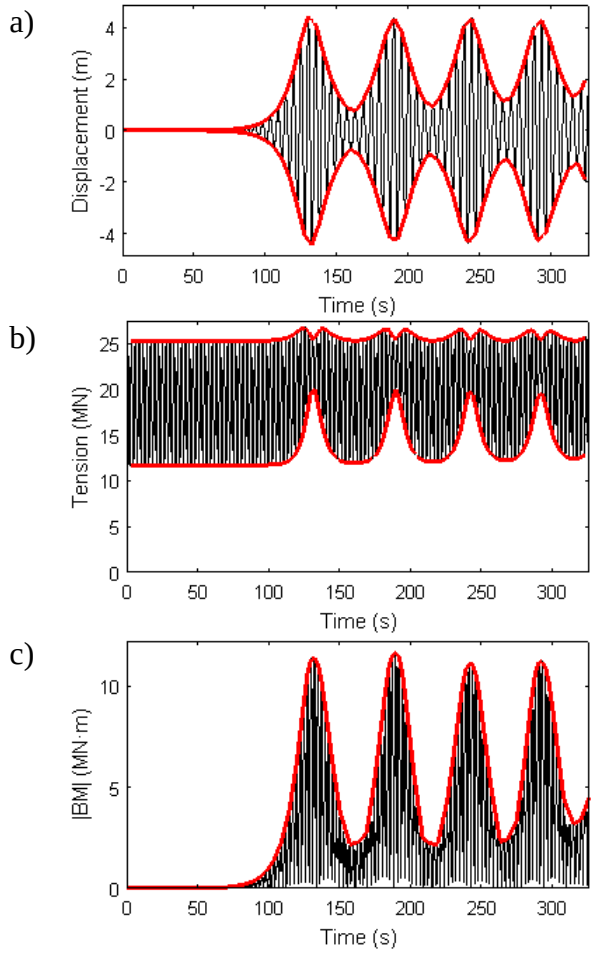

Figure E2. Tether responses under parametric resonance; a) Mid-span displacements; b) Mid-span tension values; c) Support Bending Moment in absolute value (Red lines = envelopes)

Figure E2b shows the time-history of the axial forces during parametric resonance. The tension values vary around the initial prestress tension and oscillate mainly because of the shortening and stretching of the tether length due to the imposed motion. The parametric resonance produces some small changes to the tension values. When larger lateral motions are observed (e.g. 130 s in Figure E2b), one can see an increase in tension values (both maximum and minimum) in Figure E2b. In any case, tension values never decrease and thus avoiding the risk of a temporarily slack tether. On the other hand, the maximum bending moment values on the tether clearly depend on the stability of the system as can be seen in Figure E2c. There is a clear increase in bending moment associated to an increase in the curvature of the deformed shape, which is directly related to the larger lateral motions observed during parametric resonance.

In order to compare both load effects, namely tension and bending moment, we need to define them in terms of section stresses. Normalization of the maximum section stresses over steel's yield strength gives the utilisation of the material. Utilisation values greater than one indicate yielding of steel. When calculating utilisation values separately for each load effect, the total utilisation is the sum of all. Figure E3 shows the evolution in time of the utilisation for each load effect for the dry tether during parametric resonance. The results show that, while the tension utilisation remains approximately constant, the utilisation for bending moments varies significantly and is often greater than that of tension. Note that utilisation calculations are based on the envelopes of the load effects, shown in red in Figure E2.

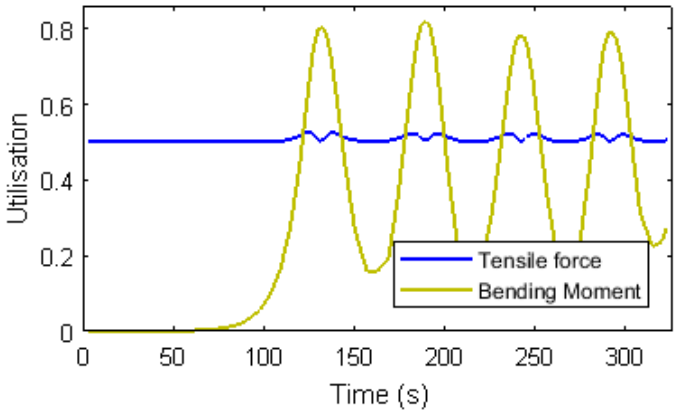

Figure E3. Utilisation of steel for a dry tether during parametric resonance

E4. Submerged tether

Hydrodynamic effects, such as drag force and added mass, are the greatest contributors to the damping of the system. Parametric resonance of a submerged tether can still occur, but the stresses and responses differ significantly due to the higher energy dissipation. This becomes very clear when analyzing the same tether and support motion as in Section E3. Figure E4 shows the temporal evolution of the utilisation, now including the hydrodynamic effects. The utilisation for tensile forces remains practically constant and is of similar magnitude as for the dry tether case (Figure E3). Whereas the bending moment utilisation grows when the system arrives at the parametric instability, which occurs approximately after 140 s. However, the maximum bending moment values and so the associated maximum utilisation value is only a fraction of that observed in previous section. While the maximum bending moment utilisation for the dry case (Figure E3) is 0.82, for the submerged case it is barely 0.10. Therefore, these results confirm that the submerged tether can also become unstable after sufficiently long excitation period. However, the effects of parametric instability are considerably smaller when including the hydrodynamic effects.

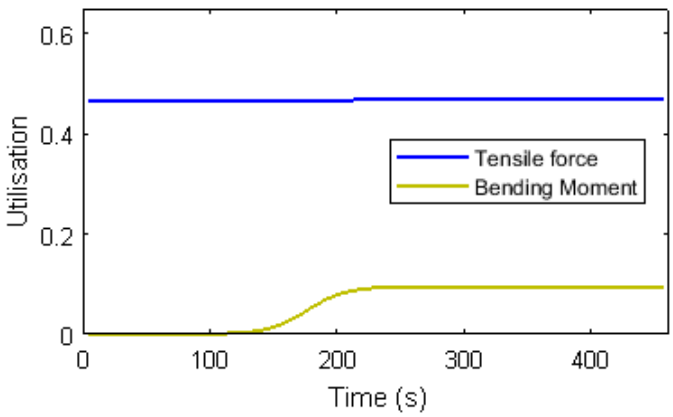

Figure E4. Utilisation of steel for a submerged tether during parametric resonance

E4.1 Effect of boundary condition

The particular technological solution used to fasten the tether to the floating structure and to the seabed will determine the tether's behavior at those locations. In other words, boundary conditions of the tether are system dependent. When numerically modelling that system, it is very important to choose the correct properties of the boundary conditions. The possibilities

range between free-to-rotate supports to fully restrained rotations. Therefore, this section investigates the effect of rotational stiffness (k_r) at the boundary conditions of the tether model. Figure E5 shows the fundamental frequency of the tether for various values of rotation stiffness. As expected, the stiffer the support, the higher the frequency.

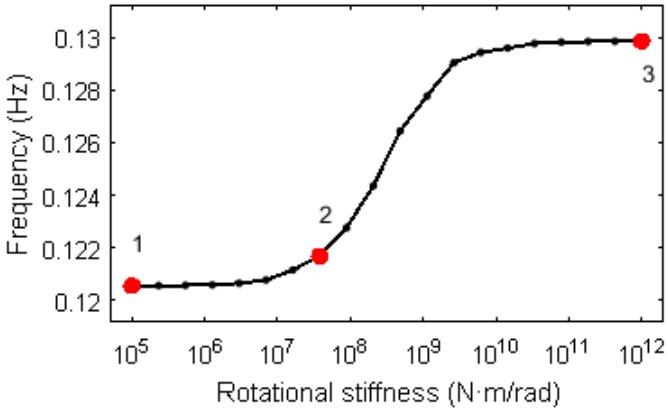

Figure E5. Tether's fundamental frequency for different rotational stiffness

Even though the frequencies change only slightly, the structural behaviour changes significantly. This is particularly pronounced for bending moments. Figure E6 shows the bending moment diagram along the tether during parametric resonance. The tethers are excited with an imposed motion with a 2:1 frequency ratio. Because the tether's fundamental frequency varies (Figure E5), the excitation frequency is different depending on the rotational stiffness considered. Three particular rotational stiffness values are considered, which correspond to the cases marked with red dots in Figure E5. If the supports are free to rotate, the maximum bending moment is located at mid-span and there is no moment at the supports (Figure E5a). However, as soon as the rotational stiffness increases more bending moments appear at the support (Figure E5b). If the rotations are fully restrained, the bending moment diagrams are dominated by the moments near the supports (Figure E5c). However, not only the location of the maximum is of interest, it is also important to note the difference in bending moment magnitudes for each case. While for the free-to-rotate case the maximum is 0.15 MN·m (Figure E5a), for the fully restrained rotation case the maximum bending moment is 1.35 MN·m (Figure E5c). For the considered tether and depending on the rotational stiffness, the maximum bending moment can be up to one order of magnitude greater.

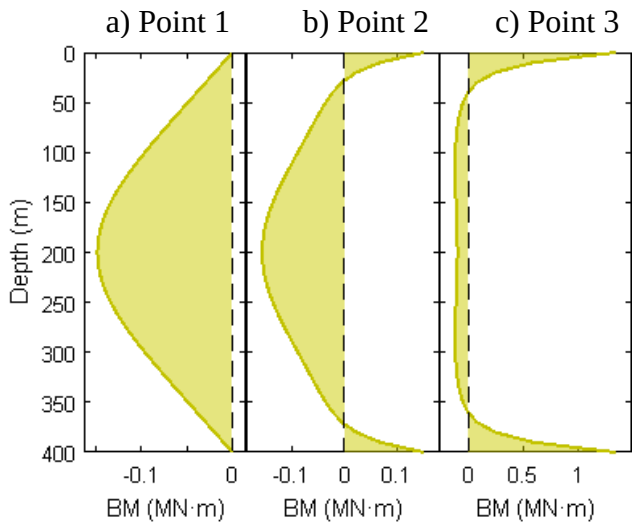

Figure E6. Bending moment diagram along the tether during parametric resonance for various rotation stiffness: a) Low stiffness (≡ free to rotate); b) Intermediate stiffness; c) High stiffness (≡ restrained rotations)

Figure E7 shows the corresponding maximum utilisation obtained during parametric resonance for each considered value of rotational stiffness. The utilisation due to tension is in practice constant, whereas for bending moment it is highest for the case with (effectively) fixed rotational supports. Therefore, to assume a high rotational stiffness is conservative and will give the highest (worst) utilisation values. A tether that allows for some rotation at the support can indeed become unstable by reaching parametric resonance, but the maximum stresses will be smaller than for the case with fully restrained rotations.

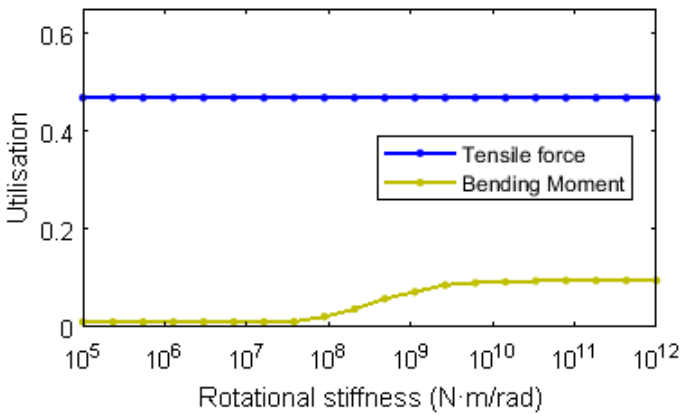

Figure E7. Maximum utilisation of steel for a submerged tether during parametric resonance for different rotational stiffness

E4.2 Support motion: Amplitude and frequency variation

The imposed support motion, directly related to the wave loading, can vary in amplitude and frequency. It is common to represent the system's stability for any amplitude-frequency combination in graphical form using stability maps or Strutt diagrams. The limits between stable and unstable regions are delimited by the transition curves. The regions grouping all unstable solutions are often called instability tongues. Figure E8 shows the stability map for the tether under consideration in this study. To generate this figure, 1320 separate simulations were necessary, each considering 120 cycles of imposed motion. Each simulated case is represented with a dot in Figure E8. Small black docks indicate that the corresponding

amplitude-frequency combination results in a stable response of the submerged tether. Whereas, large red dots indicate that the system is unstable, in other words, that it has reached parametric resonance.

Figure E8 also displays the theoretical transition curves based on the analytical expressions derived in (Cantero et al. 2017). This formulation gives the transition curves for a dry tether with internal damping. No analytical solution exist that includes hydrodynamic effects. For this reason, an internal damping of 10% is used to approximate the energy dissipation effects of the submerged case. This formulation provides a set of transition curves for each mode of vibration considered. Figure E8 shows as gray areas the instability tongues of the first three modes. The agreement between numerical and analytical results is acceptable.

This stability map shows that reasonably small amplitudes of support motions can lead to important unstable tether responses. Furthermore, the greater the amplitude of the support motion is, the more frequencies there are that result in unstable motions.

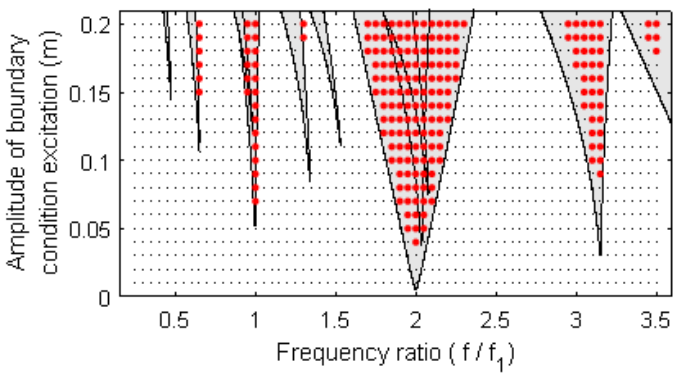

Figure E8. Stability map for submerged tether (stable = small black dot, unstable = large red dot) and theoretical instability tongues (see Appendix) associated to tether's 1st mode (Blue), 2nd mode (Green) and 3rd (Red) mode

As it is customary, the stability criteria to generate the Strutt diagram in Figure E8 is based on the values of lateral displacements of the tether. However, it is interesting to investigate the effect of the system's stability on other load effects for the same amplitude-frequency combinations. Figure E9 shows the maximum utilisation values due tension. It clearly shows a steady increase of the utilization with the amplitude of the support motion regardless of the particular excitation frequency. The effect of the system's stability is barely visible.

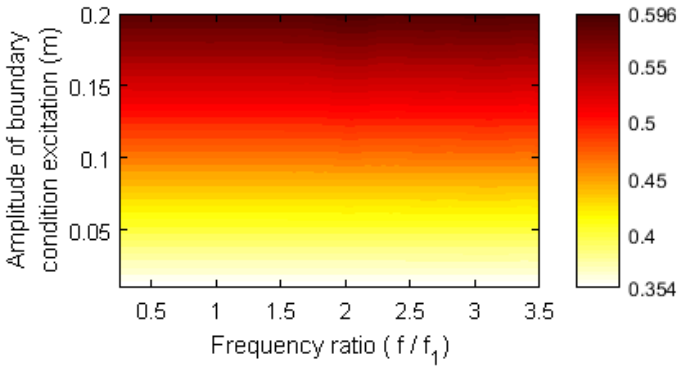

Figure E9. Maximum utilisation of steel due to tension

On the other hand, the maximum utilisation due to bending moments, shown in Figure E10, is strongly related to the stability of the system. The same instability tongues observed for lateral displacements (Figure E8) can be observed on the bending moment utilisation values (Figure E10). However, the magnitude of the utilisation values due to bending moment is rather small compared to those due to tension.

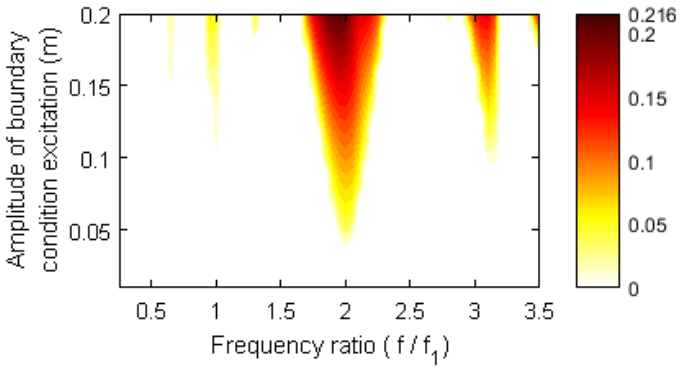

Figure E10. Maximum utilisation of steel due to bending moment

E5. Conclusion

This document has investigated the effect of parametric excitation on the response of taut mooring lines. It extended existing studies in order to analyse other load effects that are generally not investigated. In particular, this study focused on maximum tension values and bending moments along the tether length. In order to compare both load effects, the results are expressed in terms of sectional stress values and normalized by the yield strength of the material, which gives the utilisation of steel. First, parametric resonance is investigated for the case of a dry tether. The instability produces significant dynamic effects that translate into large variations of bending moment utilisation. Then, the same tether is studied including the hydrodynamic effects. Larger energy dissipation mechanisms reduce the effect of parametric resonance. Tension utilisation is practically not influenced by the instability, whereas bending moments show only a moderate increase. Furthermore, the study of the influence of rotational stiffness at the supports has shown that the fully restrained rotational support leads to the highest stresses and is thus regarded as conservative. Finally, the analysis of multiple amplitude-frequency combinations for the support motion produced the stability diagram for the considered tether. With respect to the axial forces, the simulations confirm that the tension utilisation is practically independent of the systems stability and that it is directly proportional to the tethers elongation due to the imposed support motion. As for the bending moments, the system's stability clearly influences the results, obtaining larger utilisation values at the instability tongues. However, the magnitude of the utilisation values due to bending moment is rather small compared to those due to tension.

Acknowledgements

The research presented in this manuscript was possible thanks to the financial support of The Fjord Crossing research program for the Coastal Highway Route E39.

References

Aage, C., Bernitsas, M.M., Choi, H.S., Crudu, L., Incecik, A. & Murray, J.J. 2000. The Specialist Committee on Deep Water Mooring. Final report and recommendations to the 22nd ITTC. *International Towing Tank Conference*, Seoul, 2000.

Abaqus 2011. *Analysis User's Manual*. Dassault Systèmes, Providence.

Cantero, D., Rønnquist, A. & Naess, A. 2017. Tension during parametric excitation in submerged vertical taut tethers. Applied Ocean Research 65: 279-289.

Franzini, G.R. & Mazzilli, C.E.N. 2016. Non-linear reduced-order model for parametric excitation analysis of an immersed vertical slender rod. *International Journal of Non-Linear Mechanics* 80: 29–39.

Lei, S., Zhang, W., Lin, J., Yue, Q., Kennedy, D. & Williams, F.W. 2014. Frequency domain response of a parametrically excited riser under random wave forces. *Journal of Sound and Vibration* 333:485-498:

Lilien, J.L. & Da Costa, A.P. 1994. Vibration amplitudes caused by parametric excitation of cable stayed structures. Journal of Sound and Vibration 174: 69-90.

Vegvesen 2012. Ferjefri E39 English summary. http://www.vegvesen.no/vegprosjekter/ferjefriE39/English (accessed 14.11.17).

Appendix F - Static deformation of cable

F1. The Catenary

The catenary is the profile adopted by a uniform inextensible cable that hangs between two fixed points at the same level. The cable is assumed to have no flexural rigidity and that it can only sustain tensile forces. The cable is inextensible, which means that the length of the cable remains the same. Derivations below are based on the equations published in [F1].

The definition of the forces in a differential element of the cable is:

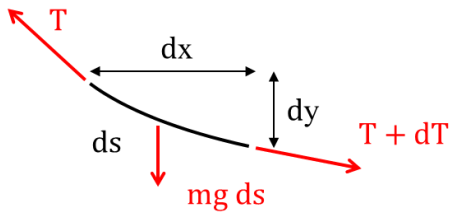

Figure F1: Forces in cable element

We need to project the tension forces on X- and Y-axis. To project on X-axis we multiply the vector by the ratio dx to ds, this is dx/ds. Whereas to project on the Y-axis we multiply by dy/ds. Thus our force equilibrium diagram is:

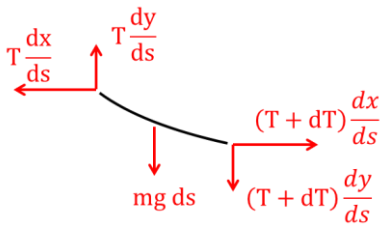

Figure F2: Forces in cable element projected on X and Y axis

The sum of vertical forces gives

$$T\frac{dy}{ds} - (T + dT)\frac{dy}{ds} - mg\ ds = 0 \qquad \text{Eq. (F1)}$$

which is equal to

$$\frac{dy}{ds}\left(\frac{dT}{ds}\right) = -mg \qquad \text{Eq. (F2)}$$

which can be expressed also as

$$\frac{d}{ds}\left(T\frac{dy}{ds}\right) = \frac{dT_y}{ds} = -mg \qquad \text{Eq. (3)}$$

The sum of horizontal forces

$$(T + dT)\frac{dx}{ds} - T\frac{dx}{ds} = 0 \qquad \text{Eq. (F4)}$$

that can also be expressed as

$$\frac{d}{ds}\left(T\frac{dx}{ds}\right) = \frac{dT_x}{ds} = \frac{dH}{ds} = 0 \qquad \text{Eq. (F5)}$$

The last equation can be integrated directly and shows that the horizontal component of the axial force in the cable is constant, since there are no horizontal loads acting. This gives:

$$T\frac{dx}{ds} = H \qquad \text{Eq. (F6)}$$

This expression can be substituted in Eq. (F3)

$$\frac{d}{ds}\left(H\frac{ds}{dx}\frac{dy}{ds}\right) = -mg \qquad \text{Eq. (F7)}$$

which is

$$H\frac{dy}{dx} = -mg\ ds \qquad \text{Eq. (F8)}$$

differentiating by dx and knowing that H is constant gives

$$H\frac{d^2y}{dx^2} = -mg\frac{ds}{dx} \qquad \text{Eq. (F9)}$$

Because of the geometric relationship

$$dx^2 + dy^2 = ds^2 \qquad \text{Eq. (F10)}$$

which, by dividing it over dx^2, we can express as

$$1 + \left(\frac{dy}{dx}\right)^2 = \left(\frac{ds}{dx}\right)^2 \qquad \text{Eq. (F11)}$$

Thus the governing differential equation of the catenary takes the form

$$H\frac{d^2y}{dx^2} = -mg\sqrt{1 + \left(\frac{dy}{dx}\right)^2} \qquad \text{Eq. (F12)}$$

This differential equation can be solved knowing the following hyperbolic identities

$$\cosh^2 t - \sinh^2 t = 1 \qquad \text{Eq. (F13)}$$

$$\frac{d}{dt}(\cosh t) = \sinh t \qquad \text{Eq. (F14)}$$

$$\frac{d}{dt}(\sinh t) = \cosh t \qquad \text{Eq. (F15)}$$

The solution that satisfies Eq. (F12) and the boundary conditions is:

$$y = \frac{H}{mg}\left(\cosh\left(\frac{mgL}{2H}\right) - \cosh\left(\frac{mg}{H}\right)\left(\frac{L}{2} - x\right)\right) \qquad \text{Eq. (F16)}$$

The length of a portion of the cable is

$$s = \int_0^x \sqrt{1 + \left(\frac{dy}{dx}\right)^2}\, dx = \frac{H}{mg}\left(\sinh\left(\frac{mgL}{2H}\right) - \sinh\left(\frac{mg}{H}\right)\left(\frac{L}{2} - x\right)\right) \qquad \text{Eq. (F17)}$$

So if a cable of length L_0 is used, the horizontal component of the cable tension may be found by solving

$$\sinh\left(\frac{mgL}{2H}\right) = \frac{mgL_0}{2H} \qquad \text{Eq. (F18)}$$

The tension at any point is

$$T = H\cosh\left(\frac{mg}{H}\right)\left(\frac{L}{2} - x\right) \qquad \text{Eq. (F19)}$$

F2. Small sag case

Certain assumptions can be done if the sag of the cable is considered small. Following derivations are based on the work published in [F2].

For flat-sag cables with constant weight, the slope of the profile is very small and so

$$dx \cong dx \qquad \text{Eq. (F20)}$$

Eq. (F9) becomes

$$H\frac{d^2y}{dx^2} = -mg \qquad \text{Eq. (F21)}$$

and its solution is the parabola

$$y = \frac{mgL^2}{2H}\left(\frac{x}{L} - \left(\frac{x}{L}\right)^2\right) \qquad \text{Eq. (F22)}$$

The cable deflection at mid-span is for $x = L/2$ is the sag

$$d = \frac{mgL^2}{8H} \qquad \text{Eq. (F23)}$$

The horizontal component of the tension can be calculated from this last equation directly.

F3. The elastic Catenary

Now the cable is modelled considering its elastic properties assuming a linear-elastic behaviour. This section shows then the derivation of the static response of single cable between two rigid supports not necessarily at the same level. The cable has constant mass and cross-section (when unloaded). Derivations presented here is based on the results published in [F1].

The cable is suspended between two fixed points A and B with coordinates $(0,0)$ and (l,h) as seen in Figure F3.

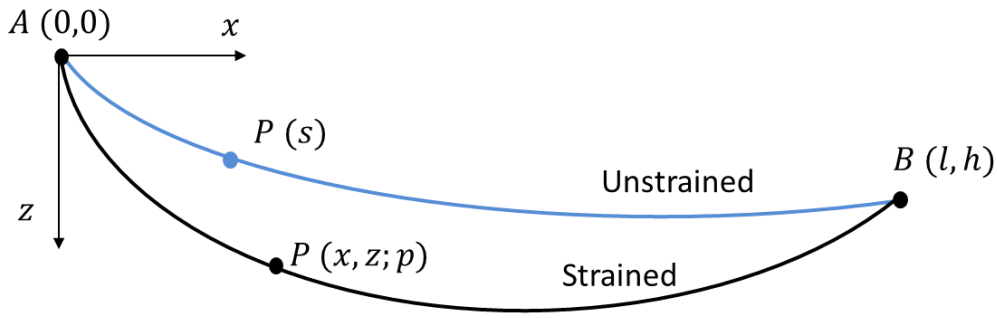

Figure F3: Coordinates of the elastic catenary

The unstrained length of the cable is L_0, which could be smaller than the distance between points A and B, but not much less.

It is convenient to define Lagrangian coordinates:

s = is the length of the cable from the origin to a point when the cable is unloaded.
p = the new length of the cable under self-weight

Self-weight is defined as

$$W = mgL_0 \qquad \text{Eq. (F24)}$$

Similar to Eq. (F11) it is possible to define a geometric constraint

$$\left(\frac{dx}{dp}\right)^2 + \left(\frac{dz}{dp}\right)^2 = 1 \qquad \text{Eq. (F25)}$$

The forces on a segment of the cable can be seen in Figure F4.

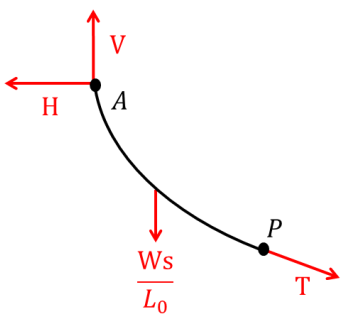

Figure F4: Forces on segment of strained cable

Balancing horizontal and vertical forces gives

$$T\frac{dx}{dp} = H \qquad \text{Eq. (F26)}$$

$$T\frac{dy}{dp} = V - W\frac{s}{L_0} \qquad \text{Eq. (F27)}$$

The constitutive relation, mathematically consistent with Hook's law is

$$T = EA_0\left(\frac{dp}{ds} - 1\right) \qquad \text{Eq. (F28)}$$

where E is the Young's modulus and A_0 the cross-sectional area of the unstrained cable. The end conditions at supports A and B are

$$\begin{matrix} x = 0 & z = 0 & p = 0 & s = 0 \\ x = l & z = h & p = L & s = L_0 \end{matrix} \qquad \text{Eq. (F29)}$$

where L is the length of the strained cable.

a) Solution for $T = T(s)$

Eq. (F26) and Eq. (F27) are squared and added together

$$T^2\left(\frac{dx}{dp}\right)^2 + T^2\left(\frac{dy}{dp}\right)^2 = H^2 + \left(V - W\frac{s}{L_0}\right)^2 \qquad \text{Eq. (F30)}$$

that reduces to the following, when considering Eq. (F25):

$$T = \sqrt{H^2 + \left(V - W\frac{s}{L_0}\right)^2} \qquad \text{Eq. (F31)}$$

b) Solution for $x = x(s)$

Noting that

$$\frac{dx}{ds} = \frac{dx}{dp}\frac{dp}{ds} \qquad \text{Eq. (F32)}$$

and from Eq. (F26)

$$\frac{dx}{dp} = \frac{H}{T} \qquad \text{Eq. (F33)}$$

and from Eq. (F28)

$$\frac{dp}{ds} = \frac{T}{EA_0} + 1 \qquad \text{Eq. (F34)}$$

and so

$$\frac{dx}{ds} = \frac{H}{T}\left(\frac{T}{EA_0} + 1\right) = \frac{H}{EA_0} + \frac{H}{T} \qquad \text{Eq. (F35)}$$

using Eq. (F31) gives

$$\frac{dx}{ds} = \frac{H}{EA_0} + \frac{H}{\left(H^2 + \left(V - W\frac{s}{L_0}\right)^2\right)^{\frac{1}{2}}} \qquad \text{Eq. (F36)}$$

The solution of the differential equation, taking into account the end conditions at support A, gives the following solution

$$x(s) = \frac{Hs}{EA_0} + \frac{HL_0}{W}\left[\sinh^{-1}\left(\frac{V}{H}\right) - \sinh^{-1}\left(\frac{V - Ws/L_0}{H}\right)\right] \qquad \text{Eq. (F37)}$$

c) Similarly the solution for $z = z(s)$

$$z(s) = \frac{Ws}{EA_0}\left(\frac{V}{W} - \frac{s}{2L_0}\right) + \frac{HL_0}{W}\left[\left(1 + \left(\frac{V}{H}\right)^2\right)^{\frac{1}{2}} - \left(1 + \left(\frac{V - \frac{Ws}{L_0}}{H}\right)^2\right)^{\frac{1}{2}}\right] \qquad \text{Eq. (F38)}$$

d) Solutions for H and V

Using the other end conditions we arrive to the following transcendental equation

$$l = \frac{HL_0}{EA_0} + \frac{HL_0}{W}\left[\sinh^{-1}\left(\frac{V}{H}\right) - \sinh^{-1}\left(\frac{V - W}{H}\right)\right] \qquad \text{Eq. (F39)}$$

and the following algebraic equation

$$h = \frac{WL_0}{EA_0}\left(\frac{V}{W} - \frac{1}{2}\right) + \frac{HL_0}{W}\left[\left(1 + \left(\frac{V}{H}\right)^2\right)^{\frac{1}{2}} - \left(1 + \left(\frac{V - W}{H}\right)^2\right)^{\frac{1}{2}}\right] \qquad \text{Eq. (F40)}$$

F. References

[F1] Max Irvine. *Cable Structures*, The MIT Press, Cambridge, 1981.
[F2] Max Irvine. Studies in the statics and dynamics of simple cable systems. Master thesis. California Institute of Technology, Pasadena, 1974.

Appendix G - Parametric Excitation of Arch Bridge

This document explores the parametric excitation phenomena and the possibility of parametric resonance. The bridge under investigation is a 4602 m long horizontally-arched floating bridge. The bridge properties have been taken from the document "Bilag B – Input to Novaframe and Orcaflex" [G1].

This document presents first a brief introduction to parametric excitation and clarifies some important aspects. Then the arch bridge is modelled using a simplified beam model. Numerical studies using this model show what responses are expected during parametric resonance and investigate the contribution of several key aspects, such as excitation amplitude and frequency and system damping. This document ends giving an overview of the findings and provides some recommendations.

G.1. Parametric excitation (PE)

In order to understand what parametric excitation is, it is convenient to start with the simplest configuration. Assume that we have a single degree of freedom system, like the one shown in Figure G1. This system is not subjected to any external load ($F = 0$). However, the system features a time-varying parameter, in this case the spring stiffness ($k(t)$). The system's response depends on the values of that parameter, thus called parametric excitation.

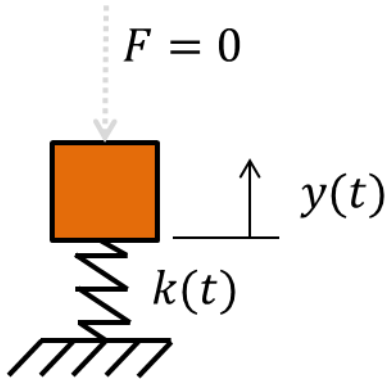

Figure G1: Model of single DOF system

The equation of motion of the system in Figure G1 is:

$$m\,\ddot{y}(t) + k(t)y(t) = 0 \qquad \text{Eq. (G1)}$$

If we say that the variation of the spring stiffness is harmonic, it can be described by:

$$k(t) = k_0 + A\cos(\Omega t) \qquad \text{Eq. (G2)}$$

where k_0 is the initial stiffness, A the amplitude of variation and Ω the frequency of variation. Performing the change of variable:

$$\tau = \Omega\, t \qquad \text{Eq. (G3)}$$

renders the equation:

$$m\Omega^2\ddot{y}(\tau) + (k_0 + A\cos(\tau))y(\tau) = 0 \qquad \text{Eq. (G4)}$$

which can be rearranged by dividing over $m\,\Omega^2$ to:

$$\ddot{y}(\tau) + \left(\frac{k_0}{m\Omega^2} + \frac{A}{m\Omega^2}\cos(\tau)\right)y(\tau) = 0 \qquad \text{Eq. (G5)}$$

We know that the system frequency is:

$$\omega = \sqrt{\frac{k_0}{\mathrm{m}}} \qquad \text{Eq. (G6)}$$

thus Eq. (G5) can be written as:

$$\ddot{y}(\tau) + \left(\frac{\omega^2}{\Omega^2} + \frac{A}{m\Omega^2}\cos(\tau)\right)y(\tau) = 0 \qquad \text{Eq. (G7)}$$

that can be expressed in the classic Mathieu equation format as:

$$\ddot{y}(\tau) + (\alpha + \beta\cos(\tau))y(\tau) = 0 \qquad \text{Eq. (G8)}$$

where

$$\alpha = \frac{\omega^2}{\Omega^2} \qquad \text{Eq. (G9)}$$

$$\beta = \frac{A}{m\Omega^2} \qquad \text{Eq. (G10)}$$

It can be shown that for certain combinations of (α, β) pairs, the solution of the equation leads to ever larger results. Then, it is said that the solution is unstable. This instability is called parametric resonance (PR). It is worth noting that parametric excitation (PE) is the general description of the way the system is excited, whereas parametric resonance (PR) corresponds to those situations where the system is unstable.

Therefore, when the solutions of the equation are studied for any combination of (α, β) values, some combinations render unstable results. All possible (α, β) pairs that lead to parametric resonance are grouped together in the so-called instability tongues. The separations between stable and unstable solutions in the (α, β) plane are defined by the transition curves. The following figure (Figure G2a) shows the transition curves for the classic Mathieu equation. Figure G2b shows the influence of damping on the shape of the instability tongues.

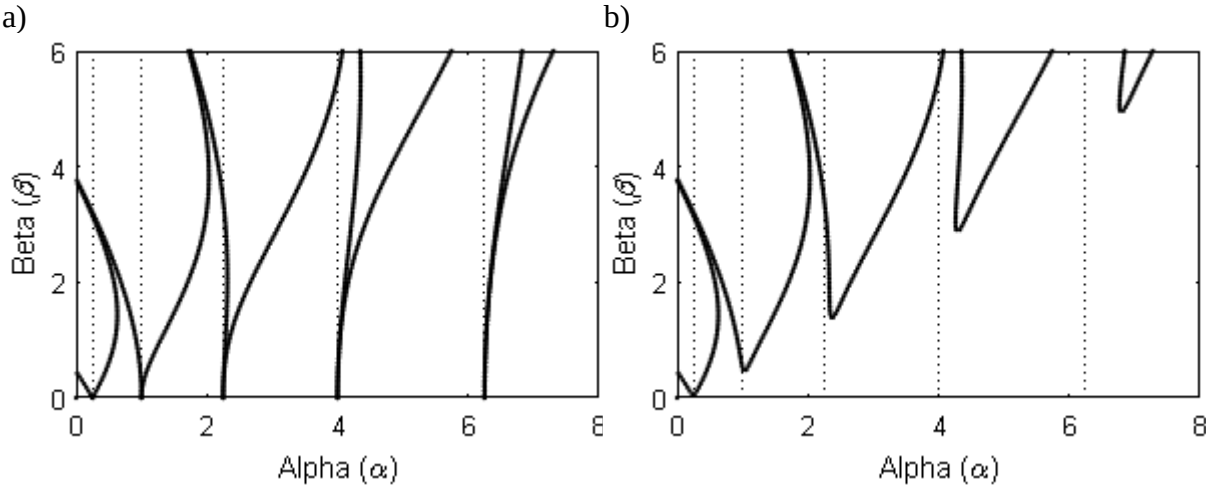

Figure G2: Transition curves; a) No damping; b) With damping

Note that Eq. (G9) is a ratio that relates the fundamental frequency of the structure to the excitation frequency. This ratio α is commonly used in studies in the field of parametric excitation. Alternatively, it is possible to define the ratio between frequencies, as the relation between the excitation frequency and the fundamental frequency of the structure (Eq. (G11)). The frequency ratio (FR) is thus the ratio of the excitation frequency (f) to the fundamental frequency (f_1). The principal parametric resonance tongue emanates from $FR = 2$, that corresponds to $\alpha = 0.25$ in Figure G2. The authors believe that this definition leads to a more intuitive interpretation of the results. Furthermore this definition confines all the critical frequencies in a range from 0 to 2.

$$FR = \frac{\omega}{\Omega} = \frac{f}{f_1} \qquad \text{Eq. (G11)}$$

G.1.1 PE of horizontal arch bridge

The horizontally arched floating bridge under investigation is loaded (among many other possible loads) by the motion of the waves. These motions produce a time-varying axial force on the bridge. This translates into a time-varying geometric stiffness of the bridge's section. Therefore, the bridge is parametrically excited by the change in section stiffness (the sum of elastic stiffness and geometric stiffness). However, this does not necessarily mean that the bridge will reach an unstable situation. Parametric resonance will only occur under certain conditions. The key aspects to assess the possibility of PR are listed below:

- The magnitude of the imposed motions due the wave loading. More precisely, the amplitude of the variation of the system's parameter.
- The frequency of the variation and its relation to other frequencies of the system.
- The amount of damping available.

The wave motion is irregular but can be defined according to its energy content in frequency domain. The waves induce some motions on the floating pontoons. However, the actual motions of the pontoons are not the same as the wave motions. In general, the broad banded process of the wave motion translates into a narrow banded motion of the pontoons. In other words, the motions of the pontoons can be simplified to a single predominant harmonic motion.

G.2 Numerical investigation

G.2.1 Simplified model

The actual bridge under investigation is a complex combination of different structural components. The goal of this simplified numerical model is not to find a precise description of the whole bridge, but rather to add some insight on the possibilities of parametric resonance. Therefore the simplified numerical model is defined considering following points:

- Geometric properties for the bridge are taken from the document [G1]
- The whole bridge is modelled as a 2D arched beam. Thus analysis includes only horizontal motions of the bridge deck.
- The geometry of the beam is almost the same as that of the original bridge. This corresponds to a circumference arc of length 4602 m and a radius of 5000 m. Geometric properties are summarized in Table G1 and Figure G3.
- The section properties are constant throughout the beam. The actual values of the section properties are summarized in Table G1, which correspond to weighted average of 'S1' and 'F1' girder sections defined in [G1].
- The boundary conditions at both ends of the beam are fixed, i.e. no rotations or displacements are allowed.
- The model considers geometric nonlinear effects.
- No hydrodynamic effects have been considered

Description	Symbol	Value	Unit
Chord width	w	4441.62	m
Chord height	h	520.27	m
Arc length	S	4602	m
Radius	R	5000	m

Table G1: Beam geometric properties

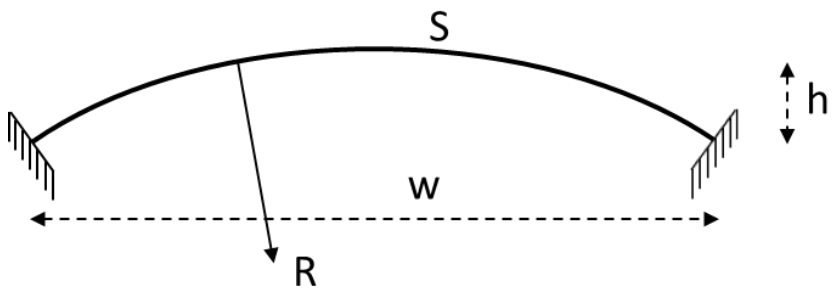

Figure G3: Geometric properties of arch

Description	Symbol	Value	Unit
Area	A	2.01	m^2
Second moment of area	I	14.46	m^4
Mass per unit length	μ	27982.5	kg/m
Young's modulus	E	$210 \cdot 10^9$	N/m^2
Poisson's ratio	ν	0.3	-

Table G2: Equivalent material and section properties

The beam is modelled using a finite element discretization with ABQUS [G3] software. A total of 160 Timoshenko beam elements (B21) are used to represent the whole structure. Figure G4 shows the nodes and geometry of the simplified numerical model.

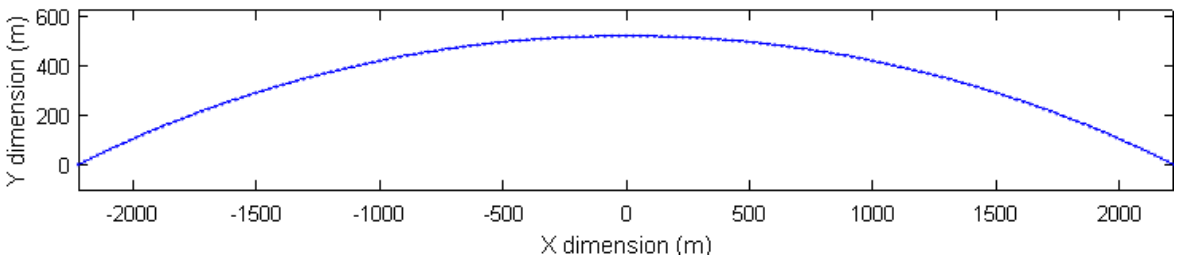

Figure G4: FEM of arch bridge

The loading on the beam has been modelled as a uniform distributed load perpendicular to the beam longitudinal axis, as can be seen in Figure G5. The time-varying nature of the load is defined according to Eq. (G12), where P_0 is the constant term, A the amplitude of the harmonic term and f the frequency of the loading.

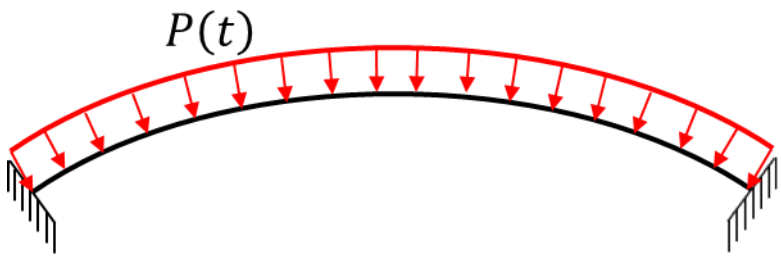

Figure G5: Time-varying uniform load on beam

$$P(t) = P_0 + A\sin(2\pi\, f\, t) \qquad \text{Eq. (G12)}$$

G.2.2 Modal analysis

The modal analysis of the presented simplified numerical model of the bridge renders the natural periods presented in Table G3 under the column "Original model". These results differ significantly from those published in [G2] and repeated in Table G3 for convenience. In order to obtain similar natural frequencies on the simplified model, the mass unit length of the bridge was modified until a better match was achieved. The adjusted mass per unit length is 2798.25 kg/m (which is 10 times smaller as the value reported in [G1]). This adjusted value of the mass per unit length is adopted for the rest of the calculations presented in this document.

Mode number	Original model	Adjusted model	From [G2]
1	214.64	67.88	68.76
2	116.76	36.92	39.38
3	64.74	20.47	22.61
4	44.45	14.06	21.39
5	30.84	9.75	15.85

Table G3: Periods of vibration in seconds (s) for first five modes

The discrepancy between solutions reported in Table G3 might be due to any or multiple of the following reasons:

- Due to the reduced complexity of the model used in this study.
- The simplified model in this study considers only boundary conditions at the abutments of the bridge. The special connection between the tower of the suspension bridge and the deck has not been included.
- The section properties reported in [G1] might have a typo.
- Or the model used in [G2] to calculate the natural periods reported in Table G3 is wrong.

In either case, the simplified numerical model used in this study, represents the dynamic properties of a certain curved beam. In might not give a precise description of the actual planned bridge. However, the insight and conclusions that can be drawn from it are still valid. Therefore, the simplified model is adopted in this study to investigate the possibility of achieving parametric resonance. Figure G6 shows the first five modes of vibration of the simplified arch beam.

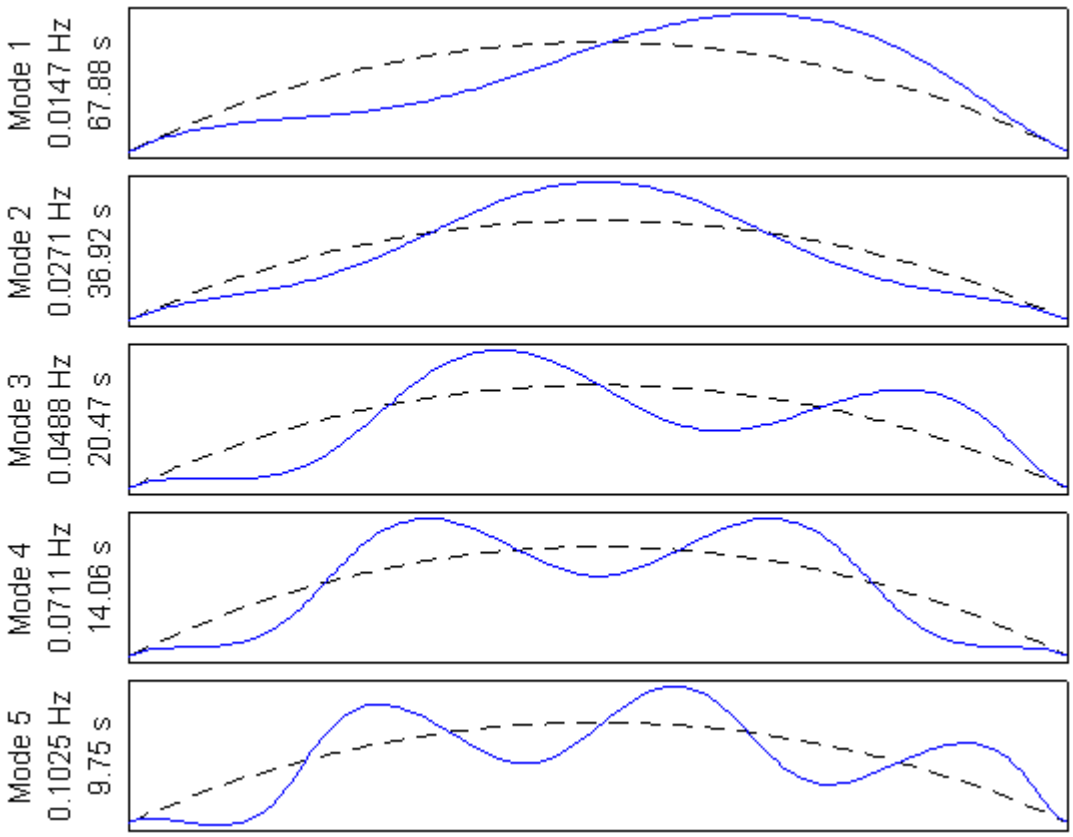

Figure G6: First five modes of vibration of numerical model

G.2.3 Typical response

This section provides a typical time series of a response that has reached parametric instability. The numerical model described above has been solved for a uniform load without constant component ($P_0 = 0$) and an amplitude A =2500 N/m (See Eq. (G12)). The frequency of variation of the load is such that the $FR = 2$. Some internal damping (5%) has been considered. Figure G7 shows the displacements of centre point of beam in both directions. The response

shows some transient response (from 0 s to 300 s) and readily reaches the steady-state regime. However, after 2000 s the response changes significantly. From that moment on the system has reached parametric instability, which is characterized by an exponential growth of the response (see between 2000 s and 2500 s in Figure G7a). Because of the nonlinearities that growth is limited but considerably greater than for the stable response.

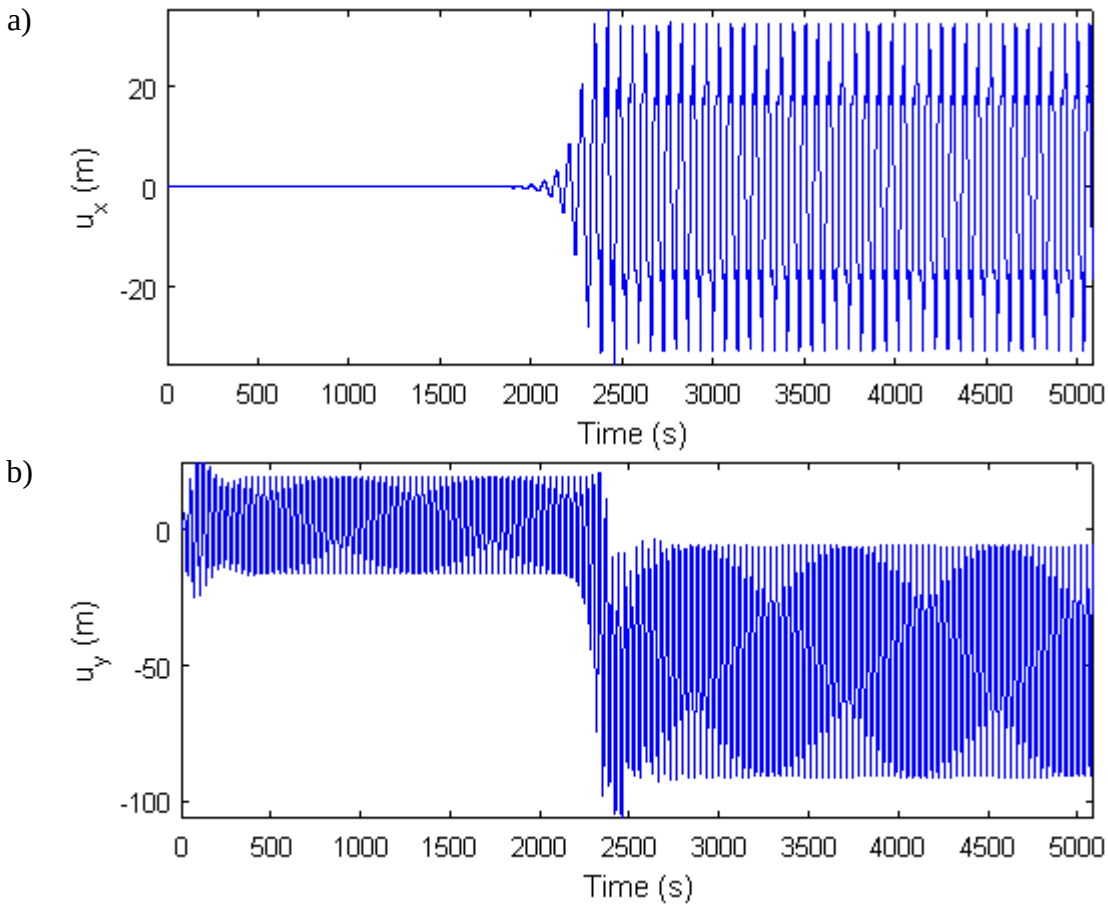

Figure G7: Mid-point displacements of beam for A=2500 N/m and FR=2; a) Horizontal direction (X axis); b) Vertical direction (Y axis)

G.2.4 Influence of amplitude and frequency ratio

Now the numerical model is evaluated for a range of loading scenarios. More precisely, 5 different loading amplitudes are considered for 11 different frequency ratios. The frequency ratios are in the proximity of FR = 2, which gives the principal parametric resonant situation. Thus a total of 55 cases have been studied, each lasting 150 loading cycles. Each time series is analysed to determine if the response has reached instability. Figure G8 shows the corresponding stability map. It shows (a discretized version) of the principal instability tongue, a clear region where the solutions are unstable. Since this simulation includes some damping (5%) the instability tongue does not start at zero amplitude. Because of damping there is a minimum amplitude necessary to trigger the parametric resonance, as could be seen in the theoretical description in Figure G2b.

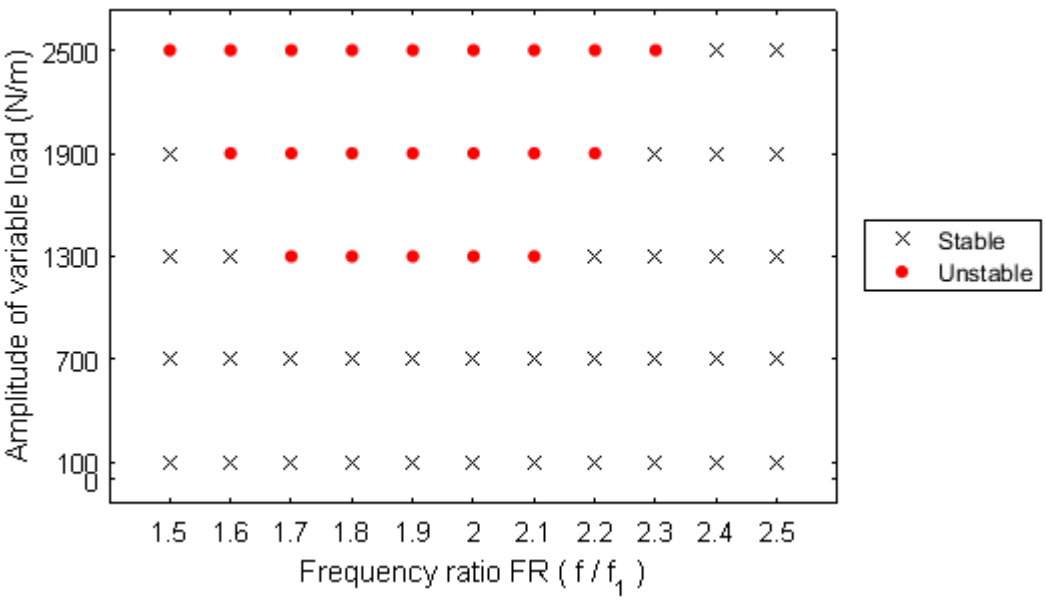

Figure G8: Instability map for simplified arch bridge model

G2.5 Influence of damping

The same example as in section 2.3 is studied now for a range of internal damping values. The most important effect of damping is that it changes the number of loading cycles necessary to reach an unstable situation. Figure G9 shows that it takes more time to trigger the parametric resonance for cases with higher damping values.

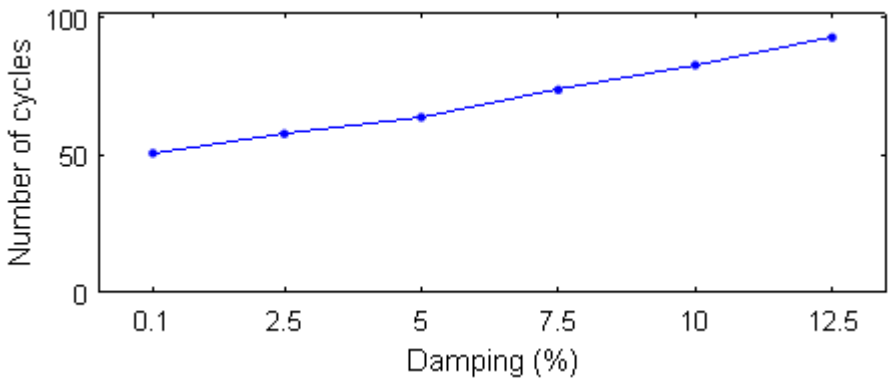

Figure G9: Influence of damping on the number of loading cycles needed to reach parametric instability.

G3. Conclusions and recommendations

Parametric excitation is a phenomenon that appears in any system that has a parameter that changes periodically. In the case of the arch bridge, this might be the cyclic variation of its geometric stiffness due to variations in axial load. On the other hand, parametric resonance is the unstable response of that system due to parametric excitation. This occurs for certain combinations of amplitudes and frequencies, where damping plays also a very important role.

This report described a simplified model of the bridge and was investigated for a range of loading scenarios and configurations. First, the example in Section 2.3 shows a typical example of how parametric resonant response would look like in such a bridge. Then Section 2.4 studied

a range of loading scenarios for different amplitudes and frequency ratios, obtaining the characteristic stability map associated to parametric excitation. Finally, section 2.5 highlights the influence of damping on the response.

Further work and suggested investigations.

- It is recommended to further explore the possibility of parametric resonance using a more elaborate model that includes detailed descriptions of all structural elements (girder, tower, pontoon, cables ...), applies the correct boundary conditions, considers the flotation of most parts of the structure and includes the hydrodynamic effects.
- Calculate the response of such a model under long series of harmonic wave loading. The wave loading should have frequencies that would lead to frequency ratios of 2. Study this for several of the modes of vibration of the bridge. In other words, apply harmonic wave loading with frequencies $2f_1$, $2f_2$, $2f_3$ and so on.
- Investigate the time series and look for sudden changes in the response, which would indicate the presence of parametric instabilities.

G. References

[G1] Bilag B – Input to Novaframe and Orcaflex. Curved bridge south – Environmental loading analyses.

[G2] Yanyan Sha, Jørgen Amdahl. Design of floating bridge girders against accidental ship collision loads. 19th IABSE Congress Stockholm, 21-23 September 2016.

[G3] ABAQUS, Analysis User's Manual, Dassault Systèmes, Providence, 2011.

Appendix H - Equations of motion of inclined cable

This appendix shows the derivation of the equations of motion of an inclined cable.

H.1 Derivation of equation of motion

A plane model (2D) of a cable, with distributed loading q in the lateral direction, including second order effects. See Figure H1.

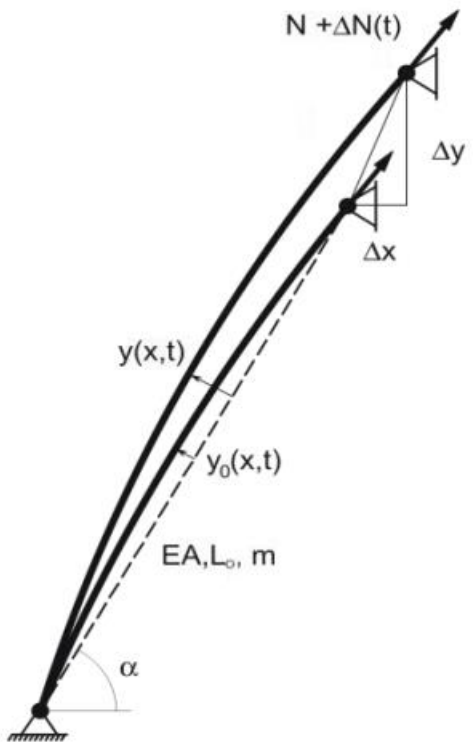

Figure H1: Planar model of single cable

To derive the differential equation, $\alpha = 0$ is assumed. See Figure H2.

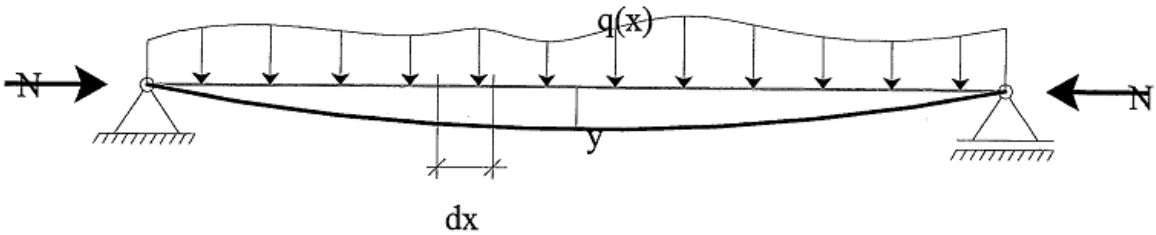

Figure H2: Horizontal cable model

Taking one small element from Figure H2, one can establish equilibrium. Using D'Alembert's principle and including damping, one can establish the equations of dynamic equilibrium.

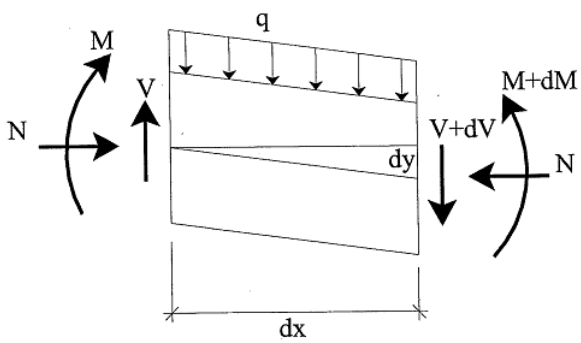

Figure H3: Equilibrium derivation

The sum of forces in Y-direction gives (considering that positive y is downwards):

$$\sum F_y = m\,dx\frac{d^2y}{dt^2} = -V + q\,dx + (V + dV) - c\,dx\frac{dy}{dt} \qquad \text{Eq. (H1)}$$

rearranging and dividing by dx gives the dynamic equilibrium equation

$$\frac{dV}{dx} = m\frac{d^2y}{dt^2} + c\frac{dy}{dt} - q \qquad \text{Eq. (H2)}$$

Taking the sum of moments at the left end of the beam element gives

$$\sum M = I\frac{d^2\theta}{dt^2} = M + q\,dx\frac{dx}{2} + (V + dV)dx - (M + dM) + N\,dy \qquad \text{Eq. (H3)}$$

Assuming that the rotations are small compared to the displacement, one can discard the rotations in the dynamic equilibrium. Therefore, rearranging Eq. (H3) and dividing by dx gives:

$$\frac{q}{2}dx + (V + dV) - \frac{dM}{dx} + N\frac{dy}{dx} = 0 \qquad \text{Eq. (H4)}$$

Neglecting lower order magnitudes

$$V = \frac{dM}{dx} - N\frac{dy}{dx} \qquad \text{Eq. (H5)}$$

Invoking the moment curvature relationship from beam theory:

$$EI\frac{d^2y}{dx^2} = -M \qquad \text{Eq. (H6)}$$

Eq. (H6) in Eq. (H5) gives:

$$EI\frac{d^3y}{dx^3}+N\frac{dy}{dx}+V=0 \qquad \text{Eq. (H7)}$$

Differentiating Eq. (H7) over x the whole equation

$$EI\frac{d^4y}{dx^4}+N\frac{d^2y}{dx^2}+\frac{dV}{dx}=0 \qquad \text{Eq. (H8)}$$

and substituting Eq. (H2) gives:

$$EI\frac{d^4y}{dx^4}+N\frac{d^2y}{dx^2}+m\frac{d^2y}{dt^2}+c\frac{dy}{dt}=q \qquad \text{Eq. (H9)}$$

This is the general dynamic equilibrium equation for a beam with axial load (column).

Our case is a cable with an initial deformation of y_0. We have a very long span, in which case we can discard the contribution of the flexural strength:

$$N\frac{d^2y}{dx^2}+m\frac{d^2y}{dt^2}+c\frac{dy}{dt}=q \qquad \text{Eq. (H10)}$$

Adapting Eq. (H10) to our situation in Figure H1, we will call now:

$$N\rightarrow-\big(N+\Delta N(t)\big) \qquad \text{Eq. (H11)}$$

$$y\rightarrow y+y_0 \qquad \text{Eq. (H12)}$$

$$q\rightarrow q(x,t)+m\,g \qquad \text{Eq. (H13)}$$

Thus equation Eq. (H10) becomes:

$$-\big(N+\Delta N(t)\big)\frac{d^2}{dx^2}(y+y_0)+m\frac{d^2y}{dt^2}+c\frac{dy}{dt}=q(x,t)+m\,g \qquad \text{Eq. (H14)}$$

From the static analysis, once it is assumed that the sag is small, the static curve can then be reasonably approximated as parabolic. In this case, the simplification is made so that $ds/dx\approx 1$, which means that the length of the cable is similar to the length of the chord. In this situation the non-linear second order differential equation of the static displacement of the cable is (see Appendix F)

$$N\frac{d^2y_0}{dx^2}+mg\sqrt{1+\left(\frac{dy_0}{dx}\right)^2}=0 \qquad \text{Eq. (H15)}$$

that reduces to

$$N\frac{d^2y_0}{dx^2}=-mg \qquad \text{Eq. (H16)}$$

that substituted in Eq. (H14) gives:

$$-\left(N+\Delta N(t)\right)\frac{\partial^2 y}{\partial x^2}-\Delta N(t)\frac{\partial^2 y_0}{\partial x^2}+m\frac{\partial^2 y}{\partial t^2}+c\frac{\partial y}{\partial t}=q(x,t) \qquad \text{Eq. (H17)}$$

where:

N is the initial axial force
ΔN the variation of the axial force
m mass per unit length
c cable damping

H.1.1 Calculation of support displacement Δ

We know that

$$N=\frac{EA}{L_0}\Delta \qquad \text{Eq. (H18)}$$

where:

E is the elastic modulus of the cable material
A is the area of the cable section
L_0 the chord length (distance between cable supports)
Δ the length increment of the cable

It is possible to calculate the total length increment as the sum of four contributions

$$\Delta=\Delta_1+\Delta_2+\Delta_3+\Delta_4 \qquad \text{Eq. (H19)}$$

Note the directions of the system of reference in the following derivations. The X-direction is along the cable chord and the Y-direction is perpendicular to it.

The general expression of cable length increment due cable deformation $y(x,t)$ can be derived from Pythagoras' theorem

$$ds^2=dx^2+dy^2 \qquad \text{Eq. (H20)}$$

dividing the expression over dx^2 gives

$$\left(\frac{ds}{dx}\right)^2=1+\left(\frac{dy}{dx}\right)^2 \qquad \text{Eq. (H21)}$$

and integrating the expression along the chord length

$$s=\int_0^{L_0}\sqrt{1+\left(\frac{dy}{dx}\right)^2}\,dx \qquad \text{Eq. (H22)}$$

Length of cable without changes in axial force remains constant and so

$$\Delta = s - L_0 \qquad \text{Eq. (H23)}$$

H.1.1a) Support displacement in x-direction

Assuming a displacement in the X-direction of $\Delta_1 = \Delta x(t)$ as shown in Figure H4.

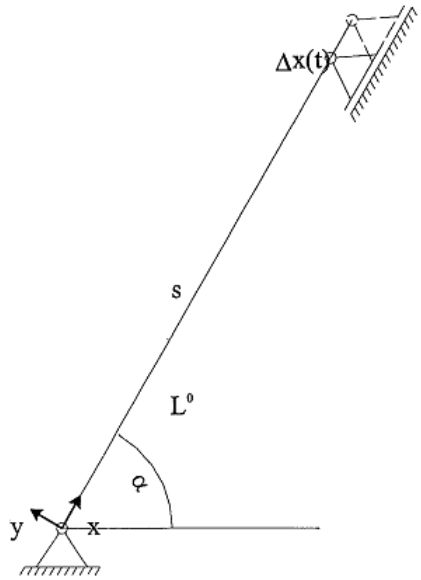

Figure H4: Support displacement in x-direction

Based on the expression of deformation due to axial load in Eq. (H18), one can write:

$$\Delta N = \frac{EA}{L_0}\Delta x(t) \qquad \text{Eq. (H24)}$$

or

$$\Delta_1 = \Delta \mathrm{x}(t) = \frac{\Delta \mathrm{N}\ \mathrm{L}_0}{EA} \qquad \text{Eq. (H25)}$$

H.1.1b) Support displacement in y-direction

The cable length increment Δ_2 due to a support displacement of $\Delta y(t)$ is represented in Figure H5.

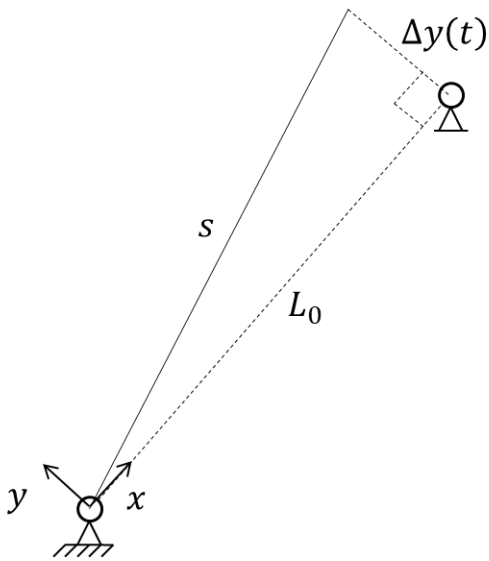

Figure H5: Support displacement in y-direction

The cable length is now

$$\mathrm{s} = \sqrt{L_0^2 + \Delta y(t)^2} \qquad \text{Eq. (H26)}$$

and so

$$\Delta_2 = \mathrm{s} - L_0 = \sqrt{L_0^2 + \Delta y(t)^2} - L_0 \qquad \text{Eq. (H27)}$$

Performing a Taylor expansion Eq. (H27) at $\Delta y(t) = 0$ and knowing that $L \geq 0$ gives:

$$\Delta_2 = \frac{1}{2L_0}\Delta \mathrm{y}(t)^2 - \frac{1}{8L_0^3}\Delta \mathrm{y}(\mathrm{t})^4 + \cdots \qquad \text{Eq. (H28)}$$

Because $L_0 \gg \Delta y(t)$ we case reduce it to

$$\Delta_2 = \frac{1}{2L_0}\Delta \mathrm{y}(t)^2 \qquad \text{Eq. (H29)}$$

H.1.1c) Cable length increment due to dynamic displacement (first mode only)

Assuming that the cable deformation can be described with one mode

$$\mathrm{y}(\mathrm{x}, \mathrm{t}) = \mathrm{Y}(\mathrm{t})\Phi(x) \qquad \text{Eq. (H30)}$$

where

$$\Phi(\mathrm{x}) = \sin\left(\frac{\pi x}{L_0}\right) \qquad \text{Eq. (H31)}$$

We know the general expression of the total length of the deformed cable s (Eq. (H22)). Substituting Eq. (H30) and Eq. (H31) in to Eq. (H22)

$$s = \int_0^{L_0} \sqrt{1 + \left(\frac{\partial}{\partial x}\left(\mathrm{Y(t)} \sin\left(\frac{\pi x}{L_0}\right)\right)\right)^2} \, dx \qquad \text{Eq. (H32)}$$

which is

$$s = \int_0^{L_0} \sqrt{1 + \left(\frac{\pi}{L_0}\mathrm{Y(t)} \cos\left(\frac{\pi x}{L_0}\right)\right)^2} \, dx \qquad \text{Eq. (H33)}$$

Performing a Taylor expansion of the integrand for $Y(t) = 0$)

$$s = \int_0^{L_0} \left(1 + \frac{\pi^2}{2L_0^2} cos\left(\frac{\pi x}{L_0}\right)^2 Y(t)^2 - \frac{\pi^4}{8L_0^4} \cos\left(\frac{\pi x}{L_0}\right)^4 Y(t)^4 + \cdots\right) dx \qquad \text{Eq. (H34)}$$

Discarding higher order terms

$$\mathrm{s} = \mathrm{L_0} + \frac{\pi^2}{4L_0^2} Y(t)^2 \qquad \text{Eq. (H35)}$$

And thus

$$\Delta_3 = \mathrm{s} - \mathrm{L_0} = \frac{\pi^2}{4L_0^2} Y(t)^2 \qquad \text{Eq. (H36)}$$

H.1.1d) Cable sag (Horizontal cable)

The Eq. (H16) can be rearranged to:

$$\frac{d^2 y_0}{dx^2} = -\frac{mg}{N} \qquad \text{Eq. (H37)}$$

the solution is

$$\mathrm{y_0}(x) = -\frac{mg}{N}(x^2 + c_1 x + c_2) \qquad \text{Eq. (H38)}$$

and knowing that the boundary conditions are $y(0) = 0$ and $y(L_0) = 0$ gives

$$\mathrm{c_1} = \frac{1}{2}\frac{mgL_0}{N} \qquad \text{Eq. (H39)}$$

$$\mathrm{c}_2 = 0 \qquad \text{Eq. (H40)}$$

and thus the solution is

$$\mathrm{y}_0(x) = \frac{1}{2}\frac{mg}{N}(L_0 - x)x \qquad \text{Eq. (H41)}$$

The displacement at mid-span of the cable is

$$\mathrm{a}_0 = \frac{1}{8}\frac{mgL_0^2}{N} \qquad \text{Eq. (H42)}$$

Eq. (H41) can be rearranged in terms of a_0 when multiplying and dividing by L_0^2 the right hand side

$$\mathrm{y}_0(x) = \frac{1}{2}\frac{mgL_0^2}{N}\left(1 - \frac{x}{L_0}\right)\frac{x}{L_0} \qquad \text{Eq. (H43)}$$

which can be rewritten as

$$\mathrm{y}_0(x) = 4a_0\left(1 - \frac{x}{L_0}\right)\frac{x}{L_0} \qquad \text{Eq. (H44)}$$

The cable length considering the sag can be calculated using Eq. (H22) again. The integrand

$$\sqrt{1 + \left(\frac{d}{dx}\left(4a_0\left(1 - \frac{x}{L_0}\right)\frac{x}{L_0}\right)\right)^2} \qquad \text{Eq. (H45)}$$

should be expanded using Taylor expansion around $a_0 = 0$

$$1 + 8\left(1 - \frac{2x}{L_0}\right)^2\left(\frac{a_0}{L_0}\right)^2 - 32\left(1 - \frac{2x}{L_0}\right)^4\left(\frac{a_0}{L_0}\right)^4 + \cdots \qquad \text{Eq. (H46)}$$

and integrating between 0 and L_0 gives

$$\mathrm{s} = \mathrm{L}_0 + \frac{8}{3}\frac{a_0^2}{L_0} - \frac{32}{5}\frac{a_0^4}{L_0^3} \qquad \text{Eq. (H47)}$$

Neglecting higher order terms

$$\Delta_4 = \mathrm{s} - \mathrm{L}_0 = \frac{8}{3}\frac{a_0^2}{L_0} \qquad \text{Eq. (H48)}$$

H.1.1e) Cable sag (Inclined cable)

Section H.1.1d calculated the cable sag of a horizontal cable. However, the cable has some inclination and the expression of the cable sag depends on the inclination angle. The new expression can be derived with a change of variable. Figure H6 shows the deformation of the cable with the coordinate system used in the derivation of the original differential equation of the static deformation. Note that the coordinate system is different to the one used in the derivation of Δ_i.

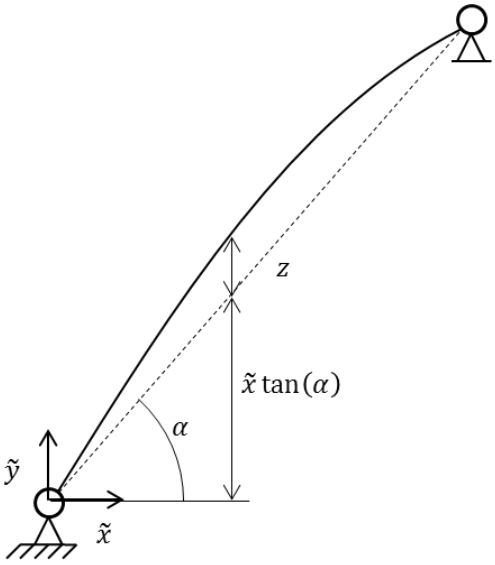

Figure H6: Inclined cable static deformation

The change of variable is

$$\tilde{y} = \tilde{x}\tan(\alpha) + z \qquad \text{Eq. (H49)}$$

which gives the following relations

$$\frac{d\tilde{y}}{d\tilde{x}} = \tan(\alpha) + \frac{dz}{d\tilde{x}} \qquad \text{Eq. (H50)}$$

$$\frac{d^2\tilde{y}}{d\tilde{x}^2} = \frac{d^2z}{d\tilde{x}^2} \qquad \text{Eq. (H51)}$$

Substituting in static deformation differential equation gives

$$H\frac{d^2z}{d\tilde{x}^2} = -mg\sqrt{1 + \left(\tan(\alpha) + \frac{d\tilde{y}}{d\tilde{x}}\right)^2} \qquad \text{Eq. (H52)}$$

which is

$$H\frac{d^2z}{d\tilde{x}^2} = -mg\sqrt{1 + \tan(\alpha)^2 + \left(\frac{d\tilde{y}}{d\tilde{x}}\right)^2 + 2\tan(\alpha)\frac{d\tilde{y}}{d\tilde{x}}} \qquad \text{Eq. (H53)}$$

If $dz/d\tilde{x}$ is considered sufficiently small for its square to be ignored, then this can be rewritten [H2] leading to the vertical displacement of the cable as

$$\mathrm{z} = \frac{\mathrm{mg}\sec(\alpha)\,{L_H}^2}{H}\left[\frac{1}{2}\frac{\tilde{x}}{L_H}\left(1-\frac{\tilde{x}}{L_H}\right)\left(1+\frac{mgL_H\,sin(\alpha)}{6}\left(1-2\frac{\tilde{x}}{L_H}\right)\right)\right] \qquad \text{Eq. (H55)}$$

where

$$\mathrm{L_H} = L_0\cos(\alpha) \qquad \text{Eq. (H56)}$$

$$\mathrm{H} = \mathrm{N}\cos(\alpha) \qquad \text{Eq. (H57)}$$

Thus Eq. (H55) for $\alpha = 0$ gives: (the same as Eq. (H44))

$$for\ \alpha = 0 \qquad \mathrm{z} = \frac{\mathrm{mg}L_H^2}{2H}\left(1-\frac{\tilde{x}}{L_H}\right)\frac{\tilde{x}}{L_H} = \frac{\mathrm{mg}L_0^2}{2N}\left(1-\frac{x}{L_0}\right)\frac{x}{L_0} \qquad \text{Eq. (H58)}$$

Again, the cable length considering the sag can be calculated using Eq. (H22). The integrant can be approximated using Taylor expansion (for $m = 0$) which gives:

$$s = \frac{1}{24}\frac{m^2\mathrm{g}^2{L_H}^3\sec(\alpha)^2}{H^2} + L_H \qquad \text{Eq. (H59)}$$

and so the length increment due to sag of an inclined cable can be expressed as:

$$\Delta_4 = \mathrm{s} - \mathrm{L_0} = \frac{1}{24}\frac{m^2\mathrm{g}^2{L_H}^3\sec(\alpha)^2}{H^2} + L_H - L_0 \qquad \text{Eq. (H60)}$$

using the expressions in Eq. (H56) and Eq. (H57) gives:

$$\Delta_4 = \frac{1}{24}\frac{m^2\mathrm{g}^2{L_0}^3}{N^2\cos(\alpha)} + (\cos(\alpha)-1)L_0 \qquad \text{Eq. (H61)}$$

which is an expression in terms of α that does not depend on the coordinate system used in its derivation. This expression for the case of $\alpha = 0$ is equivalent to the one derived in previous section in Eq. (H48).

$$for\ \alpha = 0 \qquad \Delta_4 = \frac{1}{24}\frac{m^2\mathrm{g}^2{L_0}^3}{N^2} = \frac{8}{3}\frac{a_0^2}{L_0} \qquad \text{Eq. (H62)}$$

H.2 Solution of the parametric excitation equation by generalized coordinates

The equation of motion of the cable vibration is given in Eq. (H17).

We assume a solution in the form

$$y(x,t) = Y(t)\phi(x) \qquad \text{Eq. (H63)}$$

where

$$\phi(x) = \sin\left(\frac{\pi x}{L_0}\right) \qquad \text{Eq. (H64)}$$

The initial deformation is defined in Eq. (H44), and we know that

$$y_0\left(\frac{L_0}{2}\right) = a_0 \qquad \text{Eq. (H65)}$$

If we assume the solution in the form of Eq. (H63), then

$$y_0(x) = y(x,0) = Y(0)\phi(x) \qquad \text{Eq. (H66)}$$

and thus at mid-span using Eq. (H65) gives:

$$y_0\left(\frac{L_0}{2}\right) = y\left(\frac{L_0}{2},0\right) = Y(0)\phi\left(\frac{L_0}{2}\right) = a_0 \qquad \text{Eq. (H67)}$$

which gives

$$Y(0) = \frac{a_0}{\phi\left(\frac{L_0}{2}\right)} = \frac{a_0}{\sin\left(\frac{\pi}{2}\right)} = a_0 \qquad \text{Eq. (H68)}$$

And so

$$y_0(x,0) = y_0(x) = a_0\phi(x) \qquad \text{Eq. (H69)}$$

Each term of Eq. (H17) in terms of Eq. (H63) is:

$$\frac{\partial^2 y}{\partial x^2} = Y(t)\frac{\partial^2\phi(x)}{\partial x^2} = -\frac{\pi^2}{L_0^2}Y(t)\phi(x) \qquad \text{Eq. (H70)}$$

$$\frac{\partial^2 y_0}{\partial x^2} = -\frac{\pi^2 a_0}{L_0^2}\phi(x) \qquad \text{Eq. (H71)}$$

$$\frac{\partial^2 y}{\partial t^2} = \ddot{Y}(t)\phi(x) \qquad \text{Eq. (H72)}$$

$$\frac{\partial y}{\partial t} = \dot{Y}(t)\phi(x) \qquad \text{Eq. (H73)}$$

And so, substituting Eq. (H63) into Eq. (H17) gives:

$$m\ddot{Y}(t)\phi(x) + c\dot{Y}(t)\phi(x) + \big(N + \Delta N(t)\big)\frac{\pi^2}{L_0^2}Y(t)\phi(x) + \Delta N(t)\frac{\pi^2 a_0}{L_0^2}\phi(x) = q(x,t) \qquad \text{Eq. (H74)}$$

multiplied by $\phi(x)$ gives

$$m\ddot{Y}(t)\phi^2(x) + c\dot{Y}(t)\phi^2(x) + \big(N + \Delta N(t)\big)\frac{\pi^2}{L_0^2}Y(t)\phi^2(x) + \Delta N(t)\frac{\pi^2 a_0}{L_0^2}\phi^2(t) = q(x,t)\phi(x) \qquad \text{Eq. (H75)}$$

we know that

$$\int_0^{L_0}\phi^2(x)dx = \int_0^{L_0}\sin^2\left(\frac{\pi x}{L_0}\right)dx = \frac{L_0}{2} \qquad \text{Eq. (H76)}$$

and integrated over length of cable

$$\frac{mL_0}{2}\ddot{Y}(t) + \frac{cL_0}{2}\dot{Y}(t) + \frac{\pi^2}{2L_0}\big(N + \Delta N(t)\big)Y(t) + \frac{\pi^2 a_0}{2L_0}\Delta N(t) = \int_0^{L_0} q(x,t)\sin\left(\frac{\pi x}{L_0}\right) \qquad \text{Eq. (H77)}$$

Assuming a harmonic time variation:

$$Y(t) = Y_1\sin(\omega t) + Y_2\cos(\omega t) \qquad \text{Eq. (H78)}$$

and so

$$\dot{Y}(t) = \omega Y_1\cos(\omega t) - \omega Y_2\sin(\omega t) \qquad \text{Eq. (H79)}$$

$$\ddot{Y}(t) = -\omega^2 Y_1\sin(\omega t) - \omega^2 Y_2\cos(\omega t) \qquad \text{Eq. (H80)}$$

Substituting Eq. (H78) to Eq. (H80) into Eq. (H77), and if one neglects the lateral load:

$$\frac{mL_0}{2}(-\omega^2 Y_1\sin(\omega t) - \omega^2 Y_2\cos(\omega t)) + \frac{cL_0}{2}(\omega Y_1\cos(\omega t) - \omega Y_2\sin(\omega t)) + \frac{\pi^2}{2L_0}\big(N + \Delta N(t)\big)(Y_1\sin(\omega t) + Y_2\cos(\omega t)) + \frac{\pi^2 a_0}{2L_0}\Delta N(t) = 0 \qquad \text{Eq. (H81)}$$

The increment in axial force can be taken from Eq. (H24) together with the individual increments derived in previous section:

$$\Delta N = \frac{EA}{L_0}\left[\Delta \mathrm{x}(t) + \frac{1}{2L_0}\Delta \mathrm{y}(t)^2 + \frac{\pi^2}{4L_0^2}Y(t)^2 + \frac{8}{3}\frac{a_0^2}{L_0}\right] \qquad \text{Eq. (H82)}$$

with Eq. (H78) gives:

$$\Delta N(t) = \frac{EA}{L_0}\left[\Delta \mathrm{x}(t) + \frac{1}{2L_0}\Delta \mathrm{y}(t)^2 + \frac{\pi^2}{4L_0^2}(Y_1 \sin(\omega t) + Y_2 \cos(\omega t))^2 + \frac{8}{3}\frac{a_0^2}{L_0}\right] \qquad \text{Eq. (H83)}$$

Substituting Eq. (H83) into Eq. (H81) gives the final equation of motion of the cable excited by support motions, expressed in terms of generalized coordinates.

H References

[H1] Anders Rønnquist, Svein Remseth, Geir Udahl. Possible unstable non-linear dynamic response from parametric excitation of taut mooring elements a submerged floating tunnel. *Procedia Engineering* 2010.

[H2] Max Irvine. *Cable Structures*, The MIT Press, Cambridge, 1981.